HIGH IMPEDANCE FAULT DETECTION AND LOCALIZATION IN 11kV DISTRIBUTION SYSTEM

MOHD SYUKRI BIN ALI

INSTITUTE OF GRADUATE STUDIES
UNIVERSITY OF MALAYA
KUALA LUMPUR

2018

HIGH IMPEDANCE FAULT DETECTION AND LOCALIZATION IN 11kV DISTRIBUTION SYSTEM

MOHD SYUKRI BIN ALI

THESIS SUBMITTED IN FULFILMENT OF THE REQUIREMENTS FOR THE DEGREE OF DOCTOR OF PHILOSOPHY

INSTITUTE OF GRADUATE STUDIES
UNIVERSITY OF MALAYA
KUALA LUMPUR

2018

UNIVERSITY OF MALAYA

ORIGINAL LITERARY WORK DECLARATION

Name of Candidate: Mohd Syukri Bin Ali

Matric No: HHD130001

Name of Degree: Doctor of Philosophy

Title of Thesis: High Impedance Fault Detection and Localization in 11kV Distribution System

Field of Study: Power System

I do solemnly and sincerely declare that:

(1) I am the sole author/writer of this Work;
(2) This Work is original;
(3) Any use of any work in which copyright exists was done by way of fair dealing and for permitted purposes and any excerpt or extract from, or reference to or reproduction of any copyright work has been disclosed expressly and sufficiently and the title of the Work and its authorship have been acknowledged in this Work;
(4) I do not have any actual knowledge nor do I ought reasonably to know that the making of this work constitutes an infringement of any copyright work;
(5) I hereby assign all and every rights in the copyright to this Work to the University of Malaya ("UM"), who henceforth shall be owner of the copyright in this Work and that any reproduction or use in any form or by any means whatsoever is prohibited without the written consent of UM having been first had and obtained;
(6) I am fully aware that if in the course of making this Work I have infringed any copyright whether intentionally or otherwise, I may be subject to legal action or any other action as may be determined by UM.

Candidate's Signature Date:

Subscribed and solemnly declared before,

Witness's Signature Date:

Name:

Designation:

HIGH IMPEDANCE FAULT DETECTION AND LOCALIZATION IN 11KV DISTRIBUTION SYSTEM

ABSTRACT

High impedance fault (HIF) is a type of fault, where the fault current flow is restricted by the high impedance element. The insufficient fault current will not trigger the fuse or conventional overcurrent protection relay. As such, any undetected HIF will lead to potential hazards to human life and equipment damages. On the long run, it can affect power system quality in terms of service continuity, disturbance propagation and energy losses if HIF left untreated. In order to overcome the stated problems, it is imperative for the utilities to detect the HIF and its location in distribution system quickly. However, the detection of HIF is challenging as the resultant distortion on the voltage profile and increment in harmonic content are similar to the non-HIF events such as load switching, motor starting and capacitor switching. Moreover, locating the HIF is also a complicated task especially for a distribution network. This is due to the complexity of the network such as the presence of non-homogeneous line, lateral branches and load variations. Considering the importance of detecting and locating HIF in the distribution system, this study proposes a combined technique comprising of two independent techniques utilizing single measurement point. The first technique, based on Phase Displacement Computation (PDC) is proposed to detect the occurrence of HIF utilizing the three-phase voltage waveforms. Concurrently, the proposed technique is able to discriminate the HIF from non-HIF events. The second technique, based on intelligent approach is proposed to identify the location of HIF. For this purpose, the measured three-phase voltage and current waveforms are analyzed using the wavelet transform (WT). Then, the extracted approximation features from WT are fed into Artificial Neural Network (ANN) to be trained. In this process, the grey wolf optimization (GWO) technique is adopted in order to provide the optimal value of ANN parameters. Fault simulations were carried out using

the PSCAD/EMTDC software to obtain the distorted voltage and current waveforms during the HIF events. Subsequent algorithm simulation results show that the proposed methods are able to detect and subsequently locate the faults with high accuracies. In addition, the proposed methods are found to be effective and economical since the methods require only single measurement of voltage and current waveforms.

Keywords: High impedance fault, fault distance, fault type, fault impedance and faulty section.

PENGESANAN DAN PENYETEMPATAN KESALAHAN HALANGAN TINGGI DALAM 11KV SISTEM PENGAGIHAN

ABSTRAK

Kesalahan halangan tinggi (HIF) merupakan sejenis kesalahan, yang mana aliran arus bersalah dihadkan oleh unsur halangan tinggi. Oleh itu, aliran arus bersalah yang tidak mencukupi tidak dapat mencetuskan fius atau penyampai konvensional perlindungan arus terlebih. Kejadian HIF boleh menyebabkan satu cas elektrik diantara mesin yang membawa kepada potensi bahaya kepada kehidupan manusia dan alam sekitar. Selain itu, risiko kebakaran kerana cas elektrik diantara mesin boleh menimbulkan kemungkinan kerosakkan peralatan sistem kuasa. Pada jangka masa panjang, ia boleh menjejaskan kualiti sistem kuasa dari segi kesinambungan perkhidmatan, gangguan penyebaran dan kerugian tenaga jika HIF tidak dirawat. Untuk mengatasi masalah ini, syarikat utiliti kuasa perlu mengesan dan mencari HIF secepat yang mungkin. Walaubagaimanapun, untuk mengesan berlakunya HIF adalah mencabar kerana hasil herotan pada profil voltan serta kenaikan kandungan harmonik adalah hampir sama dengan kejadian bukan-HIF seperti penukaran beban, pemulaan motor dan penukaran kapasitor. Selain itu, mencari HIF juga merupakan tugas yang rumit terutamanya bagi rangkaian pengedaran. Ini adalah disebabkan oleh kerumitan rangkaian seperti kewujudan line homogen, cawangan sisian dan variasi beban. Memandangkan kepentingan mengesan dan mencari HIF dalam sistem pengagihan, kajian ini mencadangkan teknik gabungan yang terdiri daripada dua teknik yang berbeza menggunakan satu titik pengukuran. Teknik yang pertama berdasarkan Pengiraan Anjakan Fasa (PDC) dicadangkan untuk mengesan kejadian HIF menggunakan tiga fasa gelombang voltan. Serentak dengan itu, teknik yang dicadangkan ini juga mampu untuk mendiskriminasikan antara kejadian HIF dan bukan-HIF. Teknik ynag kedua berdasarkan pendekatan bijak dicadangkan untuk mengenalpasti lokasi HIF. Bagi tujuan ini, tiga fasa gelombang voltan dan arus dinilai dan dianalisis menggunakan

pengubah wavelet. Kemudian, ciri-ciri butiran dan penghampiran yang diekstrak dari WT akan dimasukkan ke dalam Rangkaian Tiruan Neural (ANN) untuk dilatih. Dalam proses ini, teknik Pengoptimuman Serigala Kelabu (GWO) digunapakai untuk memberi nilai yang optimum bagi parameter ANN. Simulasi telah dijalankan menggunakan perisian PSCAD/EMTDC untuk mendapatkan gelombang voltan dan arus bersalah semasa kejadian HIF. Keputusan simulasi menunjukkan bahawa kaedah yang dicadangkan mampu untuk mengesan dan seterusnya mencari kesalahan dengan jayanya. Tambahan pula, kaedah yang dicadangkan dianggap efektif dan jimat kerana kaedah ini hanya memerlukan satu pengukuran untuk gelombang voltan dan arus.

Katakunci: Kesalahan halangan tinggi, jarak kesalahan, jenis kesalahan, halangan kesalahan dan seksyen kesalahan.

ACKNOWLEDGEMENTS

ALHAMDULILLAH, all praises to Almighty ALLAH S.W.T with HIS blessing, prayers of my family and friends as well as kind supervision and guidance of my respected supervisors, I able to complete this thesis.

I would like to acknowledge special thanks to my respected supervisors Prof. Ir Dr. Ab Halim Abu Bakar, Dr. Tan ChiaKwang and Prof. Dr. Hamzah Arof for their constant motivation and support during my PhD research. I truly appreciate their esteemed guidance and encouragement from the beginning to the end of this report.

I would also like to express my greatest thanks to my father, Ali Bin Hj Mohd Said, my siblings, Zarinah, Azizun, Azizie, Nur Hana, Zulailah, Mohd Azrin, Suraya and Nur Syuhaily as well as my brothers and sisters in law for their morale support, understanding and encouragement until I finish my PhD. I would like to express appreciation to all my colleagues, Fahmi, Shahrir Razhey, Hazwan and others as well as my labmates for their help and support throughout my study. My greatest thanks to Prof. Ir Dr. Hazlie Mokhlis for allowing me to do my research in his lab.

Last but not least, all thanks to those who either directly or indirectly gave cooperation, motivation and support along my journey to complete PhD.

TABLE OF CONTENTS

LIST OF FIGURES

LIST OF TABLES

LIST OF SYMBOLS AND ABBREVIATIONS

LIF	:	Low Impedance Fault
HIF	:	High Impedance Fault
PDC	:	Phase Displacement Computation
WT	:	Wavelet Transform
DWT	:	Discrete Wavelet Transform
CWT	:	Continuous Wavelet Transform
MRA-DWT	:	Multi-Resolution Analysis Discrete Wavelet Transform
ST-DWT	:	Spanning-Tree Discrete Wavelet Transform
FT	:	Fourier Transform
GPS	:	Global Positioning System
ANN	:	Artificial Neural Network
GWO	:	Grey Wolf Optimization
ANN-GWO	:	Artificial Neural Network-Optimized by Grey Wolf Optimization
PSO	:	Particle Swarm Optimization
EP	:	Evolutionary Programming
Bior	:	Biorthogonal Mother Wavelet
Db	:	Daubechies Mother Wavelet
Sym	:	Symlet Mother Wavelet
SLGF	:	Single Line to Ground Fault
LLGF	:	Double Line to Ground Fault
LLF	:	Double Line Fault
LLLGF	:	Triple Line to Ground Fault
LLLF	:	Triple Line Fault
BF	:	Balanced Fault

MaxError	:	Maximum Error
AverError	:	Average Error
StD	:	Standard Deviation
ObjFunc	:	Objective Function
trainlm	:	Levenberg-Marquardt Backpropagation
cA	:	Approximation Coefficients
cD	:	Detail Coefficients
lr	:	Learning Rate
mc	:	Momentum Constant
p	:	Number of Neurons in Hidden Layer
V_{ref}	:	Reference Voltage Signal
$V_{measured}$	:	Measured Voltage Signal During Fault
V_{min}	:	Minimum Voltage Signal
V_{max}	:	Maximum Voltage Signal
I_{min}	:	Minimum Current Signal
I_{max}	:	Maximum Current Signal
P	:	Active Power
Q	:	Reactive Power
E	:	Energy Content
sE	:	Difference in Energy Content
$\Delta\Phi_{diff}$	:	Phase Angle Difference
D-index	:	Detection Index
Id-index	:	Identification Index
L1	:	Lower Boundary of Length
L2	:	Upper Boundary of Length

LIST OF APPENDICES

CHAPTER 1: INTRODUCTION

1.1 Introduction

Faults in a power distribution network are mainly caused by natural disasters and degradation as well as human factors. Examples of these factors include storms, lightning strikes, a fallen tree trunk, animal encroachment, heat cycling, water, aging components, broken insulation and a host of human errors in the forms of accidents or other activities carried out in the vicinity of the power system (Filomena, Resener et al. 2009). The above mentioned events can lead to short-circuit.

The accompanying power quality disturbances during fault will cause interruptions to manufacturing processes in surrounding regions where sensitive equipment such as automated machines, power drive and process control in semiconductor factories are forced to shut down (Melhorn, Davis et al. 1998). In addition, the continuity of supply in the downstream network will be interrupted when the protection relay isolates the fault.

Based on the survey done by (Abraham;, Dhaliwal; et al. 2004), it was found that more than 80% of the interruptions that occurred in the distribution systems were caused by faults. Therefore, it is important for the utility companies to detect, identify and locate the fault speedily to minimize the impact of the fault to power system equipment and losses due to power supply interruption. Reducing the interruption time also improves the reliability indices of the utility companies. The System Average Interruption Duration Index (SAIDI), Customer Average Interruption Duration Index (CAIDI) and System Average Interruption Frequency Index (SAIFI) are examples of indices that examines the reliability and efficiency of a utility company.

1.2 Problem Statement

The detection and localization of faults in a power network are important to ensure the supply of electrical power that is reliable, efficient, safe and secure. Thus, immediate and accurate detection and localization of a fault are crucial. However, the detection of HIF with a low fault current is very challenging. Many methods have been proposed and tested and they can be broadly divided into two categories namely mechanical and electrical HIF detection approaches (Adamiak, Wester et al.).

Mechanical HIF detection techniques use devices that make contact with the ground to provide a low impedance ground fault when a HIF occurs. Consequently, sufficient fault current is generated to activate the overcurrent protection relay. These techniques work best when the devices are stationed at each pole. However, since there are many poles in a distribution network, it becomes prohibitively expensive and impractical.

Electrical HIF detection techniques are favorable since they only utilize voltage and current signals to detect the occurrence of a HIF. Once a HIF is detected, its location must be identified correctly. Unfortunately, it is difficult to pinpoint the HIF location due to the complex nature of the distribution network, which contains lateral branches, unbalanced network and non-homogeneous lines. The most popular conventional methods in use are trial-and-error switching, visual inspection and fault indicators (Krajnak 2000). These methods can be easily adopted but they are time-consuming and unsuitable for underground power systems.

Numerous works have been reported in locating low impedance faults (LIFs) on the transmission and overhead distribution lines. Unfortunately, only a few works have been dedicated to locate the high impedance faults (HIF), especially in an underground distribution network. The most common practice used by the utilities to locate the HIF is using a surge generator that injects high voltage pulses at each cable section, which is

also known as thumping. However, if all cables at each section are thumped, especially for a long cable, it could take days to locate the fault. Furthermore, this will reduce the lifespan of cables. Besides that, there are several other techniques have been proposed such as network topology, traveling wave, analytical formulation and knowledge-based techniques. However, most of the techniques only consider the fault distance. Therefore, the exact fault location still difficult to be pinpointed due to the lateral branches of the distribution network. Consequently, it is of utmost importance for a project to be initiated to develop an efficient HIF detection and localization techniques that are fast, reliable and do not accelerate cable ageing.

1.3 Research Objectives

The focus of this research is mainly to develop a novel technique to detect and locate HIF events. Considering the importance of HIF detection and localization in a distribution network, the following main objectives are outlined as follows:

1. To detect and differentiate HIF events from non-HIF events such as capacitor switching, motor starting and load switching.
2. To propose fault location method through fault type identification, fault impedance estimation and fault distance calculation.
3. To propose an enhanced fault location method incorporating faulty section identification algorithm to enhance fault distance estimation.
4. To compare and evaluate the effectiveness of the proposed method against existing fault detection and localization techniques in terms of accuracy and reliability.

The proposed method uses only voltage and current waveforms to detect and locate the HIF. These data can be obtained from any type of measurement devices such as Fault Recorder located at the primary substation. It is expected to be effective and economical

since the method considers only a single measurement of voltage and current waveforms and does not require any communication links to access remote nodes.

1.4 Research Contribution

To achieve the outlined objectives, the background of the distribution network and HIF event is first studied. Then, a distribution network model is developed and HIF events are simulated using PSCAD/EMTDC software. Subsequently, the measured voltage waveforms at the primary substation are analyzed to detect the occurrence of HIF event. To classify the fault type, estimate the fault impedance and distance values as well as identify the faulty section, both voltage and current waveforms are analyzed using digital signal processing techniques. The MATLAB algorithms are employed to extract important features from the voltage and current waveforms in both HIF detection and localization techniques.

1.5 Scope of Work

The scope and limitations of this research are as follows:

1. The scope of this research is limited to the 132/11kV distribution system.
2. The high impedance faults considered in this study range from 50-150Ω.
3. Distributed generator in the distribution system is not included in this study.
4. Only one measurement point is considered at the primary substation to measure voltage and current waveforms.
5. The application of an optimization technique in this research is mainly to provide an optimal values of ANN parameters.
6. All the simulations are conducted using the PSCAD/EMTDC software.

1.6 Thesis Outline

This thesis comprising of six chapters. **Chapter 1** provides an overview of faults in power distribution system, the importance of fault detection and localization, the objectives of the research, a brief methodology as well as the scope and limitations of the research.

Chapter 2 reviews the existing techniques on fault detection and localization in distribution systems. First, the overview for general fault detection and localization methods are discussed. Special emphasis is then placed on HIF and the various HIF detection and localization techniques. There are several types of HIF localization techniques comprising of network topology, traveling wave, analytical formulation and knowledge-based techniques.

In **Chapter 3**, the theoretical background of the wavelet transform is presented. The working principles, advantages and disadvantages for different types of wavelet transform are discussed. Besides that, the theoretical background of GWO and ANN are also presented.

The methodology of the proposed technique for HIF detection and identification is presented in **Chapter 4**. A typical 132/11kV radial distribution system consisting of 18 nodes is considered and modeled using PSCAD/EMTDC software to generate reference and faulted voltage waveforms. HIF events are simulated and distinguished from various non-HIF events such as motor starting, capacitor switching and load switching. The robustness of the proposed method is tested with regard to variation of fault inception angles and consecutive events occurrence. Finally, an automatic HIF detection and identification algorithms are developed.

In **Chapter 5**, the performance of the proposed fault location method in classifying various types of fault, estimating fault impedance and fault distance values are discussed. A typical 132/11kV radial distribution system consisting of 33 nodes is modeled using PSCAD/EMTDC software. Then, various types of HIF faults are simulated at different locations in the network. The proposed method in conjunction with an ANN classifier and GWO technique is able to classify the fault types, estimate the fault impedance and distance values. Subsequently, an enhanced fault location method is proposed incorporating the faulty section identification algorithm to enhance the fault distance estimation. Finally, **Chapter 6** concludes the study, summarizes the main findings and proposes future work to improve the proposed method further.

CHAPTER 2: OVERVIEW ON FAULT DETECTION AND LOCALIZATION FOR DISTRIBUTION SYSTEM, WAVELET TRANSFORM, OPTIMIZATION TECHNIQUE AND ARTIFICIAL NEURAL NETWORK

2.1 Introduction

There are two types of faults and they are low impedance fault (LIF) and high impedance fault (HIF). The focus of the work reported in this thesis is to detect, discriminate and locate HIF faults only. Detecting the occurrence of a HIF is challenging because it does not produce a significant fault current that can trigger the conventional overcurrent protection relay. However, a HIF can still distort the voltage profile and increase the harmonic content. To complicate matters, the pattern of the distortion is similar to that of a non-HIF event such as load switching, motor starting and capacitor switching. Due to the detrimental effects of a HIF to a power system, it is important for the utility company to detect and locate it as quickly and accurately as possible. In this chapter, the significance and issues associated with detecting, discriminating and locating HIF faults are discussed. An overview of existing LIF and HIF detection and localization methods in the forms of their working principle, advantages and disadvantages is presented.

Subsequently, an overview of wavelet transform (WT), optimization technique and artificial neural network (ANN) is presented. WT is used to extract the important features from the voltage and current signals. As such, the working principle, variety of WT and advantages of WT is explained. Then, the working principle and the effect of ANN variables is discussed. ANN is responsible to estimate the fault impedance and distance values as well as classify the fault type by utilizing the extracted features from WT. Besides that, the significance of utilizing the optimization technique to provide the

optimal values of ANN parameters is discussed. Here, the grey wolf optimization (GWO) technique is used and its working principle is explained.

2.2 Fault Classification Analysis

In fault analysis, differentiating power system faults from other similar transient events is crucial. Figure 2.1 shows the classification of power system disturbances into temporary and permanent events. A temporary event such as a transient event only occurs for a short period of time. There are several examples of transient events that resemble HIFs such as capacitor bank switching, inrush current, harmonic load, motor starting and insulator leakage current (Sarlak and Shahrtash 2011). Permanent disturbances are considered as faults and they can be categorized into two groups, which are LIF and HIF. They are similarly grouped into Single Line to Ground Fault (SLGF), Double Line to Ground Fault (LLGF), Double Line Fault (LLF), Three Line to Ground Fault (LLLGF) and Three Line Fault (LLLF). The only difference between LIF and HIF is the magnitude of fault impedance.

LIF and HIF have similar causes in the forms of bare overhead line falling on the ground, animal contact, a tree branch bridging the lines, insulation breakdown and adverse weather condition like flooding. However, as stated earlier, the difference between LIF and HIF is the amount of impedance introduced by the object that touches the live conductor. In an LIF event, the fault generates a sufficient fault current that can be detected by a conventional overcurrent protection relay or fuse. Then, the faulty line can be isolated from other faultless lines. In an HIF, the fault is due to a high impedance object, which results in a small fault current drawn. Thus the fault current is insufficient to trigger the conventional overcurrent protection relay or fuse making it hard to localize the faulted line. Since it is not isolated from the system, it poses a hazard to the system, human, and environment.

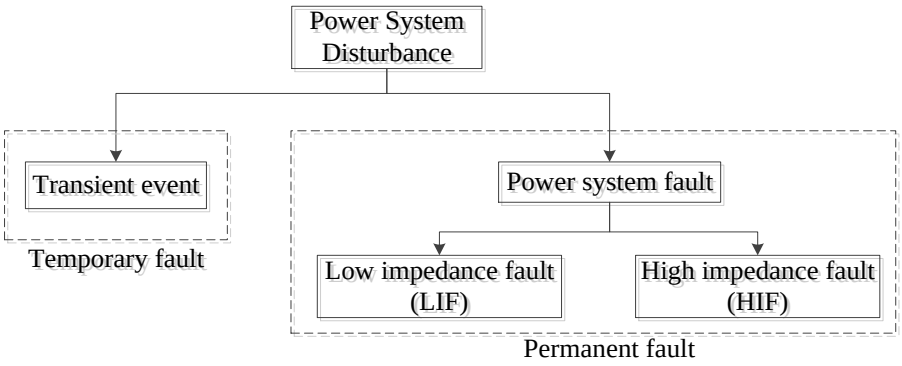

Figure 2.1: Classification of Power System Disturbance

2.3 Low Impedance Fault

2.3.1 Overview of Low Impedance Fault Localization Method

In this subsection, an overview of the methods used to locate low impedance faults are presented. They are classified as:

1. Conventional method
2. Impedance-based method
3. Travelling wave method
4. Knowledge-based method

2.3.1.1 Conventional Method

The conventional methods locate LIFs via visual inspection, trial and error switching and fault indicators (Krajnak 2000; Sharaf and Abu-Azab 2000; 2005). Visual inspection technique requires engineers to patrol along the faulty feeder to identify the fault location. Initially, an experienced engineer intelligently guesses a possible location of the fault before checking the selected location. This technique is inefficient and time-consuming since multiple locations need to be checked if the first estimated fault location is incorrect. In trial and error switching approach, every substation is switched on and off until a circuit breaker trip off is identified which indicates the faulty section. This technique is also time-consuming and exposes the equipment to additional stress due to the switch on and off

processes. The last conventional method uses fault indicators to locate the LIFs. A fault indicator is a device, which identifies the faulty section via the signal provided by two adjacent indicators. This technique is impractical since an indicator needs to be installed at each section. In addition, visual inspection is still required to ensure functionality of fault indicators.

2.3.1.2 Impedance-based Method

The impedance-based method is a mathematical technique in which the impedance is calculated from the faulted current and voltage values. There are two types of impedance-based methods. The first type is the one-ended measurement in which faulted current and voltage values are measured at one end of the line (Takagi, Yamakoshi et al. 1982; Girgis, Fallon et al. 1993; Aggarwal, Aslan et al. 1997; Santoso, Dugan et al. 2000; Filomena, Resener et al. 2009). The second one is the two-ended measurement which requires faulted current and voltage values to be measured at both ends of the line (Girgis, Hart et al. 1992; Novosel, Hart et al. 1996; Ying-Hong, Chih-Wen et al. 2002).

The advantage of this method is its simplicity to estimate the fault location. It only requires a fundamental component of current and voltage signals during the fault (Mora-Flòrez, Meléndez et al. 2008; Gazzana, Ferreira et al. 2014). This method is widely used for fault location identification in transmission line systems, but not practical to be implemented in distribution systems. This is because of the complexity of the distribution network due to the existence of non-homogeneous cable and multiple lateral branches, which contributes to inaccurate results. Besides that, this method also leads to multiple possible fault locations due to the lateral branches (Novosel, Hart et al. 1998). Generally, the error of this fault location estimation increases as the fault impedance and the distance to the fault point increases. Thus, it can be inferred that impedance-based method is only suitable for locating low impedance fault cases.

2.3.1.3 Traveling Wave Method

The principle of traveling wave method is based on the transmission and reflection of the voltage or current signal that produces traveling waves. This concept is illustrated in Figure 2.2. The voltage or current signal will be transmitted from Terminal A and then the signal will be reflected at the fault point. The reflected wave will return to Terminal A and the transmitted wave will propagate to Terminal B as shown in the figure.

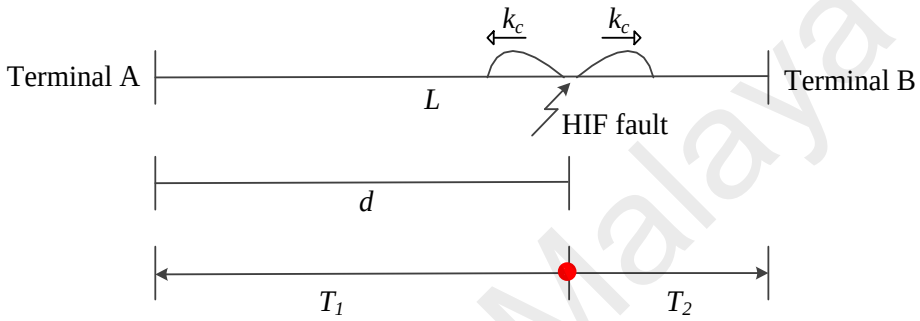

Figure 2.2: Travelling wave diagram

This method is commonly used for location of LIF on a transmission line (Elhaffar 2008). For a distribution system, this method is impractical due to the complexity of the network topology, which contains many points of electrical discontinuity. The discontinuities will cause many reflections and refractions of the transmitted signal, which is coming from the fault point and lateral junctions in the network. Besides that, the implementation of this technique is costly as it requires the sensors, high-speed data acquisition devices and a Global Positioning System (GPS) to capture the transient waveform (Lee and Mousa 1996).

2.3.1.4 Knowledge-based Method

To overcome the complexity of locating faults in a distribution network, several researchers have resorted to the knowledge-based method. It is a popular type of method, which can analyze a large amount of information. Some information such as feeder switch status, atmospheric condition, feeder measurement and the signals provided by fault

detection devices are used. The accuracy of this method is highly dependent on the amount of information available. Several examples of a knowledge-based method that are widely used are:

1. Expert system (ES)
2. Genetic algorithm (GA)
3. Artificial neural network (ANN)
4. Fuzzy set theory (FST)
5. Matching approach (MA).

(a) ***Expert System (ES)***

ES is a sort of technique that emulates human reasoning in diagnosing a problem to obtain solutions. This technique is based on pre-defined rules about system behaviors such as a breaker and relay status to estimate the fault location. Therefore, reliable and correct information from experienced engineers and data from SCADA systems are gathered and utilized. ES techniques have been successfully used in locating the faults in the works of (Martinez and Richards 1991; Yuan-Yih, Lu et al. 1991; Kumano, Ito et al. 1993). However, this technique has their own disadvantages. First, a large amount of data needs to be collected and analyzed. In addition, the task of applying pre-defined rules is difficult because the rules have to be updated and replaced according to the dynamics of the system where expertise and knowledge are again required from experts.

(b) ***Genetic Algorithm (GA)***

GA is an adaptive heuristic search algorithm based on the evolutionary idea. In this algorithm, intelligent exploitation of random search within a defined search space is performed. The basic concept of GA is to generate a random population for evolution process. In each evolution, the fitness of the populations will be evaluated. Populations with a good fitness will be selected for mutation and recombination to form a new

population. Then, this new population will undergo the same process and it will be iterated until a satisfactory fitness level is achieved. Besides that, the process can be terminated if the maximum number of iterations is reached. However, in this case, a satisfactory solution may or may not be achieved. (Wen and Han 1995) utilized GA to estimate the potential faulty sections. The main drawback of this technique is it is time consuming due to the repetition process to obtain satisfactory fitness level.

(c) ***Artificial Neural Network (ANN)***

ANN technique has also been used to locate faults in distribution systems (Glinkowski and Wang 1995; Cardoso, Rolim et al. 2004) and transmission line (Mohamed, El-Saadany et al. 2003). In order to locate a fault, a pre-defined input with respect to the expected output will undergo a training process. The pre-defined input may include feeder and circuit breaker status, voltage and current signals. The disadvantage of this technique is its dependence on correct and complete information to generate a well-trained ANN. If the information given is inaccurate or insufficient, it will affect the accuracy of ANN. Besides that, ANN needs to be re-trained when there are changes in the system.

(d) ***Fuzzy Set Theory (FST)***

In (Jarventausta, Verho et al. 1994; Wen-Hui, Chih-Wen et al. 2000; Jung, Kim et al. 2007), FST was used to determine the location of LIF. The advantage of FST is it has the capability to model uncertainty and inexactness regarding the decision making of fault location. The main drawback of this technique is it requires a large number of data, such as information obtained from the network database, data from the SCADA system such as relay and circuit breaker status and heuristic knowledge of the control center operators to form the fuzzy rules.

*(e) **Matching Approach (MA)***

MA technique requires a database of simulated faults at each node to be stored as references. When a LIF occurs, the measured data taken are compared with the simulated data (reference data stored in the database) to determine the faulty section. The faulty section is identified if the measured data fall between the simulated data of two adjacent nodes. Usually, the voltage and current signals are used for this purpose as these signals can be obtained easily at the primary substation. Voltage sag pattern and database approach have been proposed by (Li, Mokhlis et al. 2005; Mokhlis, Li et al. 2010; Mokhlis, Mohamad et al. 2011) to locate the faulty section. The faulty section is identified when the measured magnitude of voltage sag lies between two magnitudes of voltage sags that have been simulated to represent two adjacent nodes of a line section.

2.4 High Impedance Fault

2.4.1 Introduction

A HIF is defined as a fault which does not produce enough fault current that can trip the conventional overcurrent protection relay (John Tengdin, Ron Westfall et al. 1996; Torres, Guardado et al. 2014; Thomas, Bhaskar et al. 2016). This is due to the high impedance of the connecting object or surface that restricts the flow of the fault current, making it difficult to detect. HIF can occur in an overhead or underground distribution system. Normally, in an overhead system, HIF occurs when a conductor touches the ground or a high impedance object connected to the ground. This is probably due to a fallen pole or a failure of the mounting system. It is observed that a HIF can also happen without a path to ground, such as when a tree limb bridges two conductors. For an underground system, HIF is normally caused by insulation defects that expose the conductor to make contact with non-conducting elements. Common causes of insulation defects include cracking, chaffing, abrasion, flash fault and insulation degradation due to moisture and corrosive contamination. In addition, a cut to the cable insulation may

expose the conductor and cause a HIF. HIF may produce arcing, which is a potential hazard to human life and can cause damage to the power system equipment (Ghaderi, Ginn et al. 2017). Figure 2.3 shows an example of electrical arcing that was produced when the tree branch bridged across the live conductor at 7,200 Volts. Whereas an arcing at underground cable can lead to an unexpected explosion due to very high flashover energy as shown in Figure 2.4. Furthermore, it is observed that if HIF is left untreated, it will affect the power system quality in terms of service continuity and energy loss.

Figure 2.3: An electric arcing phenomenon (http://phys.org/news/2010-11-faults-vegetation-contact-lines.html#jCp)

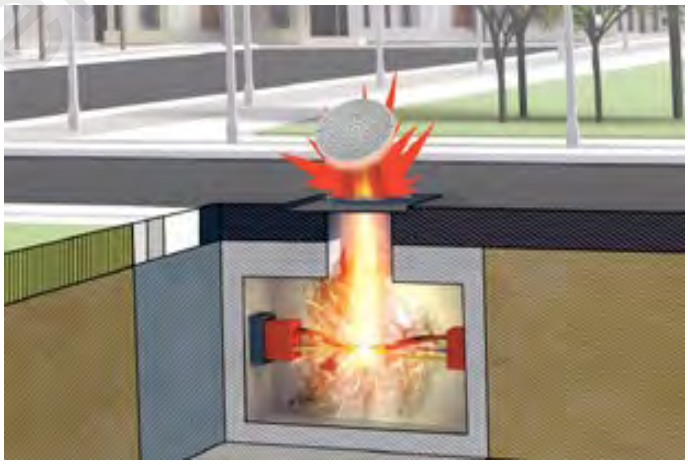

Figure 2.4: Explosion during HIF event (http://www.gedigitalenergy.com/multilin/feeder_spotlight.htm)

2.4.2 High Impedance Fault Detection Method

A HIF event must be differentiated from non-HIF events that show similar signatures to maintain the reliability of the system. The detection methods must have the capability to detect and subsequently classify the event as HIF or non-HIF. There are two types of HIF detection methods namely the mechanical and electrical HIF detection methods. A brief review of these methods is given in the following subsections.

2.4.2.1 Mechanical HIF Detection methods

Mechanical HIF detection method is a technique that utilizes a mechanical device that makes contact with the ground in order to provide a low impedance route when a HIF occurs to allow a conventional overcurrent protection relay to operate (Adamiak, Wester et al.). There are 2 common techniques for mechanical HIF detection method. The first technique employs a device that is mounted to a cross arm or pole. This device is installed under each phase wire in order to catch falling conductors. During a HIF event, the force of a falling conductor hits an internal spring that ejects a bus bar to make contact with the fallen wire. This contact will create a low impedance ground fault, which will trigger the conventional overcurrent protection relay to operate. The second technique utilizes a pendulum mounted aluminum rod with a hooked end. The device is suspended from an under-built neutral conductor. During the event of falling conductors to the ground, the hook will catch it and produce a low impedance ground fault. Thus, the conventional overcurrent protection relay will be triggered.

The disadvantage of this mechanical method is they also react to sagging conductors, which are not in contact with a grounded object or earth. Thus, they are prone to create false alarm and falsely trip the line. Besides that, this method requires a high cost of installation and maintenance. Furthermore, they are only applicable for overhead distribution network and transmission lines, not for an underground distribution system.

2.4.2.2 Electrical HIF Detection

Electrical HIF detection method utilizes voltage and current signals obtained from the measurement devices. The characteristic features are extracted from these signals periodically and the occurrence of HIF event is determined from time to time. In short, the process of electrical HIF detection using voltage and current signals consists of two basic steps, which are feature extraction and pattern recognition (classification) (Ghaderi, Mohammadpour et al. 2015). In the first step, significant features are extracted from the voltage and current signals using various feature extractors or digital signal processing techniques. Subsequently, in the second step, the extracted features will be fed into a classifier that decides whether a HIF occurs in the system. In the training stage, samples of features from voltage and current signals extracted during HIF and non-HIF events are used to train the classifier. After the classifier is successfully trained, it can be used to classify unknown features from the network to determine whether a HIF has occurred or not at any instance. Details of some famous feature extractors and classifiers are given as follows:

(a) ***Feature Extraction***

A number of feature extractors have been used to extract features from voltage and current signals for HIF analysis. They are listed as follows.

a) Fourier Transform (FT)
b) S-Transform and TT-Transform
c) Mathematical Morphology (MM)
d) Wavelet Transform (WT)

i Fourier Transform

FT is a mathematical operation that converts a signal from a function of time to a function of frequency and it can be displayed in form of magnitude and phase angle in the frequency spectrum. Generally, FT can be described as a mathematical tool that decomposes the signal waveform, *F(x)* into its sinusoidal components that consist of sine and cosine waves as shown in Equation (2.1).

$$F(x) = a_0/2 + a_1\cos(x) + b_1\sin(x) + a_2\cos(2x) + b_2\sin(2x) + \ldots + a_n\cos(nx) + b_n\sin(nx) \quad (2.1)$$

In (Zadeh 2005), Discrete Fourier Transform (DFT) was used to extract the second and third harmonic (magnitude and angle) components of the voltage and current signals to detect the occurrence of HIF. Whereas in (Aziz, Hassan et al. 2012), DFT is applied to extract the third harmonics consists of magnitude and angle of the three phases of the current signal to detect and locate the fault during HIF. As well, the fundamental component is used to classify the faulted phases. In (Zanjani and Kargar 2012), it only utilizes the third harmonic current angle to detect and distinguish the HIF event. In (Macedo, Resende et al. 2015), DFT is used to quantify the root mean square (rms) magnitude of the set of interharmonic currents that associated with electric arcs of varying length. The variation in amplitude of the third and fifth order harmonic components extracted using Fast Fourier Transform (FFT) was monitored to detect the occurrence of HIF in (Bansal and Pillai 2007).

The main disadvantage of FT is it represents a signal with perfect frequency representation without time information. FT gives poor performance when it is applied to transform the time domain signal embedded with noise. It will limit the certainty of magnitudes, phases, peak frequencies and widths to be computed by FT because the time

domain noise is distributed uniformly throughout the frequency domain during the transformation process. Furthermore, a truncated time domain signal will produce undesirable frequency domain, which makes it difficult to observe a small peak in the vicinity of a large peak.

ii S-Transform and TT-Transform

S-transform is the simplification of short-time Fourier transform (STFT) and an extension to the idea of continuous wavelet transform (CWT) (Stockwell, Mansinha et al. 1996). It is based on a moving (translation) and scalable (dilation) localizing Gaussian window. S-transform is able to give both time and frequency information with proper time and frequency resolutions respectively. Whereas TT-transform is a two-dimensional time-time representation, which is derived from one-dimensional time series based on S-transform (Pinnegar and Mansinha 2003). TT-transform represents the time–local view of the time series through the scaled windows. Therefore, TT-transform provides proper time-local properties of the time series, which is necessary to localize the frequency components. In (Samantaray, Panigrahi et al. 2008), S-transform and TT-transform are used to extract the energy and standard deviation information from the current signal to classify the HIF from no fault event.

iii Mathematical Morphology

Mathematical Morphology (MM) is a technique used in analysis and processing of geometrical structure, which is based on set theory, lattice theory, randomness and topology functions. The purpose of MM is to extract image components and provides image descriptions and representations. In (Sarlak and Shahrtash 2011), MM was utilized to detect the occurrence of HIF and differentiate it from other non-HIF events such as load switching, fault on adjacent feeders, capacitor bank switching, harmonic load and

insulator leakage current. In that analysis, the time-based features from the post-disturbance current waveforms are extracted using the Multi-resolution Morphological Gradient (MMG) to highlight the irregularities of the current signal during disturbances. The main drawback of MM is no information available about the moment of event occurrence. Besides that, it is difficult to discriminate a signal that has very small differences thus providing an inaccurate result.

iv Wavelet Transform

Wavelet signal is a wave-like oscillation with an amplitude that starts from zero, increases and then decreases back to zero within a limited duration that has an average value of zero. It behaves as a mathematical function that satisfies the certain mathematical requirement to represent the signal in time and frequency domains. Wavelet transform (WT) had overcome the drawback of FT in term of constructing a time-frequency representation of a signal that offers very good time and frequency localization (David Chan Tat and Xia 1998; Shyh-Jier and Cheng-Tao 1999; Sedighi, Haghifam et al. 2005; Ghaffarzadeh and Vahidi 2010; Vahidi, Ghaffarzadeh et al. 2010; Shinde and Hase 2012). WT has been widely used in extracting information for HIF detection in (Lai, Snider et al. 2005; Haghifam, Sedighi et al. 2006; Michalik, Rebizant et al. 2006; Michalik, Lukowicz et al. 2007; Elkalashy, Lehtonen et al. 2008; Etemadi and Sanaye-Pasand 2008; Akorede and Katende 2010; Rafinia and Moshtagh 2014; Ye, You et al. 2014; Costa, Souza et al. 2015; Sekar, Mohanty et al. 2018). In (Borghetti, Corsi et al. 2006; Michalik, Rebizant et al. 2006; Michalik, Lukowicz et al. 2007), continuous wavelet transform (CWT) is used to extract the important features from the current and voltage signals to determine the occurrence of HIF. Discrete wavelet transform (DWT) has been used to analyze the voltage and current signal during the HIF event in (Lai, Snider et al. 2005; Haghifam, Sedighi et al. 2006; Elkalashy, Lehtonen et al. 2008; Akorede and Katende

2010; Goudarzi, Vahidi et al. 2015; Prabhavathi, Surya Kalavathi et al. 2017). Whereas in (Etemadi and Sanaye-Pasand 2008), the multi-resolution analysis-discrete wavelet transforms (MRA-DWT) was utilized to extract the input features from the nonlinear behavior of the current waveform for the HIF detection.

The main advantage of the wavelet transform is its localization property in both time and frequency domain. It can represent the signal that has tiny discontinuity and sharp peaks. It also gives an indication of the frequency content of the disturbance signal and reveals the important features in the signal by partitioning the signal energy at a different frequency band.

(b) ***Pattern Recognition (Classification)***

There are several types of classifiers have been widely used to classify HIF and LIF events. They include artificial neural network (ANN), fuzzy inference system (FIS), moving window (MW) and nearest neighbor rule (NNR).

i Artificial Neural Network

ANN is an information processing method that is motivated by the nerve system. The ANN structure can deal with the imprecise, complicated and large amount of data as input when properly trained or adjusted. There are several types of ANN such as feedforward neural network, probabilistic neural network and learning vector quantization neural network.

The feedforward neural network (FNN) is the simplest type of ANN where the information is moving in one direction (do not form a directed cycle or loops). The information travels forward, from the input layer through the hidden layer and lastly to the output layer. Thus, the output of any layer does not affect the previous layer. The second type of neural network is a probabilistic neural network (PNN). PNN is based on

a statistical algorithm called Kernel Fisher discriminant analysis. PNN has four layers consists of the input layer, hidden layer, pattern layer/summation layer and an output layer. PNN is a supervised learning network with the fast learning process. The third type of neural network is learning vector quantization neural network (LVQNN) which is a supervised learning network. LVQNN is a technique in which the input space is divided into different regions, and for each region, a reconstruction vector is defined. When a new input is present, the vector quantizer will determine the region for that input data.

ANN had been widely used to detect and classify HIF from non-HIF events in (Zadeh 2005; Michalik, Rebizant et al. 2006; Bansal and Pillai 2007; Samantaray, Panigrahi et al. 2008; Sarlak and Shahrtash 2011; Moravej, Mortazavi et al. 2015). However, this technique requires a large amount of input data to achieve a good result. Besides that, the reliability of input data is important to ensure its accuracy.

ii Fuzzy Inference System

FIS is a process of mapping formulation for a given input using the fuzzy logic to produce an output. In FIS, the rule-based method is used to get the desired input and output mapping. Based on the input and output mapping, a decision can be made according to the distinguished patterns. In (Haghifam, Sedighi et al. 2006), FIS had been implemented for fault classification.

iii Moving Window

MW is a nonparametric approach in which a window centered at the point of interest is imposed to calculate the weighted sum of coefficients. Then, the window is moving to the adjacent point of interest to calculate again the weighted sum of coefficients. This procedure is repeated until the moving window visits all the points of interest in the study

area. In (Akorede and Katende 2010), this method was used to discriminate different types of fault based on a unique pattern obtained from the weighted sum of coefficients.

iv Nearest Neighbor Rule

NNR is a nonparametric approach in supervised learning method. NNR is a typical pattern classification method in which the object is classified based on the closest distance between the input data and the classified data in the feature space. In (Lai, Snider et al. 2005), NNR method was used to classify two categories of data based on the boundaries decision. The data and boundaries were plotted in two-dimensional contour graph to observe the distribution pattern of the data. The disadvantage of this method is when the input data falls in overlapping area of 2 boundaries.

2.4.3 High Impedance Fault Location Method

Locating a HIF event is quite challenging due to the small fault current magnitude, small changes in voltage profile and its similar signatures to other non-HIF events. There are several methods for HIF location have been proposed such as:

1) Network Topology Technique
2) Travelling Wave Technique
3) Analytical Formulation Technique
4) Knowledge-based Technique

2.4.3.1 Network Topology Technique

The network topology technique requires a sensor or measurement device to be installed at each node. The sensors or measurement devices will communicate to each other and send data to the primary substation through the Global Positioning System (GPS). Then, the data will be analyzed to determine the fault location.

In (Gohokar and Khedkar 2005), a current transformer (CT) was installed at each node whereas in (Garcia-Santander, Bastard et al. 2005), voltage sensor was installed at each end of the network branch in order to identify the faulty section. Faulty section identification based on the ratio of the residual current amplitude concept was proposed by (Elkalashy, Lehtonen et al. 2007). Besides that, (Elkalashy, Lehtonen et al. 2008) was also proposed power polarity concept to identify the faulty section. Both concepts utilized wireless sensors to be installed at each measurement node. Last but not least, in (Uriarte and Centeno 2005), the fault location is determined based on the information given by the sectionalizer and recloser devices.

This technique is efficient and gives high accuracy to identify the faulty section. The main drawback of this technique is the requirement for a sensor device or measurement unit to be installed at each node. Thus, it is costly, as it requires high installation and maintenance costs. Besides that, all sensors or measurement units must be functioning well for the technique to work.

2.4.3.2 Travelling Wave Technique

In the previous subsection, the application of traveling wave technique in locating LIF was discussed. Recently, this technique has been implemented to trace HIF events. In (Bernadić and Leonowicz 2012; Glik and Rasolomampionona 2013; Zimath, Dutra et al. 2014), traveling wave technique was applied to find the fault location in a transmission line during the HIF event.

2.4.3.3 Analytical Formulation Technique

Analytical formulation technique is a process to break down a complex and complicated problem into its constituent elements. This step reduces the complexity of the problem to its simplest form and makes it easier to be solved. This technique has been implemented in various fields of study (Ranjan, Pai et al. 1993; Guler and Menendez

2014; Siddiqui, AlOthman et al. 2017). In (Nam, Kang et al. 2012; Xiu and Liao 2014; Iurinic, Orozco et al. 2015), this technique was proposed to locate the HIF fault in the distribution network.

Synchronized zero-sequence voltage and current signals measured at the faulted node were used by (Nam, Kang et al. 2012) to calculate the fault distance. Whereas in (Xiu and Liao 2014), the fault location was estimated based on the product of the bus impedance matrix and current injected at the substation. Least square estimator based approach was proposed by (Ferraz, Iurinic et al. 2014) to locate the occurrence of HIF for short transmission lines. In (Iurinic, Orozco et al. 2015) the estimation of fault location based on parameter estimation approach using the derivation equation is used to calculate the fault distance.

2.4.3.4 Knowledge-based Technique

There are several types of knowledge-based technique have been proposed to determine the HIF locations such as Artificial Neural Network (ANN) (Jensen, Munk et al. 1998; Bretas, Moreto et al. 2006; Moshtagh and Aggarwal 2006; Baqui, Zamora et al. 2011; Zayandehroodi, Mohamed et al. 2012; Zayandehroodi, Mohamed et al. 2013; Aslan and Yağan 2016), Fuzzy Logic System (FLS) (Chunju, Li et al. 2007; Rafinia and Moshtagh 2014), Adaptive Neuro-Fuzzy Inference System (ANFIS) (Aziz, Hassan et al. 2012; Barakat, Eteiba et al. 2014), Support Vector Machine (SVM) (Thukaram, Khincha et al. 2005; Ye, You et al. 2014; Hong and Huang 2015) and Core Vector Regression (CVR) (Khorramdel, Marzooghi et al. 2014).

The main advantage of this technique is its capability to generalize the output through the learning process. Besides that, it can give fast and accurate results. However, this technique requires a large number of data to be trained and tested to produce a reliable network reference. Thus, the accuracy of this technique relies on the accuracy and validity

of the input data. Furthermore, the networks have to be retrained if there are changes in the system topology.

2.5 Wavelet Transform

2.5.1 Introduction

Wavelet transforms is a wave-like oscillation with an amplitude that starts from zero, increases and decreases in a certain amount of amplitude and goes back to zero amplitude within a limited duration, which has an average value of zero. Generally, the wavelet transform is a mathematical function that must satisfy certain mathematical requirements to represent the signal in time and frequency domains.

The fundamental idea behind the wavelet transform is to analyze the original signal according to the scale (by dilation and translation). It can be assumed as cutting the signal of interest into various lengths with the same size of the samples and then analyze each sample separately. For example, if we sample a signal with a small "window" (small dilation) and move the window along the signal (translation), we would notice the distinct features of the signal. Similarly, if we sample a signal with a large "window", vague features of the signal will be obtained. Therefore, by varying the size of the "window" and shifting the "window" across the signal, more significant and various features of the signal can be gained (Wavelet Transform).

Wavelet transform allows exceptional localization in both time and frequency domains via translation and dilation processes of the mother wavelet respectively. Figure 2.3 shows the pattern of the dilated Gaussian type of mother wavelet which is scaled by the parameter *a*. The translation and dilation operations are performed to calculate the wavelet coefficients that represent the correlation between the signal of interest and mother wavelet. Wavelet coefficients are calculated for each signal segment, giving a

time-scale function relating the correlation between wavelet and signal. Figure 2.4 shows the process of translation and dilation of mother wavelet on the signal.

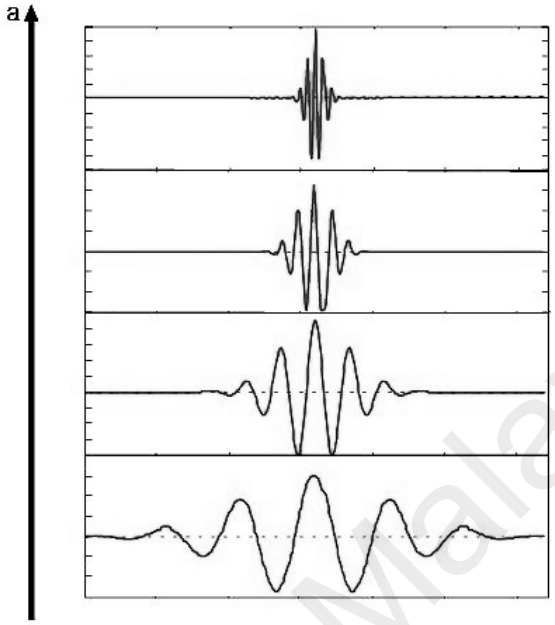

Figure 2.5: Dilation patterns of Gaussian wavelet

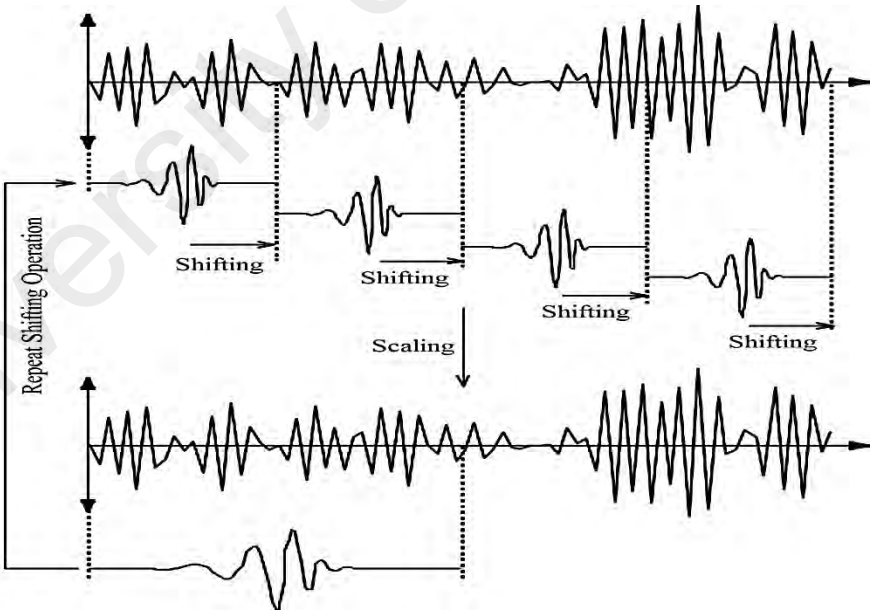

Figure 2.6: Translation and dilation of mother wavelet

Wavelet transform was widely used in various fields of research such as astronomy, signal and image processing, magnetic resonance imaging and pure mathematics applications such as solving partial differential equations. Nowadays, the application of

wavelet transform has been drastically evolving in solving the power system issues such as fault detection (Akorede and Katende 2010; Sarlak and Shahrtash 2011), power system dynamic (Wenzhong and Jiaxin 2011; Avdakovic, Nuhanovic et al. 2012), incipient fault analysis (Sidhu and Zhihan 2010) and power quality issue (Dilokratanatrakool, Na Ayudhya et al. 2003).

2.5.2 Variety of Wavelet Transforms

Wavelet transforms can be classified into two:

a) Continuous Wavelet Transform (CWT)

b) Discrete Wavelet Transform (DWT)

In CWT analysis, the wavelet coefficients are calculated based on the convolution between the input data sequence with the set of the function generated by the mother wavelet. Whereas in the DWT analysis, the continuous signal will be digitized first before the matrix of digitized data is multiplied with the matrix of discrete mother wavelets. Figure 2.5 shows the simplified operation of CWT and DWT.

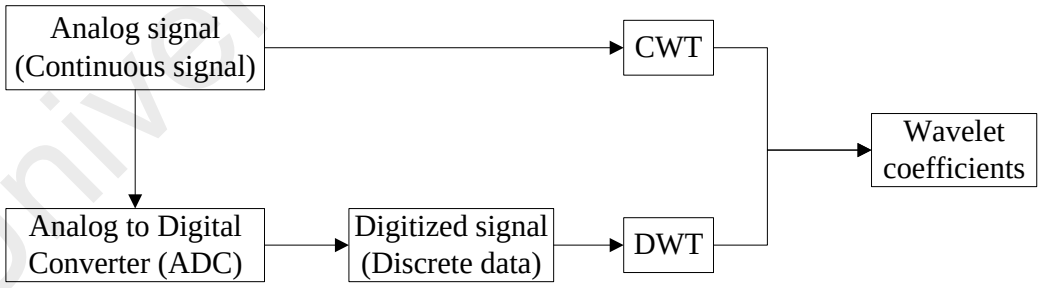

Figure 2.7: CWT and DWT operations

DWT can be further expanded into two:

- Multi-Resolution Analysis-Discrete Wavelet Transform (MRA-DWT)
- Spanning Tree-Discrete Wavelet Transform (ST-DWT)

This expanded DWT gives a better signal representation and analysis. The operations and uniqueness of each type of wavelet transform will be explained briefly in the next subsection.

2.5.3 Continuous Wavelet Transforms (CWT)

In CWT analysis, it uses the inner product of the signal, *f (t)* to measure the correlation between the signal of interest and mother wavelet, $\psi(t)$. The correlation can be measured based on the wavelet coefficient value. If the wavelet coefficient value is equal to one, it signifies a perfect matching between the signal and mother wavelet. The wavelet coefficient can be derived as below (2.2):

$$C(a,b; f(t),\psi(t)) = \int_{-\infty}^{\infty} f(t)\frac{1}{\sqrt{a}}\psi*\left(\frac{t-b}{a}\right)dt \qquad 2.2$$

where the parameter *a* and *b* represent the scale (dilation) and position (translation) values respectively and " $*$ " denotes the complex conjugate. *C (a,b)* is the continuous wavelet transform coefficients that indicate the correlation between the signal and mother wavelet.

There are four basic steps to construct the CWT analysis:

1) Correlate the selected mother wavelet with a section of the original signal.
2) Calculate the coefficient, *C* to observe the correlation between the input and wavelet signals.

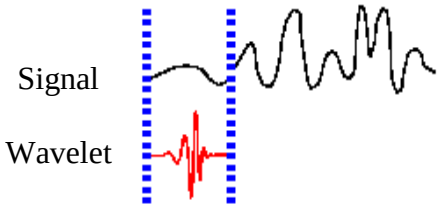

C = 0.0102

3) Step 1 and 2 are repeated by shifting the wavelet signal until it covers the entire input signal.

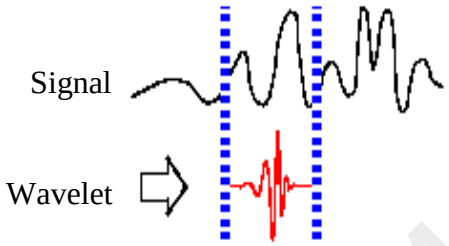

4) Step 1 to 3 are repeated by increasing the scale value of mother wavelet.

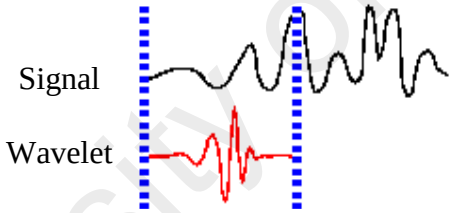

C = 0.2247

CWT has been implemented to detect and analyze power quality disturbance in power system in (Poisson, Rioual et al. 2000). In (Tria, Ovarlez et al. 2007; Briassouli, Matsiki et al. 2010), CWT was used for image processing analysis. Besides that, CWT was also employed in the medical field as reported in (Cnockaert, Migeotte et al. 2008; Hulzink, Konijnenburg et al. 2011) for diagnosis purposes.

2.5.4 Discrete Wavelet Transforms (DWT)

In DWT analysis, the original input signal is decomposed into high-frequency and low-frequency components through two complementary filters which are high-pass and low-pass filters respectively as shown in Figure 2.6. The high-frequency component is a low-

scale decomposition, which also called as details coefficients, *cD*. Whereas the low-frequency components is a high-scale decomposition, which also known as approximations coefficients, *cA* (Wavelet Transform). Generally, the low-frequency components are the crucial part as it gives the signal identity. Whereas, the high-frequency components are conveyed of flavor or nuance in the signal.

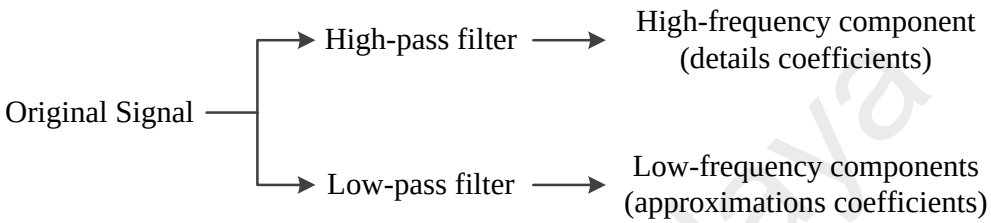

Figure 2.8: DWT decomposition process

DWT has been widely used in many applications and fields such as in signal, audio and video analysis and power system research. In (Nath, Sinha et al. 2012), power quality issue related to the location of harmonic pollution source is identified using the DWT. Detection and classification of fault in a transmission system using DWT had been proposed in (Martin and Aguado 2003; Bhalja and Maheshwari 2008). Besides that, DWT has been utilized in (Avdakovic, Nuhanovic et al. 2012) to analyze and locate the lower frequency oscillations during the power system dynamic event.

2.5.5 Multi-Resolution Analysis-Discrete Wavelet Transform (MRA-DWT)

MRA-DWT is the extension to DWT in which the decomposition process further continues with the successive approximation coefficients. MRA-DWT decomposition process will split the original signal, *S* into different levels of decomposition as shown in Figure 2.7. The main purpose of the MRA-DWT analysis is to reduce the size of the signal, but significantly maintains the similarity and the shape of the original signal. It can be obtained by eliminating the unnecessary noise signal that embedded in the original signal.

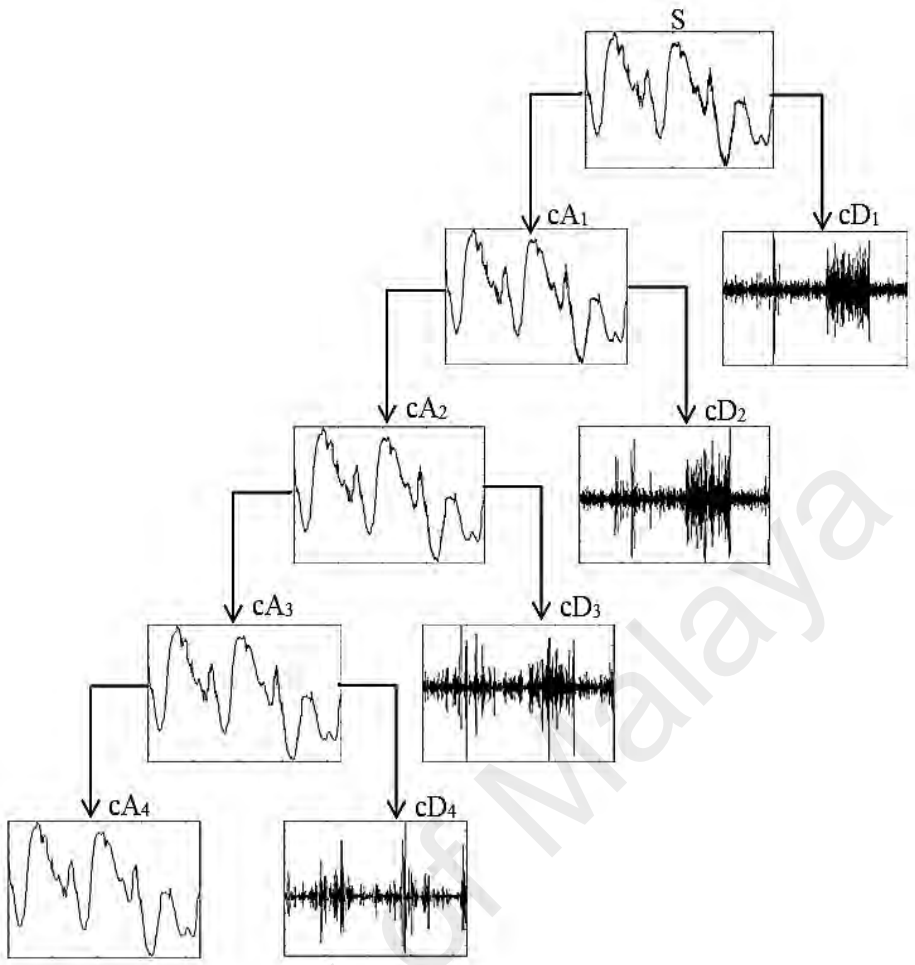

Figure 2.9: MRA-DWT operation

Recently, MRA-DWT has been applied in many power system problems such as power system protection, power system analysis, power quality detection and classification. In (Gaouda, Salama et al. 1999; S. Nath 2009), MRA-DWT was used for power quality disturbance detection and classification. Whereas in (Chanda, Kishore et al. 2003), MRA-DWT was used to determine the fault location on transmission lines.

2.5.6 Spanning Tree-Discrete Wavelet Transform (ST-DWT)

ST-DWT is a generalization of wavelet decomposition process, which provides a wide range of possibilities for signal analysis. ST-DWT is similar to MRA-DWT except that both successive approximations and details coefficients are further decomposed into different levels of decomposition as shown in Figure 2.8. The ST-DWT analysis offers

superior resolution and clarification about the signal, which cannot be obtained from other types of the wavelet transform.

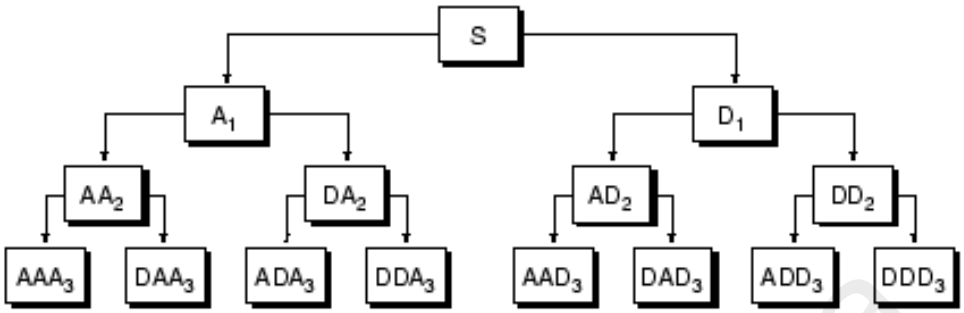

Figure 2.10: ST-DWT operation

2.5.7 Advantages of Wavelet Transform

The main advantage of wavelet transforms is its property of irregularity in shape, which make it a well-suited tool for analyzing signals with a discontinuity, sharp changes and impulse functions. Besides that, the compatibility-supported feature enables the time localization in a signal to be determined. Other than that, WT has the capability to perform a local analysis, which is to analyze a localized area of a larger signal. For instance, a small discontinuity in the signal and the exact moment of the event can be identified. Furthermore, WT can give a complete and efficient spectral analysis without losing any valuable information. WT analysis has the capability to reveal the data features, such as trends, breakdown points, discontinuities in higher derivatives and self-similarity. WT is also capable to partition the energy signal at different frequency bands. Thus, give an indication of the frequency content for the disturbance signal. Last but not least, WT is always used in compressing or de-noising image without significant degradation.

2.6 Optimization Techniques

2.6.1 Introduction

An optimization technique is an approach to determine the optimal solution with the cheapest and high performance under various constraints. In this section, the difference between heuristics and meta-heuristics technique is explained. Then, the implementation and mechanism of grey wolf optimization (GWO) are described in details. Finally, the advantages of the meta-heuristics technique are discussed.

2.6.2 Meta-heuristics Technique

An optimization technique can be classified into heuristics and meta-heuristics techniques. The main difference between these two techniques is heuristics are very specific and problem-dependent, whereas meta-heuristics are problem-independent. The main disadvantage of the heuristic technique is its easily stuck in local optima, thus fail to get the global optimum solution, which can be overcome by meta-heuristic technique. In addition, meta-heuristic technique even allows a short-term deterioration of the local solution as a return to provide them with a more thorough exploration to solution space and consequently provide a better solution which sometimes nearly to the global solution.

The meta-heuristic technique can be divided into three categories which are evolutionary strategies (ES), physics-based and swarm intelligence (SI) techniques. ES technique is inspired by evolution concepts in nature. Genetic algorithm (GA) and EP are the most popular ES technique used to provide the optimal solution in many applications. Whereas physics-based technique is inspired based on impersonation of physic rules such as ray casting, gravitational force, inertia force and electromagnetic force. The mechanism of this technique is through a random set of search agents that communicate and move throughout the search space according to the physic rules. Last but not least, the SI technique, which is inspired by the social behavior of swarms, flocks, herds or

schools of creatures in nature. The mechanism of the search agent for this technique is based on the simulated collective and social intelligence of the creatures. The most popular algorithm in this technique is particle swarm optimization (PSO) which is inspired by the social behavior of the bird flocking. One of the most recent and promising SI technique is grey wolf optimization (GWO) that is inspired by the leadership hierarchy of the grey wolves.

2.6.3 Grey Wolf Optimization (GWO)

GWO has been proposed by (Mirjalili, Mirjalili et al. 2014) which is inspired by the hunting mechanism of the grey wolves in nature and its leadership hierarchy. The leadership hierarchy of grey wolves consists of four levels known as alpha (α), beta (β), delta (δ) and omega (ω) as shown in Figure 2.9. (Muro, Escobedo et al. 2011) explains the hunting mechanism of the grey wolves, which consists of searching, encircling and attacking the prey. At first, the wolves will track the location of the prey, chase them and finally will try to approach the prey at a safe distance as shown in Figure 2.10(A). Once the group of wolves has approached the prey, they will pursue, encircle and harass the prey until the prey stop from moving as shown in Figure 2.10(B)–(D). Finally, the wolves will attack the prey when the prey is unable doing anything and stop stationary as shown in Figure 2.10(E).

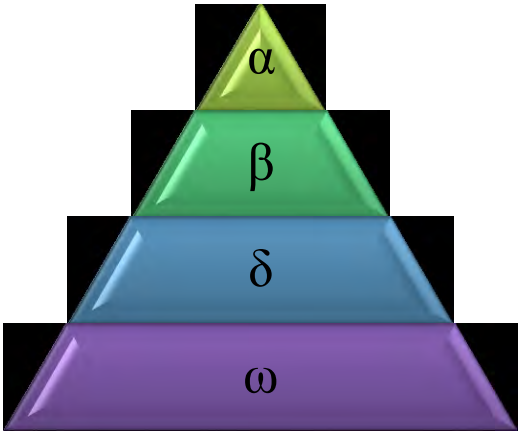

Figure 2.11: Leadership hierarchy of grey wolf

Figure 2.12: Hunting behavior of the wolves (Muro, Escobedo et al. 2011)

The GWO algorithm and its implementation process can be simplified as follows:

Step 1: Social hierarchy

Initially, it is important to describe the social hierarchy of the wolves in order to design the GWO algorithm, which consists of α, β, δ and ω. The α is considered as the fittest solution followed by the β and δ as the second and the third best solutions respectively. Whereas the ω belongs to the rest of the candidate solutions and it will follow the other three wolves (α, β, δ) when optimizing the solution.

Step 2: Hunting

It is noticed that the grey wolves have the ability to identify the potential location of the prey. Usually, the hunting process is initiated by the alpha wolf and occasionally will be participated by the beta and delta wolves. To mathematically model this hunting behavior, it is assumed that the α, β and δ wolves know the potential location of the prey. As such, these three best solutions are first saved and accordingly assist the other search agents, including the omegas to update their current position with respect to the position of the best search agents. Thus, the mathematical equations can be derived as follows:

$$\vec{D}_{\alpha} = \left| \vec{C}_1 \cdot \vec{X}_{\alpha} - \vec{X} \right|$$

$$\vec{D}_{\beta} = \left| \vec{C}_2 \cdot \vec{X}_{\beta} - \vec{X} \right|$$

$$\vec{D}_{\delta} = \left| \vec{C}_3 \cdot \vec{X}_{\delta} - \vec{X} \right|$$

$$\vec{X}_1 = \vec{X}_{\alpha} - \vec{A}_1 \cdot \vec{D}_{\alpha}$$

$$\vec{X}_2 = \vec{X}_{\beta} - \vec{A}_2 \cdot \vec{D}_{\beta}$$

$$\vec{X}_3 = \vec{X}_{\delta} - \vec{A}_3 \cdot \vec{D}_{\delta}$$

$$\overrightarrow{X}(t+1) = \frac{\overrightarrow{X_1} + \overrightarrow{X_2} + \overrightarrow{X_3}}{3} \qquad 2.3$$

where

$\vec{D}_{\alpha}$ = distance between the alpha wolf with each wolf

$\vec{D}_{\beta}$ = distance between the beta wolf with each wolf

$\vec{D}_{\delta}$ = distance between the delta wolf with each wolf

$\vec{X}(t+1)$ = position vector for each wolf with respect to position of α, β and δ

Step 3: Encircling prey

The nature of the wolves will encircle their prey during the hunting. In order to describe this behavior, the mathematical equation is derived as follows:

$$\vec{C} = 2\vec{r}_2$$

$$\vec{A} = \vec{a}(2\vec{r}_1 - 1)$$

$$\vec{D} = \left| \vec{C} \cdot \vec{X}_p(t) - \vec{X}(t) \right|$$

$$\overrightarrow{X}(t+1) = \overrightarrow{X_p}(t) - \vec{A} \bullet \vec{D} \qquad 2.4$$

where

t = current iteration

$\vec{A}$ and $\vec{C}$ = coefficient vectors

$\vec{a}$ = linearly decrease from 2 to 0 over the course of iterations

r_1 and r_2 = random vectors in [0 1]

$\vec{X}_p$ = position vector of the prey

$\vec{X}$ = position vector of the grey wolves

$\vec{D}$ = distance between the prey and the wolves

Based on these equations, it can be observed that the current position of the grey wolves can be updated in any random location according to the position of the prey.

Step 4: Attacking prey (exploitation)

After the prey being hunted and encircled, it is the time for the grey wolves start to attack the immobile prey. To model this attacking process, the value of $\vec{a}$ and $\vec{A}$ is decreasing indicate that the wolves are approaching near to the prey. The attack towards the prey is triggered if the value of $|\vec{A}| < 1$.

Step 5: Search for prey (exploration)

It is important to be noted that in this proposed GWO algorithm, it is susceptible to stagnation in local solutions. Therefore, it is required for the capability to explore. As such, to describe the divergence of the wolves from the prey, the random value of $\vec{A}$ is set either greater than 1 or lower than -1 to accommodate the search agent thus provide the global search. Concurrently, by setting the value of $|\vec{A}| > 1$, it does not just diverge the prey from the wolves, but also allowing the wolves to search for the better prey. Besides that, vector $\vec{C}$ also contributes the divergence or convergence of the wolves from the prey. The vector $\vec{C}$ contains a random value in between [0 2] which responsible to

provide the random weight for prey to stochastically emphasize or deemphasize the effect of prey in defining the distance. Apart from diverging the prey, vector $\vec{C}$ also works as the obstacle effect, which prevents the wolves from approaching the prey easily and quickly. This is due to that fact that there is always a hindrance in nature during the hunting process. As such, it gives difficulties by making the wolves get harder or farther to catch the prey or vice versa.

All the above steps can be summarized as follows. Initially, the process is started by creating a random population of grey wolves (candidate solutions) which consists of α, β, δ and ω. These candidate solutions will estimate and update their distance from the prey for each iteration. Every iteration, the value of parameter *a* will decreases from 2 to 0 in order to emphasize the exploitation and exploration process. The candidate solutions can be either diverge or converge with respect to the value of $\vec{A}$. Finally, the iteration is terminated if the optimal solution is achieved or reach the maximum number of iterations.

2.6.4 Advantages of Meta-heuristics Technique

Recently, various meta-heuristics techniques have been applied in different fields of studies. These techniques become popular due to its outstanding performance to provide the optimal solution. The advantages of meta-heuristics technique can be summarized into 4 main points, which are the flexibility, simplicity, local optima avoidance and derivation-free mechanism as follows:

1) Flexibility

   The capability of meta-heuristics to be implemented in different kind of problems without the need for special adjustment in the algorithm structure. Thus, it can be assumed as the black box. As such, it only important to know how to relate the input and output data with the application of meta-heuristics technique.

2) Simplicity

The mechanism of this technique usually gets inspired by a very simple concept, which is related to physic phenomena, animal's behaviors or evolutionary concepts. This simplicity allows a new meta-heuristics technique to be proposed, which the inspiration can be obtained through different natural concepts, hybridized different meta-heuristic techniques and modified or improve the current meta-heuristics technique. Besides that, this simplicity factor makes it easier and interesting to be learned and to be implemented in many applications.

3) Local optima avoidance

Meta-heuristics technique has the capability to avoid the local optima. This is due to the fact that, the meta-heuristics technique utilized stochastic behavior in nature to solve the problem. This gives meta-heuristics an advantage to search for a broad area of the search space and thus the capability to avoid stagnation in the local solutions.

4) Derivation-free mechanism

Last but not least, meta-heuristics technique optimizes the problem stochastically with a random solution at first. Therefore, it is not required for the sophisticated or complex formulation for the derivative of the search space in order to obtain the optimal solution. This characteristic makes meta-heuristics highly recommended to solve the real problems with unknown derivative information.

2.7 Artificial Neural Network

2.7.1 Introduction

The development of ANN gets an inspiration from the neural structure of the brain that consists of millions of cells. Each of these cells is interconnected to each other and provide the ability to analyze, remember and think. As such, the concept of ANN is developed in which the cells are introduced as neurons. ANN is used for prediction, forecasting and classification (Raza, Mokhlis et al. 2016). Figure 2.11 shows a typical diagram of ANN architecture consisting of the input layer, neurons in hidden layer and output layer.

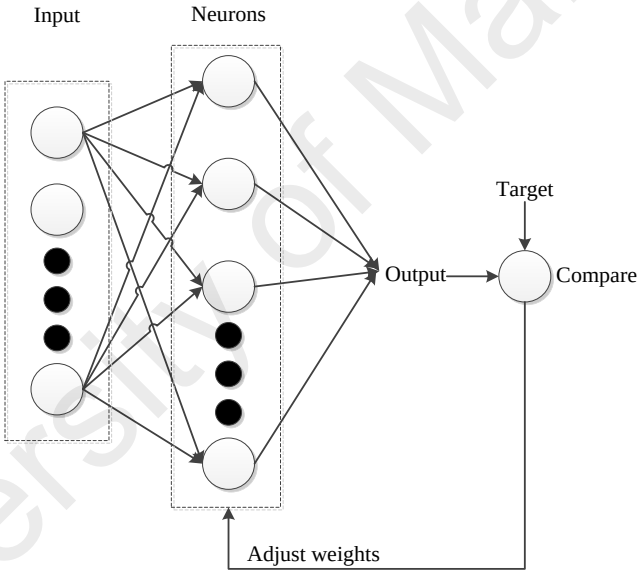

Figure 2.13: Basic artificial neural network architecture

During the training process, the input data will be trained and weighted by the neurons. Then, the estimated output during the training process will be compared with the required target based on the minimum root mean square (*rms*) error. The process is repeated by adjusting the weights inside the neurons until the estimated output is matched with the required target or minimum *rms* error is achieved. The main advantage of ANN is its ability to solve the random and non-linear problem.

2.7.2 Effect of ANN Variables

There are several variables that can influence the effectiveness of ANN such as momentum constant, learning rate, number of hidden layers, number of neurons in hidden layers and learning technique.

Momentum constant, *mc* is responsible to ensure that the system is not converging to local minima by adding the previous weight of fraction momentum to the current weight. Besides that, the *mc* assists in accelerating the training process by increasing the convergence speed of the system. If the value of *mc* is set too high, it can cause the risk of minima overshooting, thus making the system unstable. However, if the *mc* value is set too low, the training process will become slower because the system cannot avoid the local minima.

Learning rate, *lr* is used to control the size of weight and bias for the neurons. By adjusting the value of *lr*, it can accelerate the convergence of training process. If the value of *lr* is set too low, it will affect the speed of network learning, thus slow down the training process. However, if the value is set too high, it will cause the weight and objective function to diverge. The value of *lr* can be adjusted based on the value of the sum-squared error (SSE) over several consequent epochs. If the value of SSE is alternating then the value of *lr* should be decreased. Otherwise, the value of *lr* can be increased to expedite the convergence of training process.

Hidden layer is located in between the input and output layers. The number of hidden layers can be more than one depending on the complexity of the input data. Usually, the first hidden layer is involved with a linear transformation. Whereas in the second hidden layer, a squashing nonlinearity is applied. However, another function such as computing logical function, inverse transfer function and statistical function can be selected.

Basically, inside the hidden layer, there are a number of neurons in which a specific computation is involved that will mapping the input data with respect to the required target. There is no limit to the number of neurons in the hidden layer can be utilized. However, if too many neurons are applied to the hidden layer, it can cause an over-fitting. Due to over-fitting, ANN loses its ability to predict (generalize) the input data thus affect the accuracy. However, if a small number of neurons are utilized, it may give difficulties to the ANN to learn the input data. Insufficient learning will lead to ANN failure.

There are several types of learning algorithm such as Levenberg-Marquardt backpropagation, Bayesian regularization and others. Each of these learning algorithms has their own advantages and disadvantages, which can be determined based on many aspects such as the type and number of input data, the complexity of the problem, the number of weight and biases in the network. Besides that, it is also affected by the purpose of the training either for pattern recognition or function approximation.

2.7.3 Training, Validation and Testing Data for ANN Training

It is noted that there are 3 sets of data used during the ANN training process, which are training, validation and testing data. A training set of data is used to adjust the weights inside the neurons so that the fitting can be achieved between the input data and required target. However, an overfitting may occur during the ANN training process, thus the network loss its generalization. Consequently, the ANN cannot perform well when a new set of testing data are presented.

In order to avoid the ANN from overfitting, a validation set of data are required. Basically, a validation set of data are responsible to ensure that the network is capable to generalize the training set of data. The generalization is important to ensure that when the new data, which are not involved in the training process can be successfully identified. Besides that, a validation set can be used as the stopping criterion for the ANN training

process. It is important to be noted that when the validation set of data are utilized, the network weight is not adjusted. However, the process can affect indirectly the weight configuration by monitoring the obtained error values from the training and validation sets. If the obtained error is reduced for the validation set, it indicates that the accuracy of the training set is increased. However, if the obtained error is increased or remains the same for several epochs, it indicates that the ANN has been overfitted. Thus, the ANN training process has to be stopped immediately.

Finally, after the ANN training process is terminated, the test set of data are applied to the network file that is obtained from the training process. Then the errors are calculated for this test set. This error is a representative of the possible error, which can be obtained when the new set of data is tested. It also indicates the predictive capability of the network file. If the obtained error from the test set is small, thus it indicates that the network file has a powerful predictive capability.

Usually, the total number of data to be allocated for each set of data are 70%, 20% and 10% for training, validation and testing sets respectively. For this purpose, the samples used for each set will be selected randomly. As such, the accuracy of ANN can be affected by the samples used for the training, validation and testing.

2.8 Conclusion

Many methods have been proposed by researchers to tackle the complexity of detecting and locating HIF in a distribution system. Each of the methods has its merits and limitations. Mechanical HIF detection methods utilize mechanical devices that require installation and maintenance cost. Therefore, they are expensive and only applicable for overhead distribution network and transmission lines. Whereas electrical HIF detection methods comprise a feature extractor and a classifier. They utilize voltage and current signals obtained from the measurement device.

Popular electrical HIF localization techniques include network topology, travelling wave, analytical formulation and knowledge-based techniques. All the proposed techniques have the potential to estimate the location of HIF successfully. However, each of the techniques possesses drawbacks that limit its application and effectiveness. Therefore, a reliable technique that is accurate, cost-effective, efficient and practical to be implemented in a radial distribution system with lateral branches is needed.

Subsequently, the wavelet transform, grey wolf optimization technique and artificial neural network were explained. Firstly, the basic concept and types of wavelet transform had been explained. Two different types of wavelet transform which are CWT and DWT had been discussed briefly. It was followed by MRA-DWT and ST-DWT which are the successive types of DWT. Finally, the advantages of wavelet transform had been highlighted.

Secondly, the basic concept of optimization technique was studied. The difference between heuristics and meta-heuristics techniques was discussed. In a meta-heuristics technique, the GWO was explained in details. The advantages of the meta-heuristics technique were highlighted to explain it significance in most of the studies.

Lastly, the ANN was explained briefly as one of the most popular knowledge-based technique. Besides that, the effects of ANN variables toward the accuracy of the results were studied. The relationship between the training, validation and testing data during the training process were explained.

CHAPTER 3: METHODOLOGY OF PROPOSED TECHNIQUE FOR HIGH IMPEDANCE FAULT DETECTION AND LOCALIZATION

3.1 Introduction

In this research, it is our best interest to detect and locate the occurrence of high impedance fault (HIF) in the distribution system. In this chapter, the investigation is divided into three main phases. In the first phase, the occurrence of HIF is detected and differentiated from non-HIF events. Subsequently, in the second phase, the location of the HIF is identified. In the third phase, the estimated fault distance is enhanced by identifying the faulty section. In this chapter, the three main phases of the investigation are presented as follows:

a) Proposed technique for high impedance fault detection and identification
b) Proposed method for high impedance fault localization
c) Proposed enhanced fault location method

3.2 Proposed Technique for High Impedance Fault Detection and Identification

The phase displacement computation (PDC) is proposed to detect and identify HIF from non-HIF events. The different types of non-HIF events considered in this analysis include capacitor switching, load switching and motor starting. The three-phase voltage waveforms measured at the main substation is analyzed to detect and identify HIF from non-HIF events. The proposed PDC method will calculate the phase angle difference between the measured and reference voltage waveforms. The resultant PDC will then be used by detection index algorithm to detect the occurrence of a disturbance while another identification index algorithm will identify the occurrence of HIF from the various types of disturbances. Details of the above proposed algorithms are explained in the following subsection.

3.2.1 Phase Displacement Computation (PDC) Method

When a fault occurs in the network, there will be a slight distortion in the voltage waveform. This distortion can be observed clearly through the differences between the reference and faulted voltage waveforms in Figure 3.1 and Figure 3.2. Figure 3.1 shows an example of a few cycles of reference and faulted voltage waveforms when HIF occurs in the network. While Figure 3.2 shows an enlarged view of the circled part in Figure 3.1, showing the onset of fault.

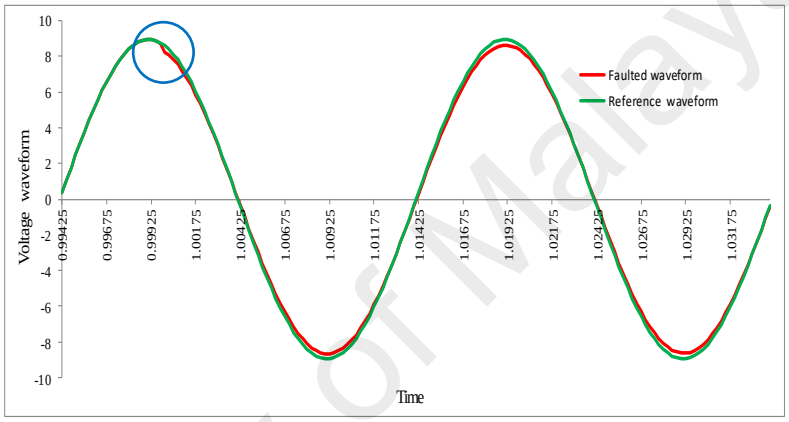

Figure 3.1: Comparison between faulted and reference voltage waveform

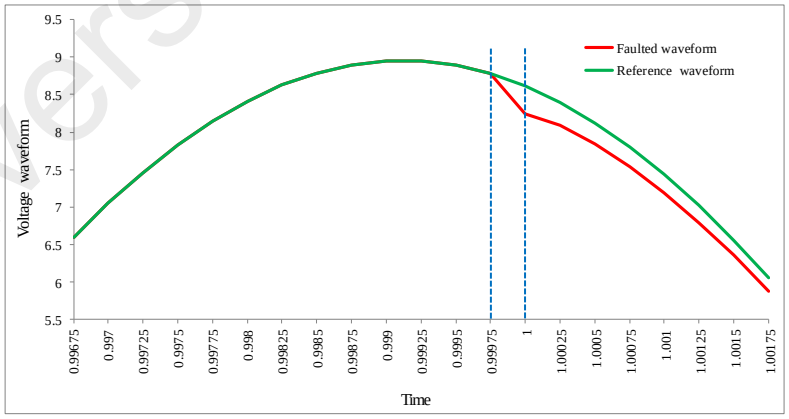

Figure 3.2: Enlarged view of the faulted and reference voltages

The distortion of the waveform in Figure 3.2 can be quantified using the PDC method as follows.

Table 3.1: Voltage magnitude

Time (s)	Faulted waveform (V)	Reference waveform (V)	Distortion = | Faulted - Reference | (V)
0.99925	8.948	8.948	0.000
0.9995	8.891	8.891	0.000
0.99975	8.779	8.779	0.000
1	**8.250**	**8.613**	**0.363**
1.00025	8.085	8.394	0.309
1.0005	7.835	8.124	0.289
1.00075	7.533	7.803	0.270

Table 3.1 shows the voltage magnitude before and after the fault occurrence. The fault is applied to the system at *t=1s*. As shown in the table, the voltage is distorted after the fault is applied. Figure 3.3 shows the plots of the faulted and reference waveforms just before and after the fault from Table 3.1. As shown in the figure, the voltage waveform starts to deviate at *t=1s*. This distortion can be represented by the PDC. The PDC will calculate the time difference between the faulted and reference waveforms in which the voltage magnitude for both waveforms are the same. As such, the time (t_{new}) at which the faulted waveform has the same magnitude as the reference waveform will first be computed.

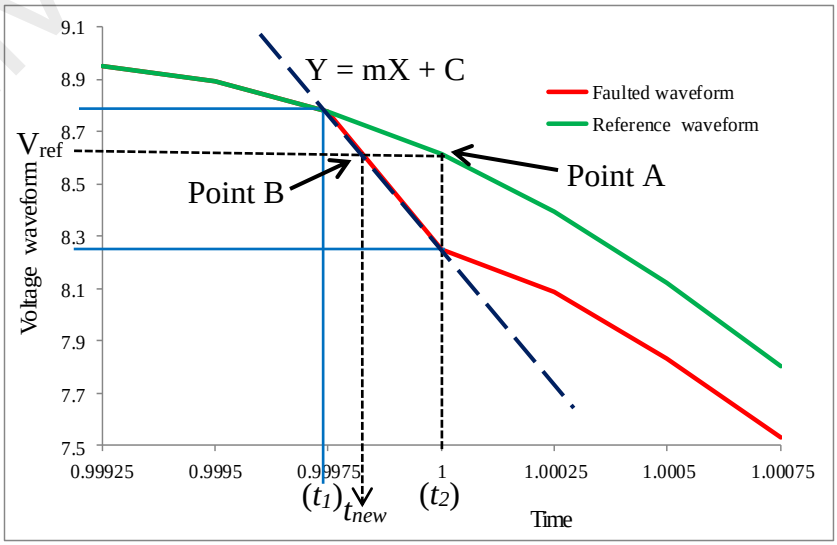

Figure 3.3: Illustration of the faulted and reference waveforms

Initially, the algorithm will continuously track for differences in magnitude between the faulted and reference voltage waveforms throughout the samples. Once the difference in magnitude was detected at t_2, the magnitude of the reference waveform at Point A will be traced to the same magnitude of the faulted waveform at Point B to obtain t_{new}. The computation of t_{new} is based on the assumption that consecutive samples in the voltage waveforms are connected through a straight line. As such, t_{new} is calculated from the straight line equation as follows.

$$Y = mX + C \tag{3.1}$$

where

X = time = t_{new}

Y = voltage magnitude = V_{ref}

m = gradient of the straight line

C = y-axis intercept of the straight line.

Therefore,

$$t_{new} = \frac{V_{ref} - C}{m} \tag{3.2}$$

Finally, the phase angle difference, $\Delta\Phi_{diff}$ between both waveforms can be calculated as follows:

$$\Delta\Phi_{diff} = \frac{|t_{new} - t_2|}{T} \times 360^{\circ} \tag{3.3}$$

where

T = time over one full cycle = 1/f

f = frequency of the system = 50Hertz

3.2.2 Phase Displacement Computation for HIF Detection and Identification

Figure 3.4 shows the flowchart of the proposed HIF detection and identification method. After measuring the three-phase voltage waveforms, the phase displacement is calculated using the time difference between the faulted and reference voltage waveforms. Then, two processes consisting of moving window and grouping window are conducted to obtain the smooth pattern of phase displacement. Finally, the detection index and identification index algorithms are executed to detect the anomaly and then identify the HIF from the various anomalies.

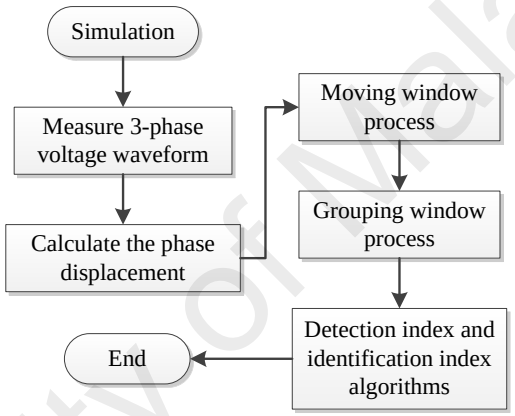

Figure 3.4: Flowchart of the proposed HIF detection and identification method

3.2.3 Phase Displacement Computation Process

Figure 3.5 to Figure 3.8 show the process of PDC method until the final pattern of PDC is obtained. Figure 3.5 shows an example of absolute PDC obtained using Eq. 3.3 during the occurrence of HIF event. The phase displacement between the reference and faulted waveforms is constantly calculated even before and after the event. It can be observed that the absolute PDC is constantly zero before the event, but starts to fluctuate after the event. The fluctuation of the absolute PDC value indicates an anomaly that has occurred in the system. Figures 3.5(a)-(c) show the absolute PDC of the voltage waveforms for phases A, B and C respectively. While Figure 3.5(d) shows the sum of absolute PDC of the three phases.

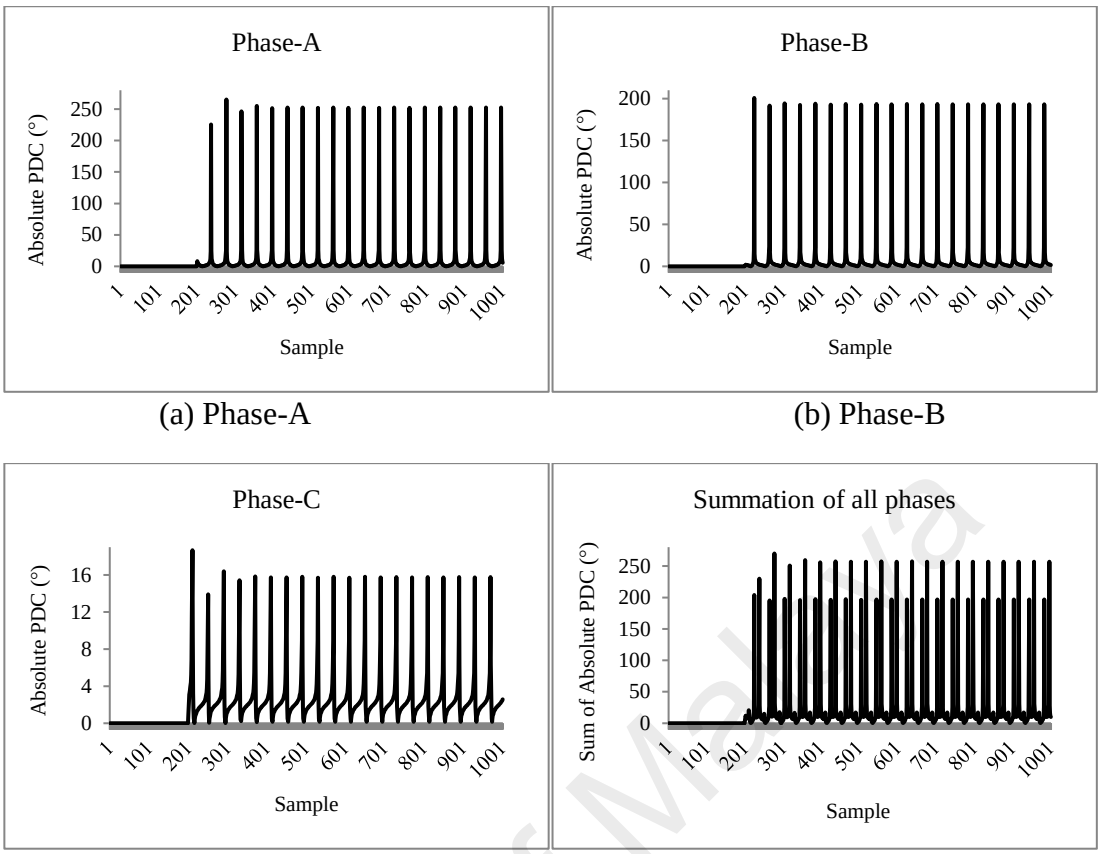

(a) Phase-A (b) Phase-B

(c) Phase-C (d) Summation for all phases

Figure 3.5: Absolute PDC during HIF event

Subsequently, the obtained sum of absolute PDC data points in Figure 3.5(d) is summed by a moving window where each window contains 80 samples (one full cycle). The position of the window is shifted point by point consecutively as illustrated in Figure 3.6. The result of the moving window process on the sum of absolute PDC is known as moving window PDC and it is displayed in Figure 3.7.

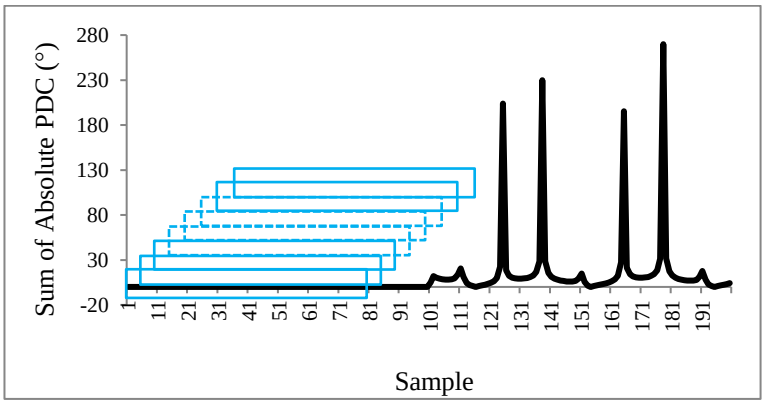

Figure 3.6: Moving window process on the sum of absolute PDC

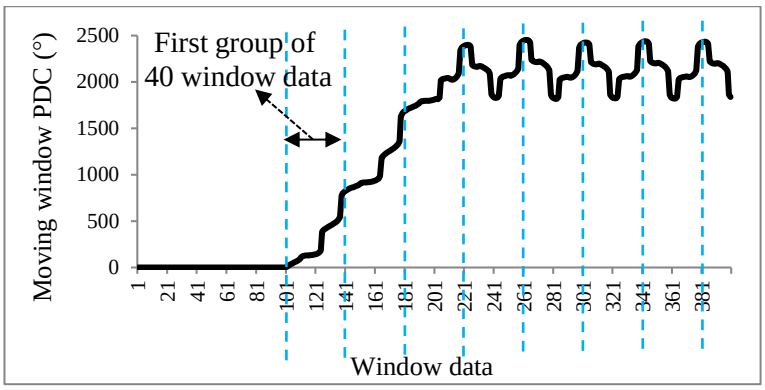

Figure 3.7: Grouping window process on moving window PDC

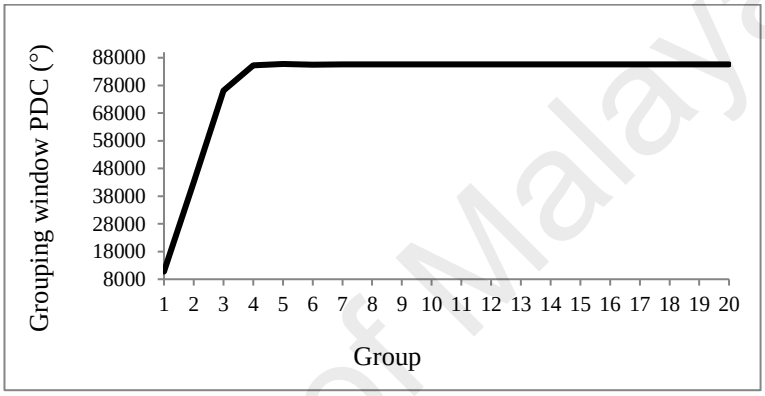

Figure 3.8: Smoothed PDC

As observed in Figure 3.7, the obtained moving window PDC is oscillatory. Thus, another grouping window is applied to smoothen the data further. The grouping window process is initiated if there is a significant change in moving window PDC. In this step, every 40 consecutive data are summed and the result is known as smoothed PDC as shown in Figure 3.8. Based on the pattern of smoothed PDC, the occurrence of HIF event is identified.

3.2.4 High Impedance Fault Detection and Identification Index

To simplify the detection and identification of HIF and non-HIF events, 2 indices are developed. The first is the detection index (*D-index*) which is used to detect the occurrence of an event in the network. The second is the identification index (*Id-index*) which is used to identify HIF from non-HIF events.

Figure 3.9 shows an example of smoothed PDC due to the occurrence of load switching event in the system. The increment in smoothed PDC value indicates that an event has occurred in the system. As such, the calculation of *D-index* is initiated. At first, the difference between two consecutive smoothed PDC data, *G(1) – G(2),* is calculated. If the difference is negative, the value is stored and the difference between the next two data, *G(2) – G(3),* is calculated. If it is still negative, the value is stored and the subtraction step is carried out for *G(3) – G(4).* This step is repeated until a positive difference is obtained. Suppose the subtraction step is repeated for *n* times before the first positive difference is obtained, then, the *D-index* is calculated as follows:

$$D-index=\frac{\sum_{i=1}^{n} G(i)-G(i+1)}{n} \qquad 3.4$$

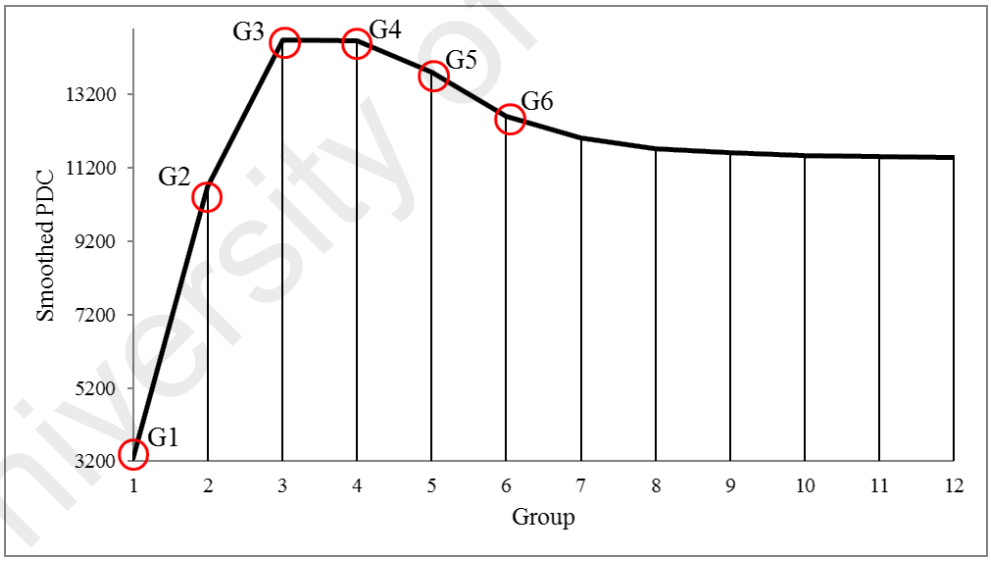

Figure 3.9: Smoothed PDC of a load switching event

Besides detecting the event occurrence in the system, the *D-index* is also used to differentiate the event with the steady state condition. Based on thorough analysis, the threshold value of *D-index* is set to -200. It specifies that if the *D-index* value is greater than -200, it indicates a normal fluctuation. Otherwise, it indicates the occurrence of an event in the system.

It is noticed that the smoothed PDC for HIF events rises to the steady state value without noticeable dip as shown in Figure 3.8. While in Figure 3.9, the load switching event experiences a dip in the subsequent group which creates a peak before reaching the steady state value. As such, the *Id-index* is developed to differentiate between HIF and non-HIF events by detecting the presence of peak before the smoothed PDC reaches its steady state value. Referring to Figure 3.9, the *Id-index* starts calculating if there exist a slope change at any smoothed PDC datum, *G(i)*, such that $(G(i-1) - G(i)) < 0$ and $(G(i) - G(i+1)) > 0$. In other words, if two consecutive differences in smoothed PDC change sign from negative to positive, then the peak is expected to occur at that position. Thus, the *Id-index* is calculated as follows.

$$Id-index = \frac{G(i) - G(i+3)}{G(i)} \qquad 3.5$$

From more simulations conducted, it is found that the best threshold value for the *Id-index* to separate HIF from non-HIF events is 0.01. If the *Id-index* falls below the threshold, it shows that the HIF event is identified. Otherwise, only a non-HIF event such as capacitor switching, load switching or motor starting is identified. Table 3.2 shows the steps for the calculation of the *D-index* and *Id-index* for the event in Figure 3.9. Whereas Figure 3.10 shows the flowchart of the steps in the whole process.

Table 3.2: *D-index* and *Id-index* calculation

Group	Summed PDC value	Difference in summed PDC value between two adjacent groups
1	3265.91	G(1)-G(2) = -7408.38
2	10674.29	G(2)-G(3) = -4024.32
3	14698.61	G(3)-G(4) = 22.31
4	14676.30	G(4)-G(5) = 862.63
5	13813.67	G(5)-G(6) = 1219.55
6	12594.12	G(6)-G(7) = 564.61
7	12029.51	G(7)-G(8) = 296.62
8	11732.89	G(8)-G(9) = 116.74

Step 1: *D-index* = (-7408.38-4024.32)/2 = -5716.35

Step 2: Conditions to initiate *Id-index* fulfilled

Step 3: *Id-index* = (14698.61-12594.12)/14698.61 = 0.1432

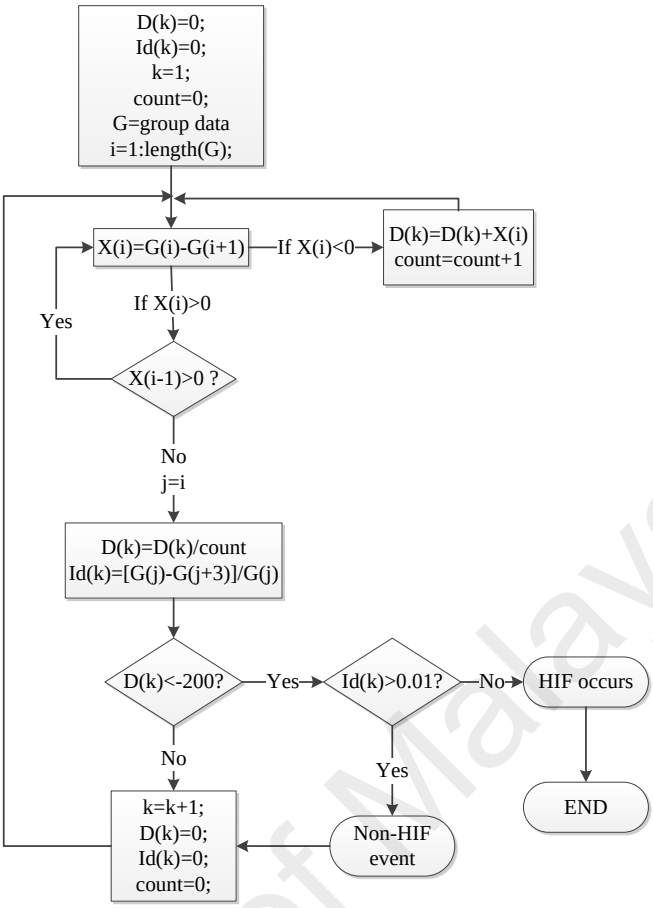

Figure 3.10: HIF detection and identification flowchart

3.3 Proposed Method for High Impedance Fault Localization

In this chapter, the overall concept of the proposed method utilizing the Multi-Resolution Analysis-Discrete Wavelet Transform (MRA-DWT) to extract the important features from the measured three-phase voltage and current waveforms to identify the fault location is presented. The proposed fault location method involves classifying the fault type and estimating the fault distance during the occurrence of high impedance fault (HIF) in the distribution network. The Artificial Neural Network (ANN) plays an integral role in the proposed fault location method where the extracted features are fed into the ANN for training and subsequently tested to evaluate the performance. In this proposed method, the Grey Wolf Optimization (GWO) technique is also utilized during the training process to determine the optimal ANN variables in order to obtain more accurate results.

3.3.1 Overall Concept of the Proposed Method

Figure 3.11 shows an example of the simple radial distribution network, which consists of one main feeder and two laterals, tapped at node 2 and 3. A line section is represented by two adjacent nodes and has its own line configuration. In this diagram, a fault is assumed to occur in the middle of line section S-R. Then, the three-phase voltage and current waveforms are measured at the measurement point, which is located at node 1.

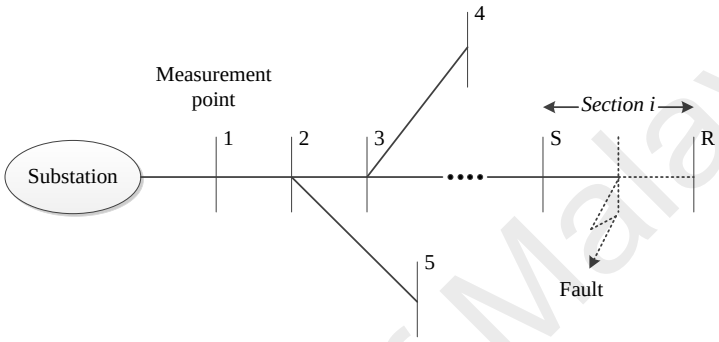

Figure 3.11: A simple radial distribution network

Figure 3.12 shows the overall flowchart of the proposed method during the occurrence of HIF. It consists of feature extraction, fault type classification, fault distance and impedance estimations as well as the faulty section identification. At first, the features of the measured three-phase voltage and current waveforms are extracted using the MRA-DWT. Based on the extracted features, the fault type is classified and the fault distance and impedance are estimated, which form the basis for the proposed fault location method. Then, the faulty section is identified based on the estimated fault distance. To enhance the estimated fault distance, the previously estimated fault distance is re-evaluated with respect to the identified faulty section, which forms the basis for the proposed enhanced fault location method.

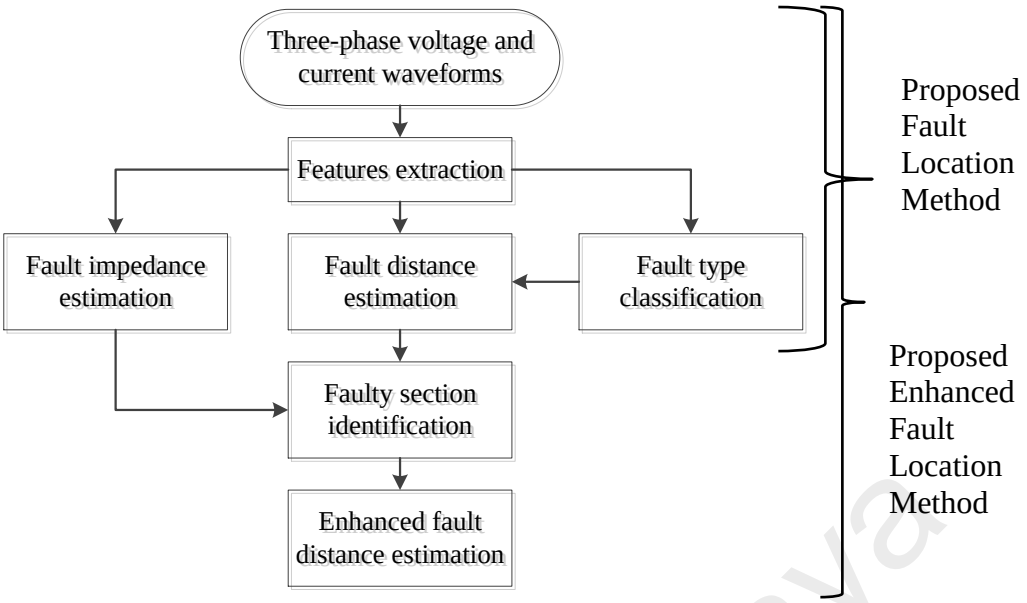

Figure 3.12: Flowchart of the fault location method

3.3.2 Multi-Resolution Analysis Discrete Wavelet Transforms

3.3.2.1 Features Extraction by MRA-DWT

During the occurrence of HIF event, the measured three-phase voltage and current waveforms are decomposed using the MRA-DWT. From this decomposition process, 2 important features can be obtained, which are:

- Approximation coefficients (*cA*)
- Detail coefficients (*cD*)

The approximation and detail coefficients are extracted after the original waveform is decomposed using the low-pass and high-pass filters respectively. Figure 3.13(a) shows an example of the original phase-A voltage waveform with phase-A to ground fault initiated at Node 1 with 100Ω fault impedance. As highlighted in the figure, it can be observed that the voltage fluctuation during the fault is not easily noticed. However, by utilizing the MRA-DWT analysis, the first level of extracted *cD* can signify the fault occurrence through the sharp peak as shown in Figure 3.13(b). While Figure 3.13(c) shows the first level of extracted *cA*.

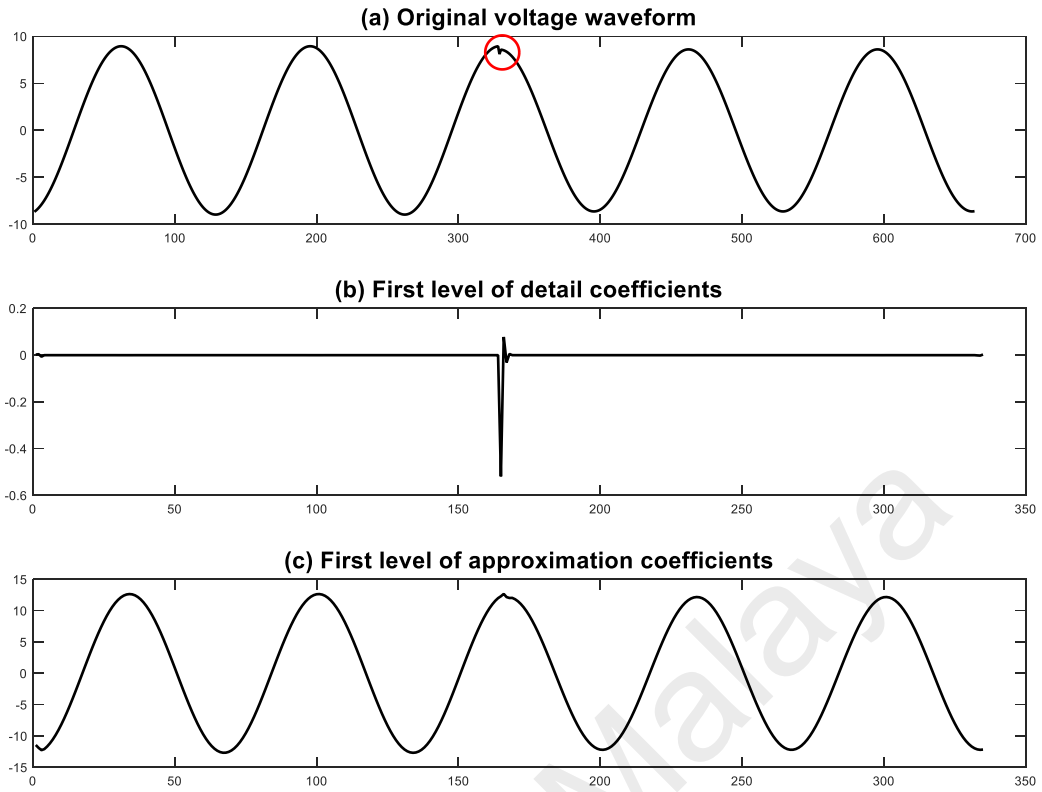

Figure 3.13: Decomposition process for voltage waveform using Db4

3.3.2.2 MRA-DWT Analysis to Estimate the Fault Distance

In this analysis, the fault distance is estimated by utilizing the energy content, E of the extracted cA from the voltage and current waveforms. The equation to calculate the E_j is shown as follows:

$$E_{j,k} = \sum_{n=\frac{128\,j-128+2^k}{2^k}}^{\frac{128\,j}{2^k}} (cA)^2 \qquad 3.6$$

where

j = frame number (1 frame is equal to one full cycle of $\frac{128}{2^k}$ samples)

k = level of decomposition ($k=1, 2,\ldots, n$)

n = number of samples

Figure 3.14 shows the application of Eq 3.6 to the waveform in Figure 3.13(c) to extract the energy content of *cA*. It can be observed that there are no significant change in the first 4 energy content as the fault is not initiated in the system. However, after the fault is initiated at *j=4*, there is a significant decrease in energy content. As such, it indicates the starting point of the fault. This rapid change in the energy content will then settle at a constant value from the 6th cycle onwards. Therefore, the difference in energy content, *sE* can be calculated between the starting point of the fault, E_j and point E_{j+3} as encircled in Figure 3.14. The point E_{j+3} is selected to ensure that the energy content is totally stabilized. The equation to calculate the *sE* is shown as follows:

$$sE = E_{j+3} - E_j \tag{3.7}$$

It is important to note that the calculated *sE* can be either negative or positive. Negative *sE* indicates the decrement of energy content, whereas positive *sE* represents the increment of energy content. In this analysis, the calculated *sE* is used to estimate the fault distance, given that the voltage and current magnitudes vary for different fault distances.

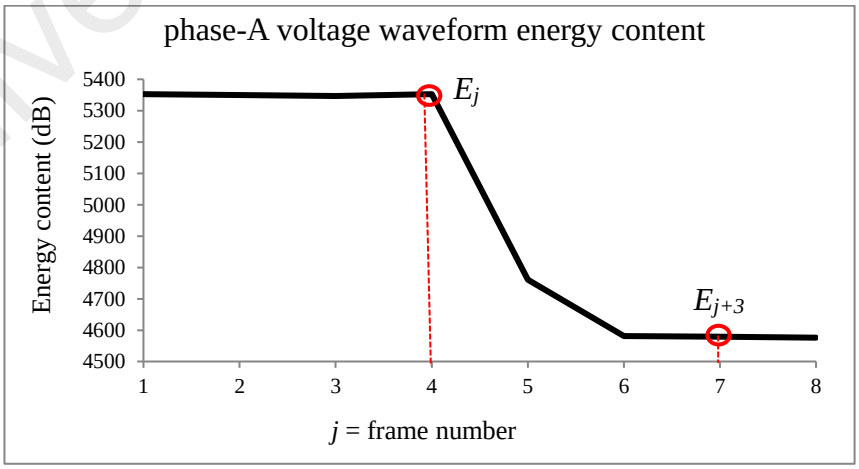

Figure 3.14: Energy content for each full cycle of phase-A voltage waveform

3.3.3 ANN Training for Determination of Optimal ANN Variables

It must be noted that before the fault location algorithm using the ANN can be applied, the ANN has to be trained first using the obtained energy content. As such, the training methodology for the ANN is presented in this section. The training methodology consists of 3 steps which are fault distance estimation, fault type classification and fault impedance estimation. In this training process, thorough investigations through the fault distance estimation are first conducted to obtain the optimal ANN variables. Subsequently, the optimal ANN variables are also used in the ANN training for fault type classification and fault impedance estimation.

3.3.3.1 Fault Distance Estimation

As mentioned earlier, thorough investigations through the fault distance estimation are conducted to obtain the optimal ANN variables. The performance is evaluated based on the average error of fault distance. First, an investigation to observe the effect of different types of wavelet transforms is conducted. In this investigation, the best combination of mother wavelet and its associated decomposition level is obtained. Then, the effect of variations in ANN parameters is investigated. The ANN parameters comprise of a number of neurons, learning rates and momentum constant. Next, the GWO technique is implemented to find the optimal values of the ANN parameters. Further investigation is also conducted to evaluate the effect of variation in the number of neurons in a hidden layer. Subsequently, the effect of different types of ANN learning algorithms is investigated to identify the best ANN learning algorithm. In addition, the effects of performing the dataset categorization and different objective functions for GWO technique are conducted. Besides that, the effect of a different number of input data to be fed into the ANN is investigated. Last but not least, the effect of different types of optimization techniques to provide the optimal values of ANN parameters are investigated and compared. In this investigation, the other 2 optimization techniques to

be compared against the GWO technique are Evolutionary Programming (EP) and Particle Swarm Optimization (PSO) techniques.

(a) ***Selection of Mother Wavelets and Its Associated Levels of Decomposition***

In this subsection, the performance of three different mother wavelets comprising of Biorthogonal (Bior3.3), Daubechies (Db4) and Symlet (Sym8) and its associated 4 levels of decomposition are investigated and compared to identify the best performing pair of mother wavelet and levels of decomposition. As such, there are 12 combinations of mother wavelets and its associated levels of decomposition to be compared.

(b) ***Effect of Variations in ANN Parameters***

In this subsection, the effect of variations in ANN parameters is investigated. The parameters involved in this investigation are:

- Learning rate (*lr*)
- Momentum constant (*mc*)
- Number of neurons in hidden layer (*p*)

In this investigation, there are 3 different scenarios related to the above 3 different ANN parameters. In each scenario, one ANN parameter is changed while the other two ANN parameters are fixed.

(c) ***Effect of Performing ANN Parameters Optimization through GWO***

In this subsection, the Grey Wolf Optimization (GWO) technique is proposed to determine the optimal values of ANN parameters comprising of *lr*, *mc* and *p*. In order to obtain the optimal values of ANN parameters, the range of values for *lr*, *mc* and *p* during initialization have to be defined. Here, the boundary limit for *lr* and *mc* are set in between [0 1], whereas the boundary of *p* is set in between [1 60].

(d) ***Effect of Different Types of ANN Learning Algorithm***

In this subsection, the effects of different types of ANN learning algorithm are investigated. The common types of ANN learning algorithm include Levenberg-Marquardt backpropagation (*trainlm*), Bayesian regularization (*trainbr*) and others, which are mentioned in Table 3.3 (Mathworks 2016). In this study, the performance of each learning algorithms in ANN is evaluated with the assistance of GWO technique.

Table 3.3: Different types of learning algorithm

Learning algorithm (Mathworks 2016)	
trainbfg	BFGS quasi-Newton backpropagation
trainbr	Bayesian regularization
traincgb	Conjugate gradient backpropagation with Powell-Beale restarts
traincgf	Conjugate gradient backpropagation with Fletcher-Reeves updates
traincgp	Conjugate gradient backpropagation with Polak-Ribiére updates
trainlm	Levenberg-Marquardt backpropagation
trainoss	One-step secant backpropagation
trainr	Random order incremental training with learning functions
trainrp	Resilient backpropagation
trainscg	Scaled conjugate gradient backpropagation

(e) ***Effect of Performing Dataset Categorization***

In this subsection, the effect of performing dataset categorization, where the training process is conducted separately for each category of fault types comprising of single line to ground fault (SLGF), double line to ground fault (LLGF), double line fault (LLF) and balance fault (BF) is investigated.

(f) ***Effect of Different Number and Combinations of Input Data***

In this subsection, the effects of different number and combinations of input data being fed into the ANN are investigated. The comparison analysis is first conducted using 3 consistent input data in each level of MRA-DWT decompositions. Then, the comparative analysis is conducted for more input data comprising of consistent data from multiple

different combinations of MRA-DWT decompositions levels. Finally, the analysis for random selection of input data is also performed. A comparison of the results with and without the GWO technique in the above analysis is also conducted in this section.

i Variation in the Number of Input Data

In this investigation, the effects of a different number of input data to be fed into the ANN are observed. There are 5 scenarios wherein the number of input data is varied between 3, 6, 12, 18 and 24 input data. The input data comprise of the 1^{st}, 2^{nd}, 3^{rd} and 4^{th} levels of three-phase voltage and current energy contents that are extracted using the Bior3.3 mother wavelet. For each scenario, the best combination of input data is determined based on the average error. Then, this best combination of input data will be further trained with the application of GWO.

ii Random Selection of Input Data (6 Input Data)

In this subsection, the best random combination of 6 input data which are randomly selected from 24 available input data is determined. The purpose of this investigation is to evaluate the strength of each input data and its combinations that may improve the ANN accuracy. For this purpose, an exhaustive technique is used to obtain the best random combination of 6 input data and there are a total of 134596 random combinations that can be obtained using this technique. At first, all 134596 random combinations are evaluated using the stand-alone ANN. Subsequently, the best random combination of input data is repeated with the assistance of GWO-ANN.

(g) Effect of Different Objective Functions for GWO Technique

In this subsection, further investigation is conducted to evaluate the effect of different objective functions for GWO technique. It is noted that in the application of an optimization technique, it is necessary to define an objective function, *ObjFunc* which is

responsible to ensure that the optimal solution is minimized or maximized. The common types of *ObjFunc* that can be assigned include standard deviation (*StD*), average error (*AverError*), maximum error (*MaxError*) or several other statistical formulations.

(h) ***Effect of Different Types of Optimization Techniques in Optimizing ANN Parameters***

In this subsection, different types of optimization technique, which are the Particle Swarm Optimization (PSO) and Evolutionary Programming (EP) are implemented. The main purpose of this research is to investigate the significance of utilizing the optimization technique to provide the optimal value of ANN parameters thus increasing the accuracy. Furthermore, the comparison between the techniques is evaluated. The performance of these optimization techniques is compared in terms of accuracy and training time. The accuracy can be determined based on the average error in which the least value of average error represents the highest accuracy. Whereas for the training time, it can be determined based on the number of neurons utilized. It is noted that more training time is required if the number of neurons is higher.

3.3.3.2 Fault Type Classification

In this subsection, the fault type is classified using the same approach to estimate the fault distance. However, it utilizes directly the optimal ANN variables, which had been obtained during the training process to estimate the fault distance. There are 11 types of fault to be classified as follows:

1) Unbalanced Fault
   - Single Line to Ground Fault (SLGF)
     - ✓ Phase A-G (AGF)
     - ✓ Phase B-G (BGF)
     - ✓ Phase C-G (CGF)

- Double Line to Ground Fault (LLGF)
    - ✓ Phase A-B-G (ABGF)
    - ✓ Phase A-C-G (ACGF)
    - ✓ Phase B-C-G (BCGF)
- Double Line Fault (LLF)
    - ✓ Phase A-B (ABF)
    - ✓ Phase A-C (ACF)
    - ✓ Phase B-C (BCF)

2) Balanced Fault (BF)

- Three Line to Ground Fault (LLLGF)
    - ✓ Phase A-B-C-G (ABCGF)
- Three Line Fault (LLLF)
    - ✓ Phase A-B-C (ABCF

3.3.3.3 Fault Impedance Estimation

In this subsection, the fault impedance is estimated using the same method as in Subsection 3.3.3.2. The fault impedance value considered in this analysis ranges from 50Ω to 150Ω. This range of HIF value is used since there is no commonly agreed or standardized range of HIF values. For instance, in (Uriarte and Centeno 2005) the recommended value of HIF is based on the type of surface where the conductor makes contacts such as dry sand and concrete. Another reported HIF value is 140kΩ in a case where the distribution network suffered from a fault due to leaning tree (Elkalashy, Lehtonen et al. 2008). While, in (Bretas, Moreto et al. 2006) and (Jung, Kim et al. 2007), the maximum HIF value is set to 100Ω and 200Ω respectively.

3.3.4 ANN Testing for Fault Location Determination

Previously, thorough investigations to obtain the optimal ANN classifier had been conducted with the integration of GWO technique in the training process. The training process involves three main objectives, which are to identify the fault types, estimate the fault distance and fault impedance values. During the training process, the generated network files for fault type identification, fault distance and fault impedance estimations were saved. Subsequently, the testing process is conducted in this section to evaluate the predictive capability of the saved network files. For that purpose, new testing data are generated which are not the same data used during the training process and the capability of the saved network files to estimate the outputs with minimum error are evaluated. Figure 3.15 shows the flowchart for the testing procedures, in which the fault type is classified first and then followed by the fault distance estimation.

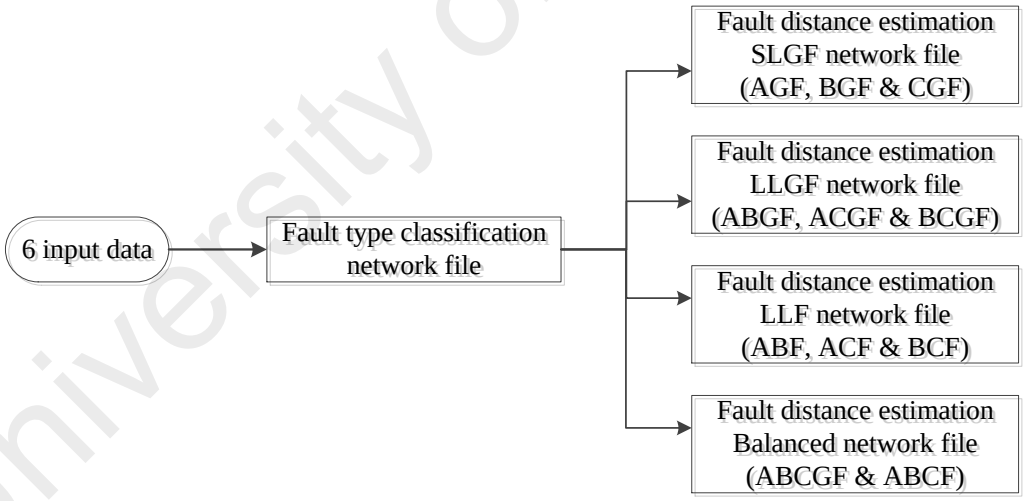

Figure 3.15: Flowchart for fault type identification and fault distance estimation

3.4 Proposed Enhanced Fault Location Method

In the previous proposed fault location method in Subsection 3.3, it only estimates the fault distance. However, the estimated fault distance may lead to multiple possible points of fault location due to the existence of lateral branches of equal distances from the measurement point. Therefore, determination of the exact fault location becomes difficult

and time-consuming. To overcome these difficulties, an enhanced fault location method is proposed in this section. In the proposed enhanced fault location method, the faulty section identification method is used to determine the most likely faulty section through a ranking process. Here, the proposed method will first identify all the possible faulty sections. Then, each of the previously estimated fault distance will be re-evaluated with respect to the identified faulty section to improve the fault location results.

3.4.1 Faulty Section Identification

The proposed faulty section identification method utilizes the previously estimated fault distance to identify the possible faulty section. The faulty section is considered if the estimated fault distance falls in between the length of the line section. However, it is important to take into account the error of the estimated fault distance. For this purpose, the error is assumed to be ±10% of the estimated fault distance. Therefore, the range of the estimated fault distance to be considered in identifying the faulty section is as follows:

Lower boundary of length, L1 = $x - 10\%$

Upper boundary of length, L2 = $x + 10\%$

where x is the previously estimated fault distance.

Figure 3.16 shows an example of simple distribution network consisting of 3 line sections. A line section is represented by two adjacent nodes. Line section 1 (S1) is located between nodes N1 and N2, line section 2 (S2) is located between nodes N2 and N3 whereas line section 3 (S3) is located between nodes N3 and N4.

Figure 3.16: Simple distribution network with 3 line sections

To consider any line section as the possible faulty section, it must fulfil one of the following 3 conditions:

Condition 1: N2 < *L1* & *L2* < N3

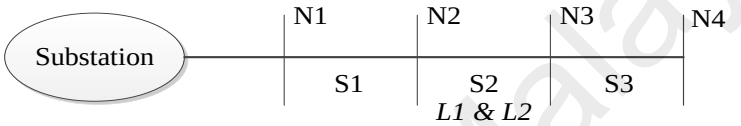

If this condition is fulfilled, then there is only 1 possible faulty section which is S2.

Condition 2: (N1 < *L1* < N2) & (N2 < *L2* < N3)

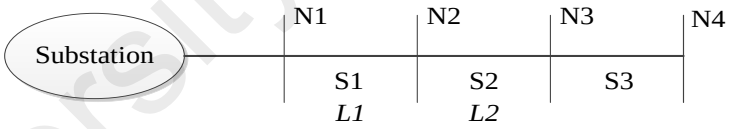

If this condition is fulfilled, there will be 2 possible faulty sections which are S1 and S2.

Condition 3: (N1 < *L1* < N2) & (N3 < *L2* < N4) – special condition

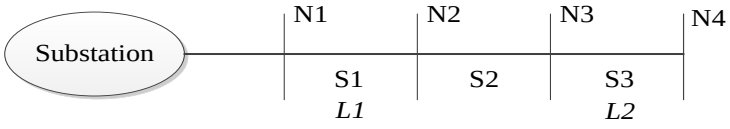

If this condition is fulfilled in which the identified faulty sections are not adjacent to each other, then there will be 3 possible faulty sections which are S1, S2 and S3. This special condition usually occurs for short line sections.

3.4.2 Ranking Process

In the previous subsection, multiple possible faulty sections with equal probability have been determined. As these faulty sections could be located far apart, the rectification process may be lengthy. Therefore, in this subsection, the identified faulty sections will be ranked from the most likely to least likely sections to generate a list of inspection sequence for the operators. Here, the database approach is adopted where the possible faulty sections are ranked based on the number of measured data that falls within the range of stored data. The measured data are the voltage and current data when the HIF event occurs in the system. Whereas the stored data are the simulated HIF event data at each node with pre-defined fault types and fault impedance values, stored in the database.

3.4.2.1 Development of Database

In this subsection, the process to develop the database is explained. Figure 3.17 shows the simple distribution network for line section *k* located between nodes *i* & *j*. To develop the database, the fault is first simulated at each node with pre-defined fault type and fault impedance values. For instance, the SLGF is simulated at node *i* with 50Ω of fault impedance. Then, the measured data will be saved together with the corresponding fault type and fault impedance value as shown in Table 3.4.

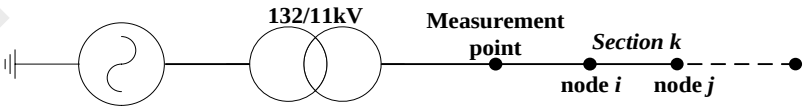

Figure 3.17: Simple distribution network (Line Section *k*)

Table 3.4: Measured data for SLGF

	50Ω	60Ω	70Ω
Node *i*	$V_{a,i}^{50}, V_{b,i}^{50}, V_{c,i}^{50}, I_{a,i}^{50}, I_{b,i}^{50}, I_{c,i}^{50}$	$V_{a,i}^{60}, V_{b,i}^{60}, V_{c,i}^{60}, I_{a,i}^{60}, I_{b,i}^{60}, I_{c,i}^{60}$	$V_{a,i}^{70}, V_{b,i}^{70}, V_{c,i}^{70}, I_{a,i}^{70}, I_{b,i}^{70}, I_{c,i}^{70}$
Node *j*	$V_{a,j}^{50}, V_{b,j}^{50}, V_{c,j}^{50}, I_{a,j}^{50}, I_{b,j}^{50}, I_{c,j}^{50}$	$V_{a,j}^{60}, V_{b,j}^{60}, V_{c,j}^{60}, I_{a,j}^{60}, I_{b,j}^{60}, I_{c,j}^{60}$	$V_{a,j}^{70}, V_{b,j}^{70}, V_{c,j}^{70}, I_{a,j}^{70}, I_{b,j}^{70}, I_{c,j}^{70}$

After each type of fault with pre-defined fault impedance values are simulated at each node, then the process to generate the database is initiated. To generate the database for a particular line section that lies between two nodes, it is best to store only the minimum and maximum values of the data. Table 3.5 shows the first database that covers 50Ω to 60Ω of fault impedance for line section *k* that lies between node *i* and *j*. For the first data which is the phase-A voltage signal, there are 4 data consisting of 50Ω and 60Ω data at node *i* and *j*. Among these 4 data, only the minimum and maximum data will be selected as shown below. The same process is repeated for the other data and the selected data will be stored as shown in Table 3.5.

$$\underbrace{V_{a,i}^{50}, V_{a,j}^{50}, V_{a,i}^{60}, V_{a,j}^{60}}_{V_{a(\min)}, V_{a(\max)}}$$

Table 3.5: Database 1

	Database 1 (50-60Ω)	
	Min	Max
Section *k* (line section *i-j*)	$V_{a(\min)}, V_{b(min)}, V_{c(min)}$ $I_{a(min)}, I_{b(min)}, I_{c(min)}$	$V_{a(\max)}, V_{b(\max)}, V_{c(\max)}$ $I_{a(\max)}, I_{b(\max)}, I_{c(\max)}$

The process is repeated for all line sections and fault impedance intervals. There will be a total of 10 generated databases as shown in Table 3.6.

Table 3.6 : Database for each fault impedance interval

Database	Fault impedance interval (Ω)
Database 1	50-60
Database 2	60-70
Database 3	70-80
Database 4	80-90
Database 5	90-100
Database 6	100-110
Database 7	110-120
Database 8	120-130
Database 9	130-140
Database 10	140-150

3.4.2.2 Faulty Section Ranking

To rank all the possible faulty section, the measured data are first compared against the stored data for each of the identified faulty sections. If the measured data fall in between the minimum and maximum values of the stored data, then it will be counted as '√', otherwise, it will be counted as '×'. Then, the total number of '√' for each identified faulty section is calculated and ranked according to the highest number of '√'.

3.5 Conclusion

In this chapter, a new algorithm using phase displacement computation (PDC) method has been proposed to discriminate HIF from non-HIF events. The proposed method utilized three-phase voltage waveforms that were measured at the main substation. The PDC data were calculated between the measured and reference three-phase voltage waveforms. To identify the HIF from non-HIF events, the smoothed PDC pattern was observed. To simplify the HIF detection and identification process, an automatic HIF classification algorithm was proposed. The proposed algorithm uses two indices, which were detection index (*D-index*) and identification index (*Id-index*). The *D-index* is used to detect the occurrence of an event in the system. Subsequently, the *Id-index* is used to identify the event as HIF or non-HIF events.

Subsequently, a hybrid technique comprising of Multi-Resolution Analysis-Discrete Wavelet Transform (MRA-DWT), Artificial Neural Network (ANN) and Grey Wolf Optimization (GWO) technique has been developed to estimate the fault location. The proposed fault location method involves classifying the fault type and estimating the fault distance and impedance values during the occurrence of HIF in the distribution network. The MRA-DWT is utilized to extract the important features from the measured three-phase voltage and current waveforms. Then, the extracted features are fed into the ANN to be trained and subsequently tested to evaluate the performance of the proposed fault

location method. Besides that, the GWO technique is also utilized during the training process to obtain the optimal ANN variables.

It is observed that the estimated fault distance may leads to multiple possibilities of faulty sections. Therefore, an enhanced fault location method was proposed where all the possible faulty sections were identified and ranked by the proposed faulty section identification algorithm.

CHAPTER 4: VALIDATION OF PROPOSED TECHNIQUE FOR HIGH IMPEDANCE FAULT DETECTION AND LOCALIZATION

4.1 Introduction

In this chapter, the proposed techniques for HIF detection and localization developed in Chapter 3 are implemented. There are three phases involved in this chapter as follows:

a) Validation of proposed technique for high impedance fault detection and identification
b) Validation of proposed method for high impedance fault localization
c) Validation of proposed enhanced fault location method

4.2 Test System Modelling for the Proposed Method

The test system used for analyzing the proposed method is 11kV and 50 Hz system as shown in Figure 4.1. The test system has 33 nodes that represent 32 line sections. All cables in the network are three-phase balanced and underground. The measurement point is located at the primary substation. The complete network data are given in the Appendix A.1. Figure 4.2 shows the test system that is modeled in PSCAD/EMTDC software.

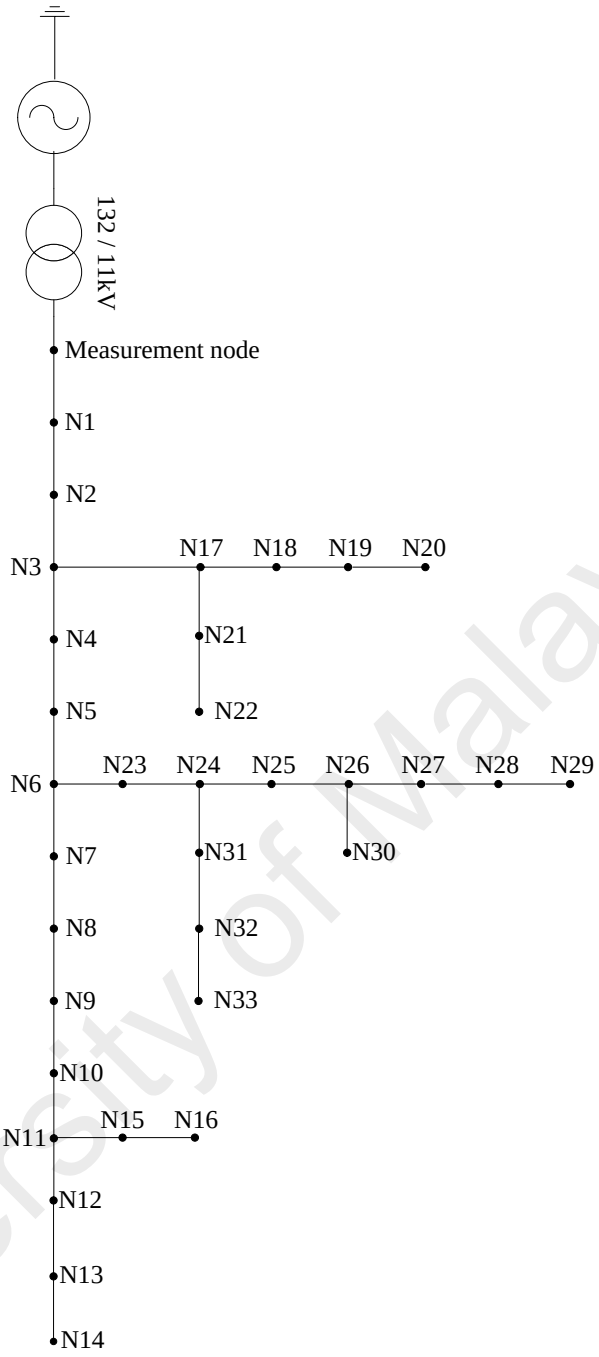

Figure 4.1: Schematic diagram of 11kV distribution network

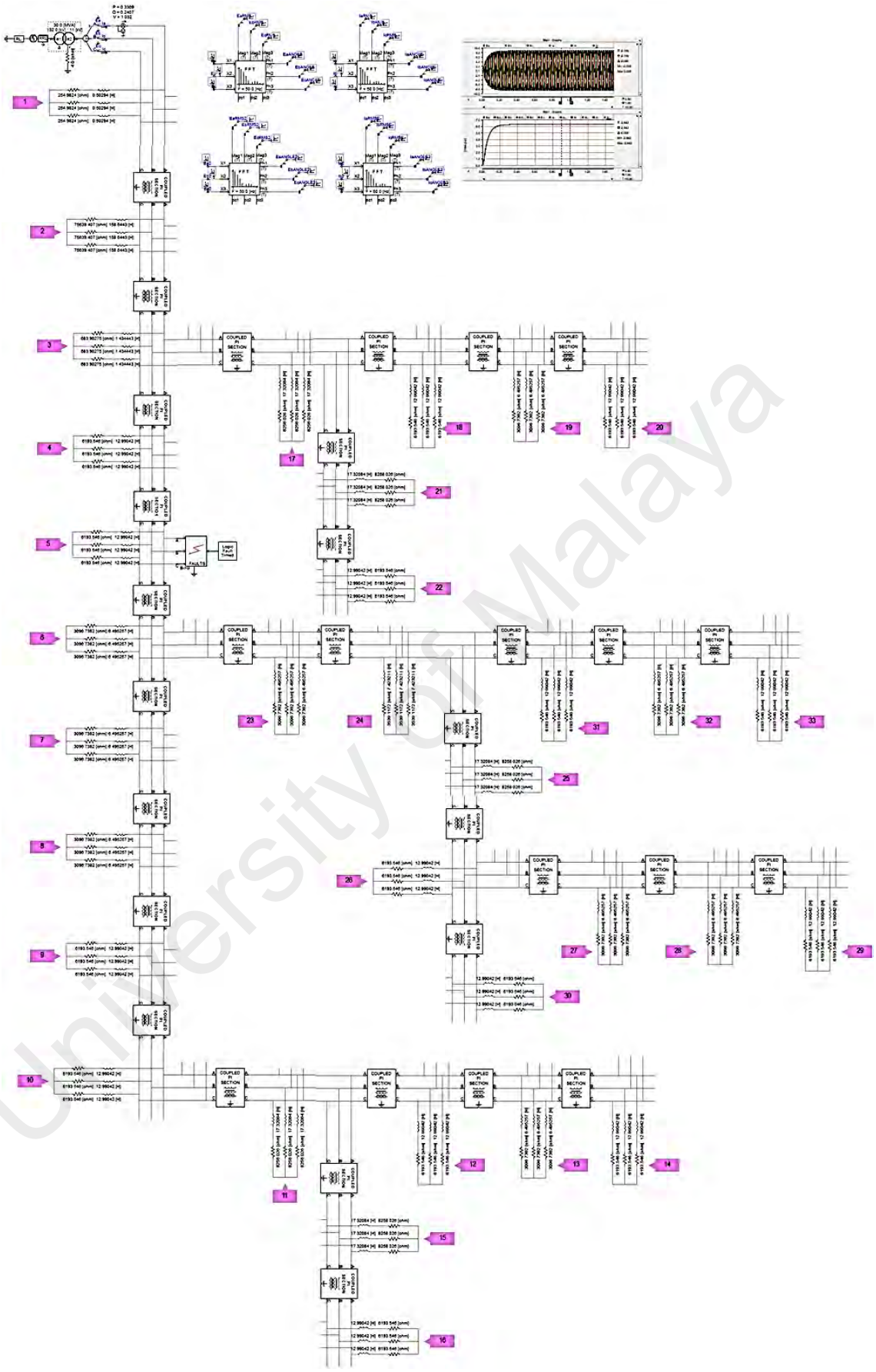

Figure 4.2: The typical 11kV distribution network modeled in PSCAD/EMTDC software

The grid is modeled by using an equivalent three-phase voltage source model. The transformer consists of three-phase 2-winding transformer and the line sections are modeled by using the π-model. The loads are modeled with a resistor (R) and inductor (L) elements, where the values are given in Appendix A.1. The multimeter is used to obtain the three-phase voltage and current waveforms at the primary substation. All of these models can be found in PSCAD/EMTDC master library.

4.3 Validation of Proposed Technique for High Impedance Fault Detection and Identification

In this subsection, the performance of the proposed PDC method to detect and identify the HIF from non-HIF events is evaluated. For this purpose, different types of disturbance are simulated in the system. Then, the transition and steady state periods for each disturbance are determined. Besides that, the robustness of the proposed method is investigated in terms of variation of fault inception angles and multiple consecutive events occurring in the system. Finally, the effectiveness of the proposed automatic HIF classification algorithm is discussed.

4.3.1 Different Types of Disturbance for HIF Detection and Identification

In order to validate the effectiveness of the proposed method to detect and identify the HIF, different sets of events are simulated. The events are described as follows:

1) HIF: different types of HIF such as single line to ground fault (SLGF), double line to ground fault (LLGF), double line fault (LLF) and three phase to ground fault (LLLGF) are simulated with different fault impedance values. In this study, 50Ω and 100Ω are chosen to represent the fault impedance. Besides that, different fault inception angles comprising of 0°, 30°, 45°, 90°, 135°, 150°, 180°, 210°, 225° and 270° are simulated to observe the robustness of the proposed method.

2) Load switching: loads of 0.3MW/0.24MVar, 0.75MW/0.36MVar and 1.5MW/0.9MVar are switched into the system.
3) Motor starting: the motor bearing the ratings of 0.6431MW, 1.245MW and 1.029MW are injected into the system.
4) Capacitor switching: the capacitor banks having the rating of 0.5MVar, 1.5MVar and 2.5MVar are connected to the system.

All of the above events are introduced at BUS2 at *t=1.0sec*. The process starts by measuring the three-phase voltage waveform at the measurement point. The measured voltage is compared to the reference voltage to calculate the absolute PDC and smoothed PDC. Based on the pattern of the smoothed PDC, the events can be identified as HIF or non-HIF event. To simplify the identification process, an automatic HIF classification algorithm is developed.

4.3.1.1 HIF event

Figures 4.3(a)-(d) show the patterns of smoothed PDC for different types of HIF with fault impedance of 50Ω and 100Ω. As shown in the figures, once the HIF occurs, the smoothed PDC starts to increase until it reaches a plateau without obvious dip, overshoot or fluctuation. Based on the results, it can be observed that the patterns are similar for each case, although the obtained smoothed PDC magnitudes are different.

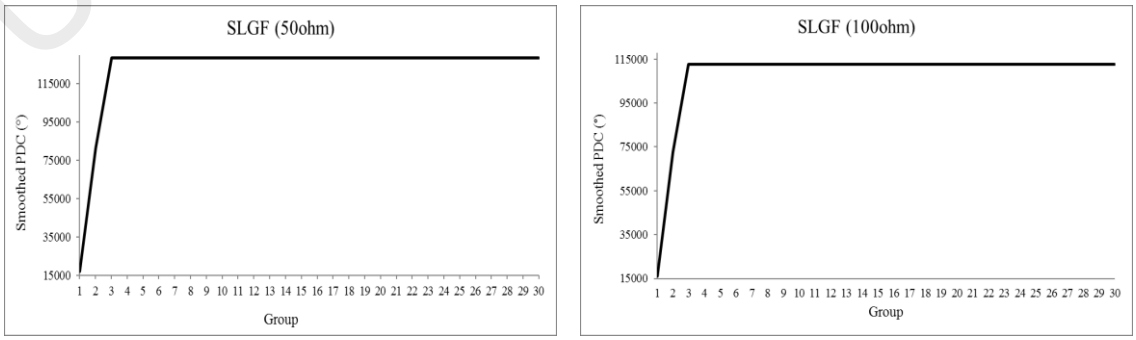

(a) SLGF type of fault

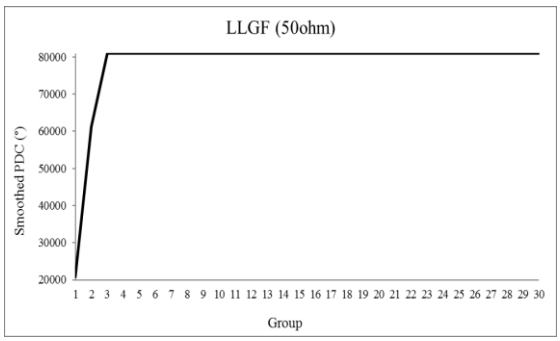

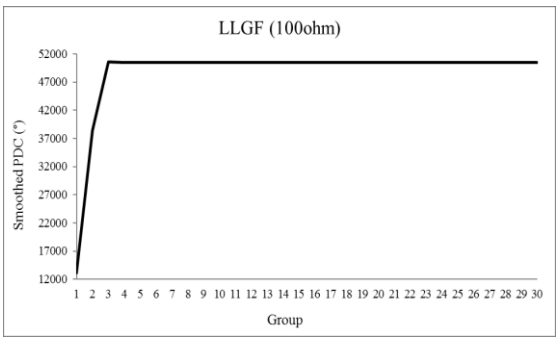

(b) LLGF type of fault

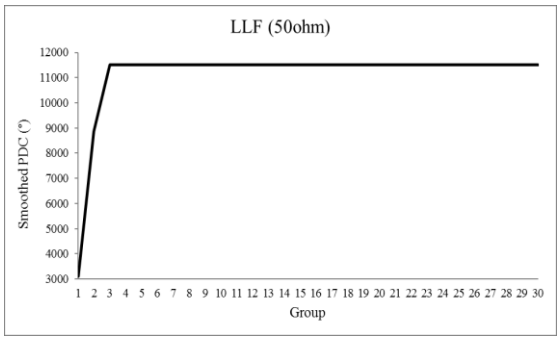

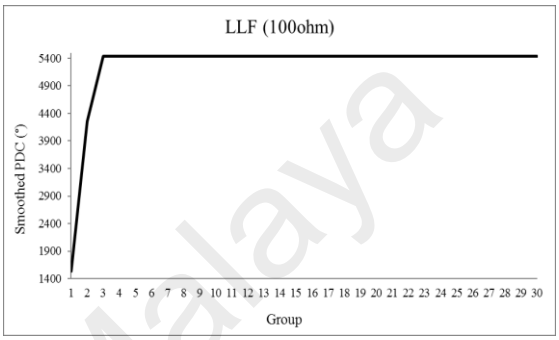

(c) LLF type of fault

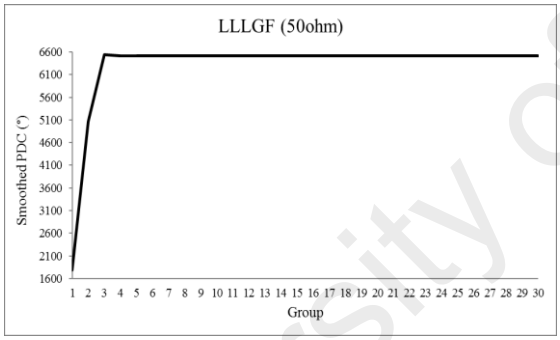

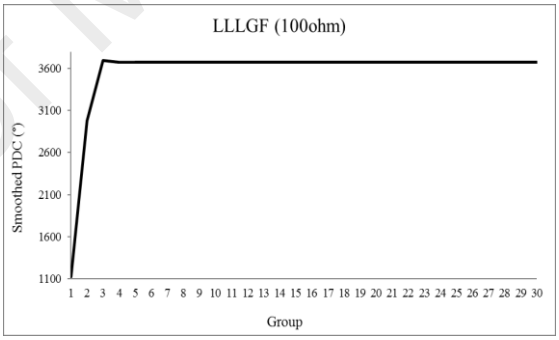

(d) LLLGF type of fault

Figure 4.3: Patterns of smoothed PDC for different types of HIF

4.3.1.2 Load switching event

Figures 4.4(a)-(c) show the changes in smoothed PDC when the loads are added to the system. It can be observed that the smoothed PDC increases to a peak value and then decreases before reaching a constant value. The peak before the dip differentiates this event from HIF events.

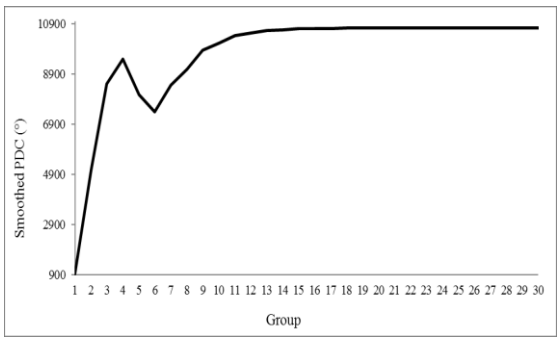

(a) 0.3MW / 0.24MVaR

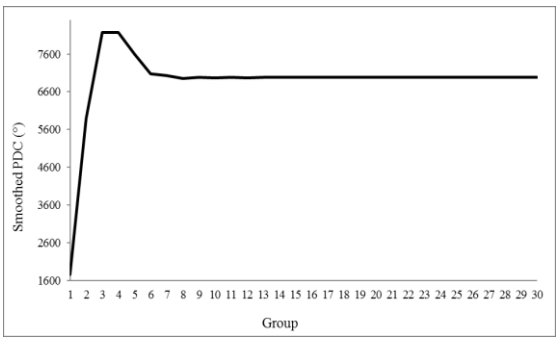

(b) 0.75MW / 0.36MVaR

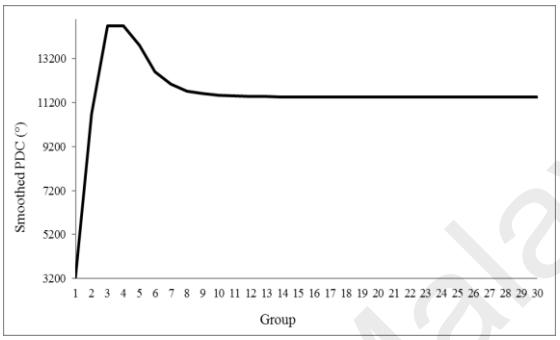

(c) 1.5MW / 0.9MVaR

Figure 4.4: Pattern of smoothed PDC for load switching event

4.3.1.3 Motor starting event

Figures 4.5(a)-(c) show the smoothed PDC patterns associated with motor starting events. It can be observed that the peak and subsequent dip is obvious. A little fluctuation is detected after the first dip.

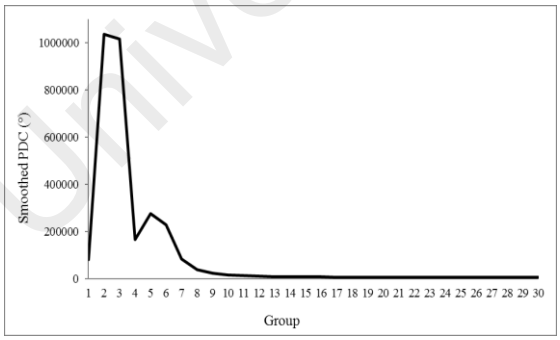

(a) 0.6431MW

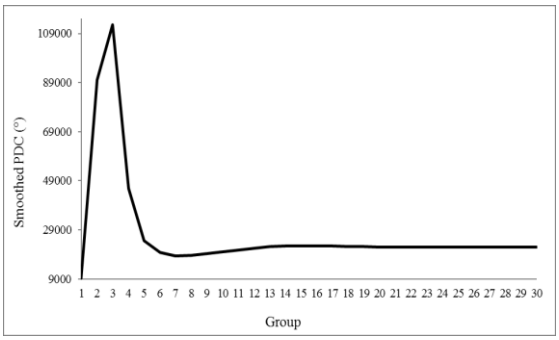

(b) 1.245MW

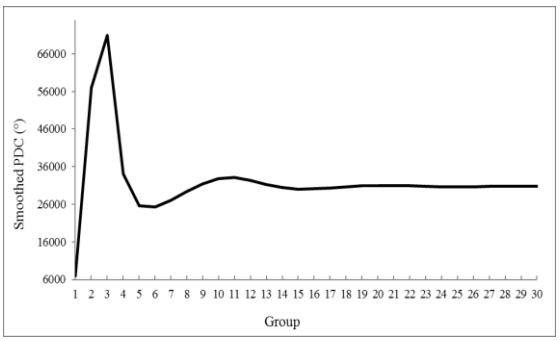

(c) 1.029MW

Figure 4.5: Pattern of smoothed PDC for motor starting event

4.3.1.4 Capacitor switching event

Finally, the smoothed PDC of capacitor switching with ratings of 0.5MVar, 1.5MVar, 2.5MVar are shown in Figures 4.6(a)-(c). It can be seen that the peak and the subsequent dip are pronounced.

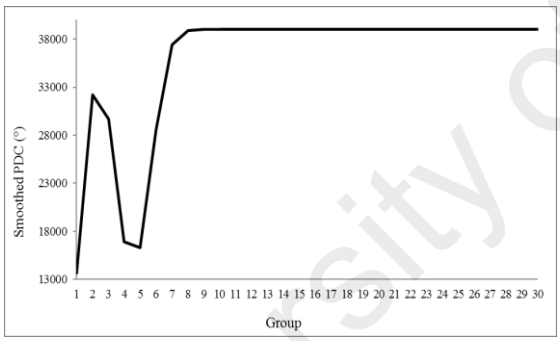

0.5MVar

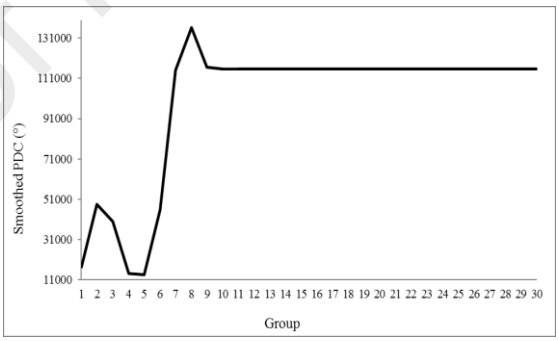

(b) 1.5MVar

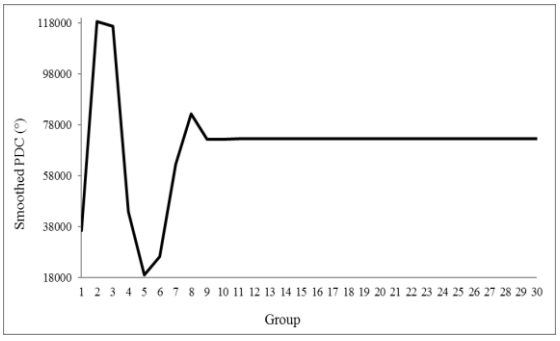

(c) 2.5MVar

Figure 4.6: Pattern of smoothed PDC of capacitor switching event

Based on the results in Figure 4.3 to Figure 4.6, it clearly shows the difference in the pattern of smoothed PDC. It can be observed that only HIF event has no obvious peak and subsequent dip in the pattern as compared to the other events. As such, the occurrence of HIF event can be differentiated from the other non-HIF events.

4.3.2 Transition and Steady State Period of Event

It is noted that the smoothed PDC pattern fluctuates after the occurrence of an event before it stabilizes to its steady state condition. The volatile period before the steady state condition is known as a transition period. Likewise, the steady state condition is achieved when there is no obvious oscillation in the smoothed PDC.

Figure 4.7 shows the transition periods for different types of events. As shown in the figures, each event has a different transition period. The HIF event has a shorter transition period as compared to the non-HIF events. It is noted that non-HIF events always oscillate before reaching the steady state condition. Through a thorough simulation and analysis process, the non-HIF events require a maximum transition period of 13 consecutive groups from the start of the event to reach the steady state condition. Therefore, if two events occur within 13 consecutive groups, only the first event is considered. While the other event is considered as a fluctuation within the transition period as shown in Figure 4.7(b)-(d). Figure 4.8 shows an example of two events that are simulated with at least 14 group apart. In this example, the occurrence of the second event is inspected from the 14^{th} group and onward.

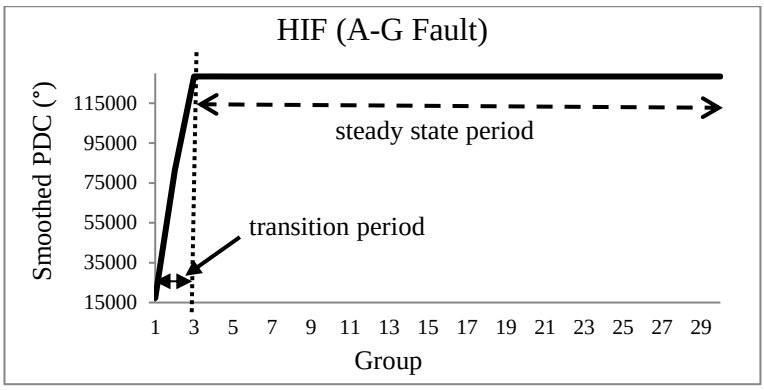

(a) HIF event

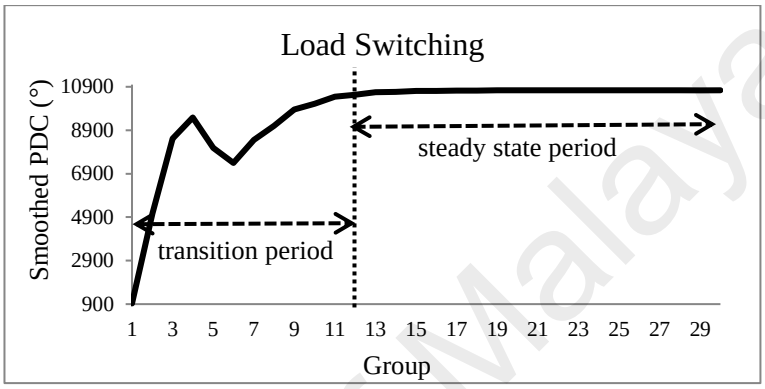

(b) Load switching event

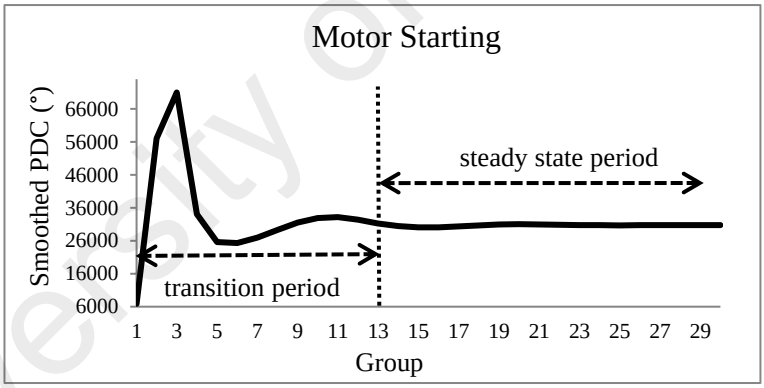

(c) Motor starting event

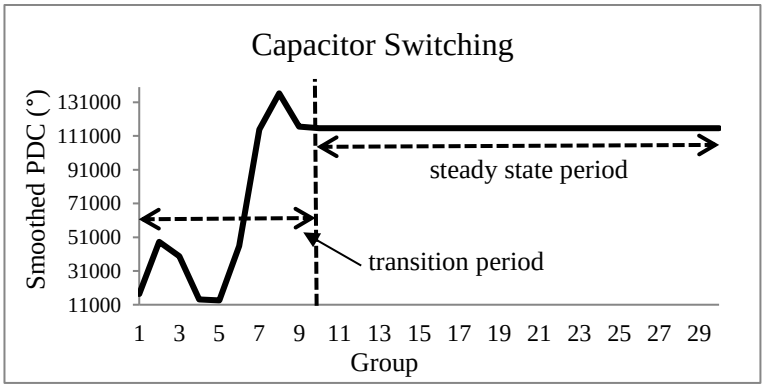

(d) Capacitor switching

Figure 4.7: Transition and steady-state period for event

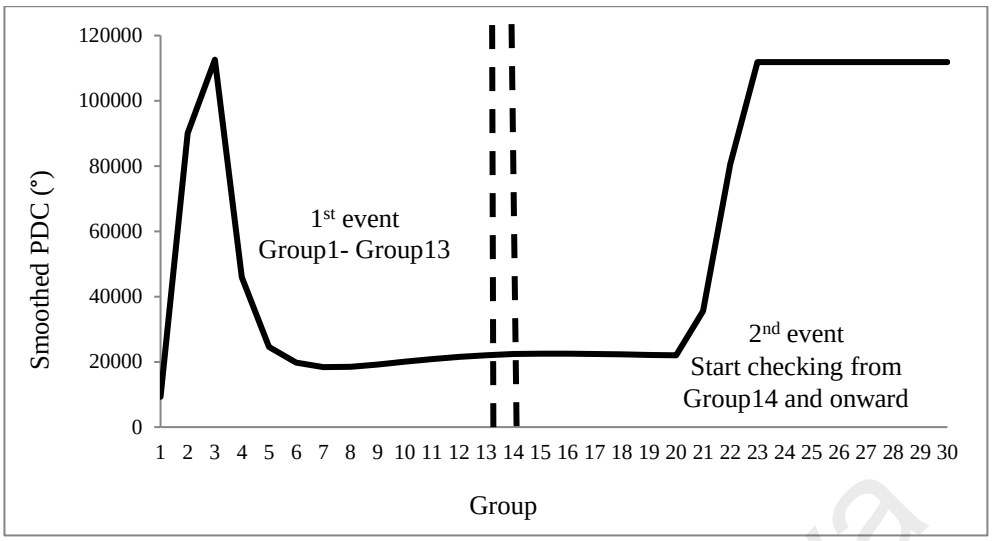

Figure 4.8: Transition and steady-state period for 2 consecutive events

4.3.3 Sensitivity studies

Based on the results above, it can be observed that the HIF and non-HIF events can be differentiated by the rising pattern of the smoothed PDC. However, it is crucial to investigate the robustness of the proposed method. For this purpose, two sensitivity studies are simulated as follows:

1) Variation of fault inception angles
2) Occurrence of multiple consecutive events

4.3.3.1 Variation of fault inception angles

In this subsection, the effect of fault inception angle towards the pattern of smoothed PDC during the occurrence of HIF event is analyzed. For this purpose, the SLGF fault with fault impedance of 50Ω is applied at BUS2. 10 different fault inception angles are simulated which are 0°, 30°, 45°, 90°, 135°, 150°, 180°, 210°, 225° and 270°. The reason for this study is to observe the existence of peak and subsequent dip in the pattern of smoothed PDC due to the variation of fault inception angles. The results of this analysis are shown in Figure 4.9.

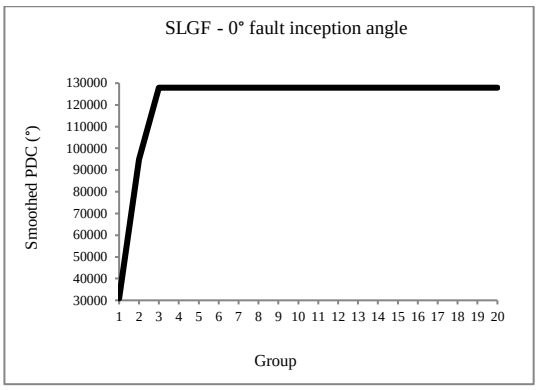

(a) 0° inception angle

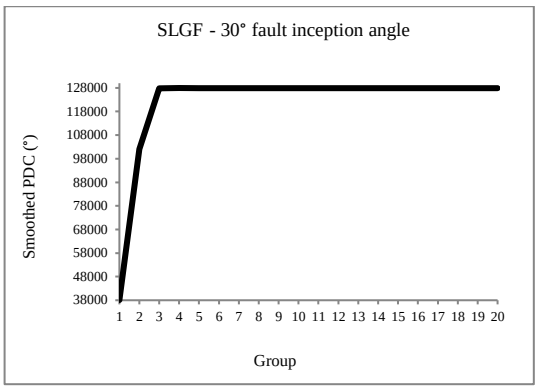

(b) 30° inception angle

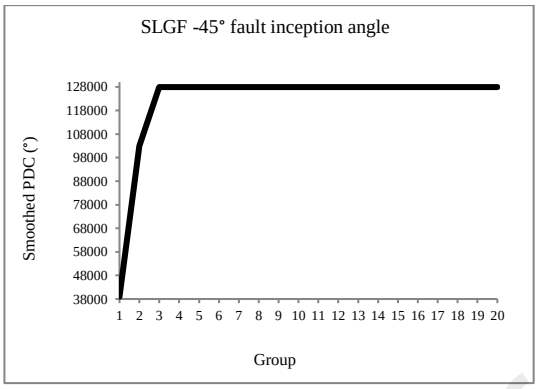

(c) 45° inception angle

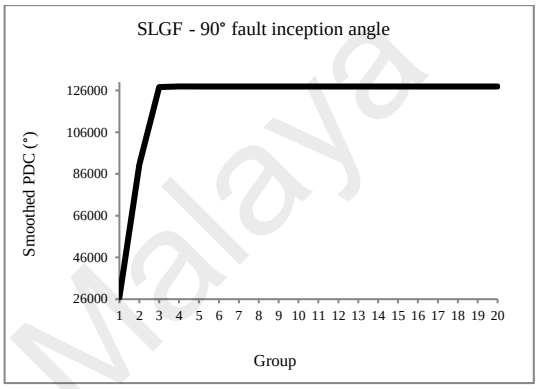

(d) 90° inception angle

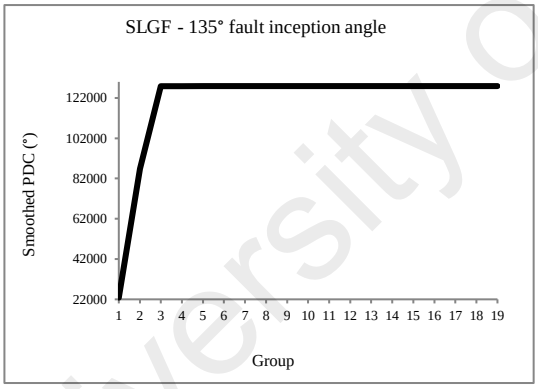

(e) 135° inception angle

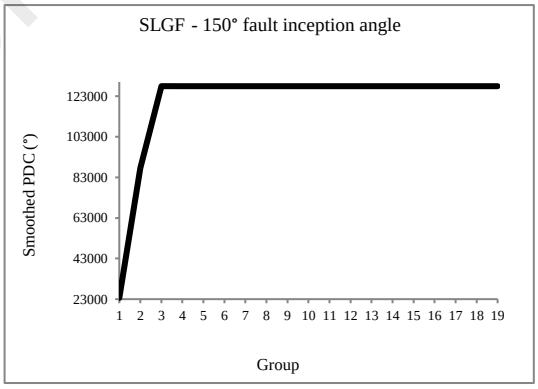

(f) 150° inception angle

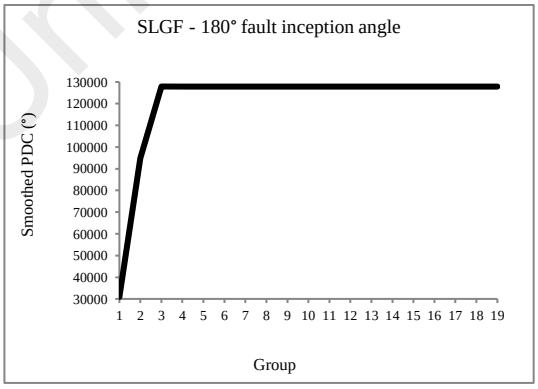

(g) 180° inception angle

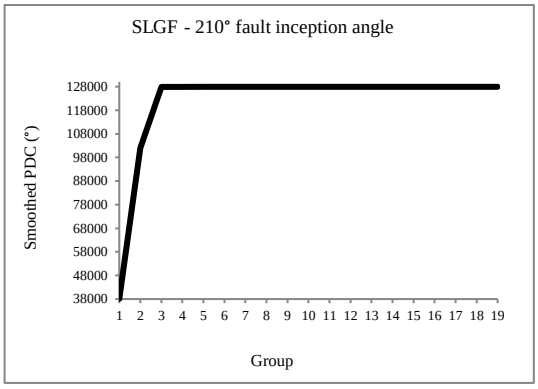

(h) 210° inception angle

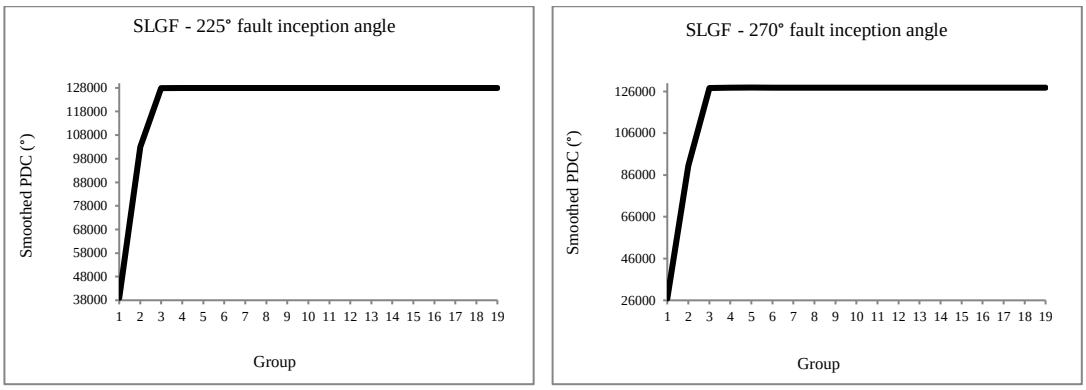

(i) 225° inception angle (j) 270° inception angle

Figure 4.9: Variation of fault inception angles

As shown in the Figure 4.9, it can be observed that there is no obvious peak and subsequent dip in the pattern of smoothed PDC if the fault inception angle is varied. Nevertheless, a small change in smoothed PDC magnitude between the different smoothed PDCs of various inception angle can be noticed.

4.3.3.2 Occurrence of multiple consecutive events

In this subsection, the occurrence of multiple consecutive events are simulated to evaluate the robustness of the proposed method. The purpose of this analysis is to observe the capability of the proposed method to identify the HIF event after a non-HIF event occurred in the system. Table 4.1 shows the sequence of events that are simulated consecutively one after another.

Table 4.1: Consecutive events occurring in the system

Figure 5.7	*t*= 1s	*t*= 1.2s	*t*= 1.4s
(a)	Motor starting	HIF fault	-
(b)	Capacitor switching	HIF fault	-
(c)	Load switching	HIF fault	-
(d)	Load switching	Capacitor switching	-
(e)	Motor starting	Load switching	Capacitor switching
(f)	Motor starting	Load switching	HIF fault

The first event occurs at *t=1s*, the second event at *t=1.2s* and the third event at *t=1.4s*. The events are simulated at BUS2 and the smoothed PDC of the events are shown in Figure 4.10. For instance, Figure 4.10(a) shows the smoothed PDC of a motor starting followed by a HIF event. As shown in the figure, a sharp peak is followed by a dip of the smoothed PDC indicating that this event is a non-HIF event. The onset of the second event is marked by the rise of the smoothed PDC to a plateau signifying that HIF has occurred.

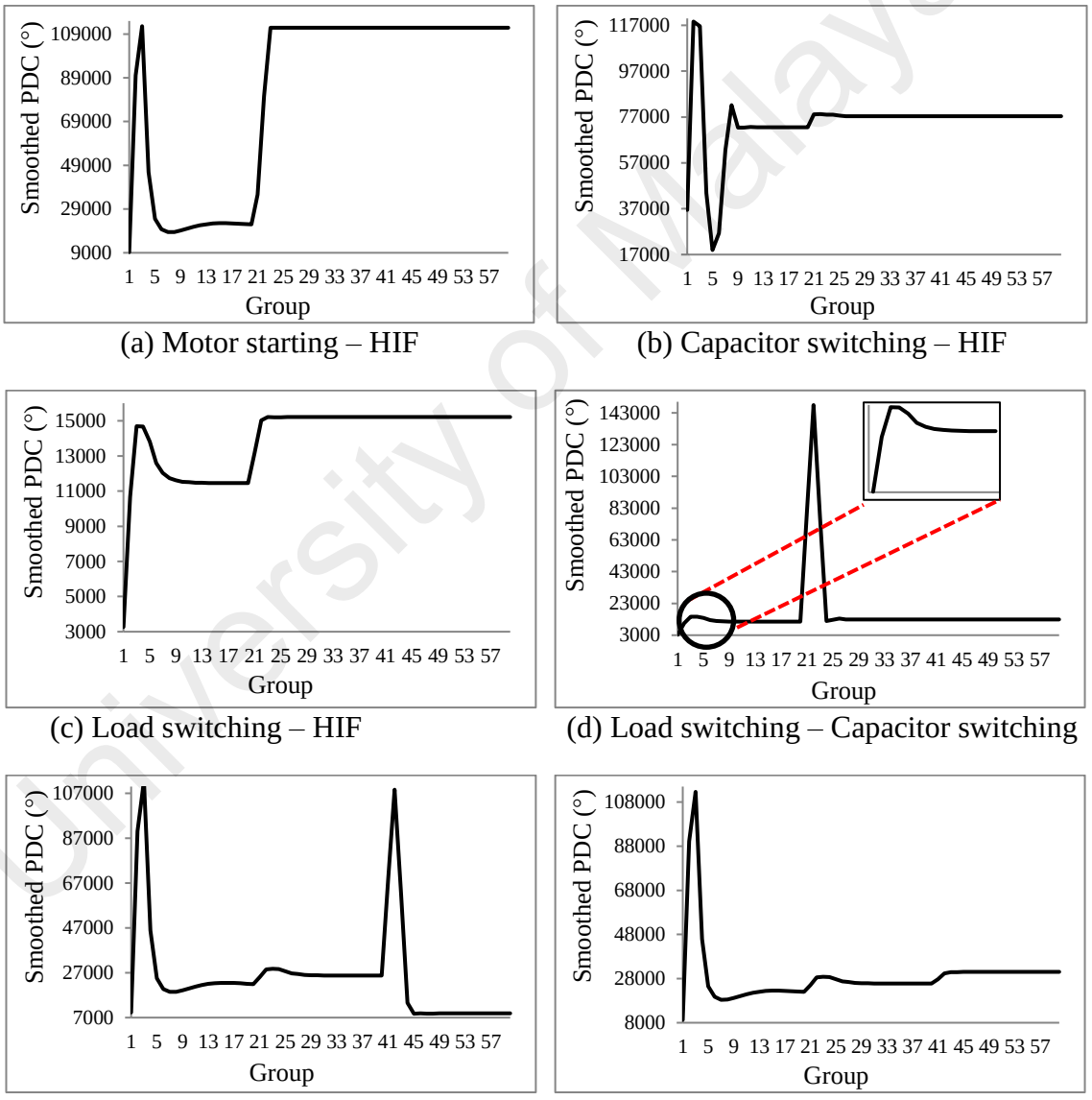

Figure 4.10: Pattern of the smoothed PDC

Figure 4.10(d) shows the pattern of smoothed PDC for two consecutive non-HIF events comprising of load switching first and then followed by capacitor switching events. As shown in the figure, it can be observed that the first event does not show noticeable peak and subsequent dip as compared to the second one. However, as depicted in the enlarged view of the circle part in the figure, it clearly shows a small peak and subsequent dip. Thus, both events are identified as a non-HIF event.

In contrast, Figure 4.10(f) shows the consecutive occurrence of motor starting, load switching and HIF events which are simulated at *t=1s*, *t=1.2s* and *t=1.4s* respectively. It can be observed that there is a peak and subsequent dip for the first two events and the peaks are pronounced for both events. Therefore, the proposed method identifies both events as non-HIF events. However, for the third event, the smoothed PDC reaches a plateau without a peak and subsequent dip. Thus, the occurrence of HIF event is identified.

4.3.4 High Impedance Fault Detection and Identification Based on Index

Previously, the occurrence of HIF is differentiated from non-HIF events based on the pattern of smoothed PDC. However, it has been noted that in some cases, it is difficult to detect the peak and subsequent dip pattern by the naked eyes as shown in Figure 4.10(d). As such, an automatic HIF classification algorithm is developed to simplify the identification process. In order to evaluate the effectiveness of the proposed algorithm, the same case studies as in Subsection 4.3.1 are repeated. Moreover, in this study, the events are simulated at four different locations that are at BUS2, BUS9, BUS14 and BUS27.

Table 4.2 to Table 4.5 show the results of the proposed automatic HIF classification algorithm for different types of event. The second column indicates the detection index (*D-index*) whereas the third column represents the identification index (*Id-index*). In this

proposed algorithm, the *D-index* is monitored first to detect the occurrence of any event in the system and also to differentiate it from normal fluctuation. An event is considered to occur if the value of *D-index* is lower than -200. Subsequently, the value of *Id-index* will be checked to determine whether it is HIF or non-HIF events. If the value of *Id-index* is lower than 0.01, then it will be considered as HIF event. Otherwise, it is a non-HIF event. Based on the obtained results, it can be observed that the proposed algorithm successfully classified the HIF and non-HIF events in all case studies.

Table 4.2: Capacitor switching event analysis

Capacitor Switching								
Q (MVaR)	BUS2		BUS9		BUS14		BUS27	
	D-index	*Id-index*	*D-index*	*Id-index*	*D-index*	*Id-index*	*D-index*	*Id-index*
2.5	-18494.89	0.49347	-28672.05	2.26460	-43461.83	0.67783	-36707.76	0.65995
1.5	-30909.55	0.71916	-66318.50	0.79723	-73841.18	0.89260	-67088.68	0.27606
0.5	-82217.08	0.83989	-106161.12	0.65645	-19307.84	0.55731	-19429.25	0.74698

Table 4.3: Load switching event analysis

Load Switching								
P/Q (3phase) (MW/MVaR)	BUS2		BUS9		BUS14		BUS27	
	D-index	*Id-index*	*D-index*	*Id-index*	*D-index*	*Id-index*	*D-index*	*Id-index*
0.3/0.24	-2852.47	0.10900	-2929.09	0.18611	-4228.74	0.08803	-4491.97	0.09665
0.75/0.36	-3203.02	0.13351	-2158.72	0.13684	-4162.06	0.17790	-4221.74	0.19221
1.5/0.9	-5716.35	0.14318	-5666.82	0.12981	-17984.52	0.12627	-19476.85	0.22009

Table 4.4: Motor starting event analysis

Motor Starting								
P (3phase) (MW)	BUS2		BUS9		BUS14		BUS27	
	D-index	*Id-index*	*D-index*	*Id-index*	*D-index*	*Id-index*	*D-index*	*Id-index*
0.6431	-955145.41	0.73453	-192120.45	0.21661	-23315.63	0.66934	-24221.66	0.67975
1.245	-51665.99	0.82490	-58663.68	0.84401	-26318.25	0.64914	-27480.54	0.66240
1.029	-32054.57	0.64355	-34748.64	0.66958	-31196.62	0.53570	-32853.08	0.55697

Table 4.5: HIF event analysis

HIF								
Fault type	BUS2		BUS9		BUS14		BUS27	
	D-index	Id-index	D-index	Id-index	D-index	Id-index	D-index	Id-index
A-G (50 ohm)	-37058.63	0.00000	-27644.10	0.00000	-33672.71	0.00000	-32631.21	0.00000
A-G (100 ohm)	-48266.71	0.00010	-49698.21	0.00004	-6736.06	0.00000	-30763.18	0.00000
A-B-G (50 ohm)	-15059.67	0.00000	-18553.23	0.00000	-10368.03	0.00000	-10720.72	0.00000
A-B-G (100 ohm)	-18685.65	0.00035	-18692.54	0.00012	-7195.17	0.00000	-7215.26	0.00000
B-C (50 ohm)	-4204.48	0.00048	-4087.50	0.00054	-2843.14	0.00000	-2892.59	0.00000
B-C (100 ohm)	-1954.98	0.00080	-1927.74	0.00086	-2006.28	0.00003	-2021.09	0.00004
A-B-C-G (50 ohm)	-2373.26	0.00315	-2353.64	0.00352	-2051.66	0.00010	-2060.97	0.00009
A-B-C-G (100 ohm)	-1286.64	0.00586	-1310.39	0.00524	-1049.94	0.00116	-1056.96	0.00089

Table 4.6 and Table 4.7 show the results of automatic HIF classification algorithm for HIF event with different fault inception angles. In this analysis, the effectiveness of the proposed algorithm regardless of fault inception angle is shown. Table 4.6 shows the results when the SLGF fault is applied at BUS2 with fault impedance value of 50Ω and 100Ω. Whereas Table 4.7 shows the results when the LLF fault is applied at BUS9 with fault impedance value of 50Ω and 100Ω. Based on the results, it is proven that the proposed automatic HIF classification algorithm is able to identify the occurrence of HIF events.

Table 4.6: Different fault inception angles (SLGF-BUS2)

Fault inception angle	A-G (50Ω)		A-G (100Ω)	
	D-index	*Id-index*	*D-index*	*Id-index*
0°	-48510.25	0.00004	-42479.51	0.00006
30°	-22453.15	0.00000	-20988.29	0.00000
45°	-44463.80	0.00013	-40568.98	0.00006
90°	-25263.60	0.00000	-23547.62	0.00000
135°	-26265.15	0.00000	-44467.02	0.00114
150°	-52177.70	0.00032	-31058.02	0.00000
180°	-48510.25	0.00004	-42479.51	0.00006
210°	-22453.15	0.00000	-20988.29	0.00000
225°	-44463.80	0.00013	-40568.98	0.00006
270°	-25263.60	0.00000	-23547.62	0.00000

Table 4.7: Different fault inception angles (LLF-BUS9)

Fault inception angle	B-C (50Ω)		B-C (100Ω)	
	D-index	*Id-index*	*D-index*	*Id-index*
0°	-4128.73	0.00172	-2005.49	0.00075
30°	-3099.12	0.00000	-1424.42	0.00000
45°	-3086.79	0.00000	-1441.83	0.00000
90°	-2906.20	0.00000	-1358.69	0.00000
135°	-3516.94	0.00238	-1498.86	0.00407
150°	-4249.14	0.00048	-1903.55	0.00037
180°	-4128.73	0.00172	-2005.49	0.00075
210°	-3099.12	0.00000	-1424.42	0.00000
225°	-3086.79	0.00000	-1441.83	0.00000
270°	-2906.20	0.00000	-1358.69	0.00000

Finally, to evaluate the robustness of the proposed automatic HIF classification algorithm, the occurrence of multiple consecutive events as in Subsection 4.3.3.2 is repeated and the results are shown in Table 4.8 and Table 4.9. Based on the results, it can be observed that the proposed algorithm has successfully identified the HIF events.

Table 4.8: Mix event analysis (BUS2)

BUS 2									
Case study	Event #1	Event #2	Event #3	*D-index #1*	*Id-index #1*	*D-index #2*	*Id-index #2*	*D-index #3*	*Id-index #3*
1	Starting Motor	HIF Fault (AGF)		-51665.99	0.82490	-29969.48	0.00038		
2	Capacitor Switching	HIF Fault (ABGF)		-82217.14	0.83989	-2939.06	0.08460		
3	Load Switching	HIF Fault (AB)		-5716.35	0.14318	-1252.25	0.00028		
4	Load Switching	Capacitor Switching		-5716.35	0.14318	-68231.77	0.91398		
5	Starting Motor	Load Switching	Capacitor Switching	-51665.99	0.82490	-2265.03	0.07121	-13818.71	0.91959
6	Starting Motor	Load Switching	HIF Fault (ABCGF)	-51665.99	0.82490	-2265.03	0.07121	-441.92	0.00030

Table 4.9: Mix event analysis (BUS9)

BUS 9									
Case study	Event #1	Event #2	Event #3	*D-index #1*	*Id-index #1*	*D-index #2*	*Id-index #2*	*D-index #3*	*Id-index #3*
1	Starting Motor	HIF Fault (AGF)		-58663.68	0.84401	-21461.57	0.00001		
2	Capacitor Switching	HIF Fault (ABGF)		-106161.12	0.65645	-1977.02	0.00712		
3	Load Switching	HIF Fault (AB)		-5666.82	0.12981	-255.92	0.00000		
4	Load Switching	Capacitor Switching		-5666.82	0.12981	-35606.50	0.84956		
5	Starting Motor	Load Switching	Capacitor Switching	-58663.68	0.84401	-1635.64	0.07239	-6941.10	0.86672
6	Starting Motor	Load Switching	HIF Fault (ABCGF)	-58663.68	0.84401	-1635.64	0.07239	-426.97	0.00076

Several other techniques that have been proposed by other authors to detect and identify the HIF events are summarized and can be compared in Table 4.10. Basically, all the previous techniques were able to discriminate between the HIF and non-HIF events with accuracy higher than 97%. However, in this proposed method, the obtained accuracy is 100%. Moreover, the proposed method is able to identify the HIF events, although multiple events were occurring consecutively.

Table 4.10 Comparison with other literatures

Techniques used in other similar paper	Type of event presented by each of the techniques				Accuracy	Subsequent events
	Non-HIF			HIF		
	Capacitor switching	Load switching	Motor starting			
WT (Shinde and Hase 2012)	Yes	No	No	Yes	-	No
DWT (Akorede and Katende 2010)	Yes	No	No	Yes	-	No
DWT and ANN (Vahidi, Ghaffarzadeh et al. 2010)	Yes	Yes	No	Yes	99%	Yes
WT, GA, fuzzy inference system and principal component analysis (Haghifam, Sedighi et al. 2006)	Yes	Yes	No	Yes	98.33%	No
WT and statistical pattern recognition (Sedighi, Haghifam et al. 2005)	Yes	Yes	No	Yes	97.60%	No
DWT, frequency range and RMS conversion (Lai, Snider et al. 2005)	Yes	No	No	Yes	97.48%	No
Proposed method	Yes	Yes	Yes	Yes	100%	Yes

4.4 Validation of Proposed Method for High Impedance Fault Localization

In this subsection, the performance of the proposed method for high impedance fault localization is evaluated. For this purpose, the ANN is trained first to obtain the optimal ANN variables. Various effects are investigated through fault distance estimation to obtain these optimal ANN variables. Subsequently, the obtained optimal ANN variables are utilized directly to train the ANN for fault type classification and fault impedance estimation. Finally, the ANN testing is conducted to evaluate the predictive capability of the saved network files during the ANN training.

4.4.1 ANN Training for Fault Distance Estimation

There are a total of 3993 ANN training cases of energy content consisting of 11 types of fault, 11 fault impedance values and 33 nodes. The energy contents for the ANN training cases are extracted using the Eq 3.6 and Eq 3.7 before they are being fed into the ANN for training. The fault impedance values range from 50Ω-150Ω (in step increment of 10Ω). Each of the 3993 resultant fault distance estimations from ANN training is then compared against the actual fault distance to calculate the average error of fault distance as follows:

$$Average\ error = \frac{\sum_{i=1}^{n} \left| fault\_dist_{estimated(i)} - fault\_dist_{actual(i)} \right|}{n} \quad 4.1$$

where

i = number of ANN training case

n = total number of ANN training cases (eg. 3993 for this case)

The training process is iterated for 50 times and only 10 iterations with the best average error results are shortlisted for analysis.

4.4.1.1 Selection of Mother Wavelets and Its Associated Levels of Decomposition

In this subsection, the performance of three different mother wavelets comprising of Biorthogonal (Bior3.3), Daubechies (Db4) and Symlet (Sym8) and its associated 4 levels of decomposition are investigated and compared to identify the best performing pair of mother wavelet and levels of decomposition. Table 4.11 to Table 4.13 show the shortlisted average error results for the 4 levels of decompositions for Biorthogonal3.3, Daubechies4 and Symlet8 mother wavelets respectively. The best combination of mother wavelet and its associated level of decomposition is determined based on the least average error.

Table 4.11: Average error results from Biorthogonal level 3.3 mother wavelet

Bior3.3				
Shortlisted Iterations	1st level	2nd level	3rd level	4th level
1	**0.0976**	0.1465	0.1400	0.1629
2	0.1018	0.1476	0.1625	0.1670
3	0.1081	0.1515	0.1627	0.1671
4	0.1210	0.1553	0.1631	0.1683
5	0.1282	0.1631	0.1641	0.1687
6	0.1491	0.1631	0.1644	0.1713
7	0.1606	0.1638	0.1673	0.1737
8	0.1731	0.1655	0.1674	0.1737
9	0.1785	0.1660	0.1684	0.1748
10	0.1851	0.1662	0.1695	0.1768

Table 4.12: Average error results from Daubechies level 4 mother wavelet

Db4				
Shortlisted Iterations	1st level	2nd level	3rd level	4th level
1	**0.1098**	0.1156	0.1403	0.1559
2	0.1292	0.1157	0.1488	0.1592
3	0.1390	0.1309	0.1537	0.1596
4	0.1444	0.1473	0.1554	0.1600
5	0.1466	0.1541	0.1569	0.1609
6	0.1530	0.1552	0.1577	0.1618
7	0.1648	0.1659	0.1651	0.1640
8	0.1701	0.1700	0.1657	0.1652
9	0.1703	0.1720	0.1671	0.1671
10	0.1707	0.1852	0.1757	0.1720

Table 4.13: Average error results from Symlet level 8 mother wavelet

Sym8				
Shortlisted Iterations	1st level	2nd level	3rd level	4th level
1	**0.1273**	0.1502	0.1540	0.1680
2	0.1374	0.1549	0.1648	0.1680
3	0.1466	0.1642	0.1657	0.1702
4	0.1649	0.1644	0.1671	0.1712
5	0.1688	0.1647	0.1724	0.1715
6	0.1700	0.1665	0.1725	0.1720
7	0.1767	0.1696	0.1727	0.1747
8	0.1767	0.1696	0.1727	0.1765
9	0.1786	0.1697	0.1730	0.1768
10	0.1791	0.1719	0.1762	0.1770

As shown in the tables, it can be observed that the least average error for each type of mother wavelet is obtained in the first level of decomposition. The obtained average error are 0.0976, 0.1098 and 0.1273 for Bior3.3, Db4 and Sym8 mother wavelets respectively. As such, Bior3.3 mother wavelet at the 1st level of decomposition is selected to represent the best combination of mother wavelet and its associated level of decomposition.

4.4.1.2 Effect of Variations in ANN Parameters

In this subsection, the effect of variations in ANN parameters comprising of learning rate (*lr*), momentum constant (*mc*) and number of neurons in hidden layer (*p*) is investigated. A total of six input data for each of the 3993 ANN training cases are fed into the ANN. The 6 input data comprises of the 3 phases voltage and current energy contents that are extracted from the 1st level of decomposition of the Bior3.3 mother wavelet. This combination of mother wavelet and its associated level of decomposition is selected based on the results obtained from the previous investigation.

Table 4.14 shows the result when the value of *lr* is changed while the values of *mc* and *p* are fixed. For this purpose, the value of *mc* is set to 0.95 and *p*=6, while the values of *lr* are set to 0.3, 0.5 and 0.8. As shown in the table, it can be observed that the obtained average error changes as the value of *lr* changes.

Table 4.14: Changing the value of *lr*

p = 6, *mc* = 0.95	
lr	Average error (km)
0.3	0.0976
0.5	0.0899
0.8	0.0910

Table 4.15 displays the results when the values of *mc* are varied between 0.35, 0.65 and 0.95. Here, the value of *lr* and *p* are fixed to 0.3 and 6 respectively. As depicted in the table, it can be observed that the average error increases as the value of *mc* increases.

Table 4.15: Changing the value of *mc*

p = 6, *lr* = 0.3	
mc	Average error (km)
0.35	0.0875
0.65	0.0921
0.95	0.0976

Lastly, the effects of changing the value of *p* is shown in Table 4.16. Here, the value of *mc* and *lr* are set to 0.95 and 0.3 respectively. Whereas, the values of *p* are varied between 3, 6 and 12. From the table, it can be observed that the average error decreases as the value of *p* increases.

Table 4.16: Changing the number of *p*

mc = 0.95, *lr* = 0.3	
p	Average error (km)
3	0.1604
6	0.0976
12	0.0250

As shown in Table 4.14 to Table 4.16, it can be noticed that the performance of ANN can be influenced by changing the values of ANN parameters such as *lr*, *mc* and *p*. A summary of the above results is shown in Figure 4.11. It can be observed that the right combinations and values for these parameters are important to ensure that the obtained average error is small. Unfortunately, it is difficult to determine the optimal values for these ANN parameters concurrently. Therefore, an optimization technique is proposed to determine the optimal values for these parameters in the next section.

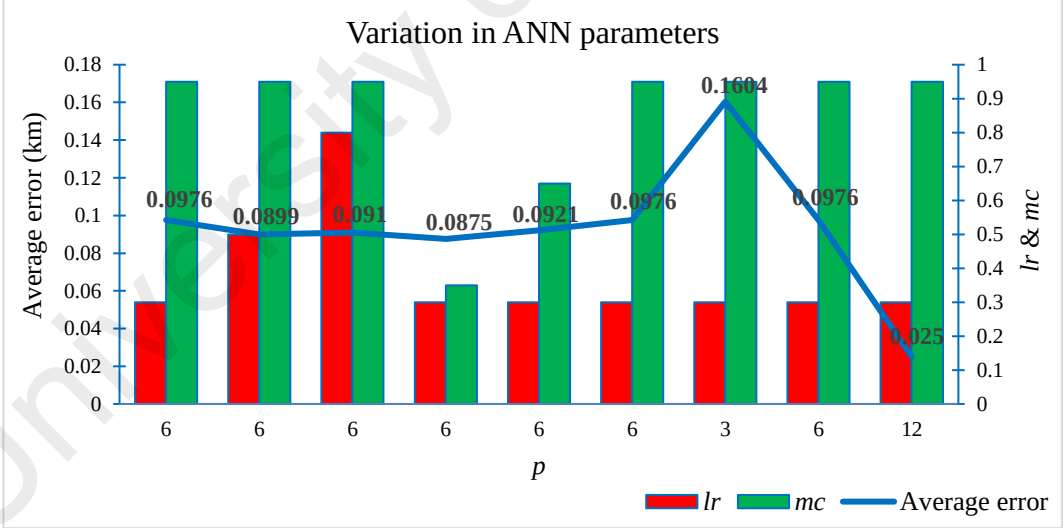

Figure 4.11: Average error results for different combinations of ANN parameter

(a) ***Effect of Performing ANN Parameters Optimization through GWO***

In this subsection, the Grey Wolf Optimization (GWO) technique is proposed to determine the optimal values of ANN parameters comprising of *lr*, *mc* and *p*. Table 4.17 shows the average error results when the 6 input data from the previous section are fed

into the ANN. The second column shows the best combination of ANN parameters that are manually determined from the previous investigation. The third column shows the best values of ANN parameters that are determined using the GWO. It can be seen that GWO managed to identify the optimal ANN parameters, thus deliver a least average error in the fault distance algorithm.

Table 4.17: Average error results for different combinations of ANN parameters

	The best combination of ANN parameters that are manually determined	The best combination of ANN parameters that determined by GWO
lr	0.30	0.4137
mc	0.95	0.4091
p	12	58
Average error (km)	0.0250	0.0069

4.4.1.3 Effect of Different Types of ANN Learning Algorithm

In this subsection, the effects of different types of ANN learning algorithm are investigated. The performance of each learning algorithms in ANN is evaluated with the assistance of GWO technique. Table 4.18 shows the average error results for different types of learning algorithms. As shown in the table, *trainlm* delivered the least average errors with the values of 0.0174.

Table 4.18: Average error results for different types of learning algorithm

Learning algorithm (Mathworks 2016)	*lr*	*mc*	*p*	Average error (km)
trainbfg	0.414	0.6648	9	0.1261
trainbr	0.0065	0.6041	15	0.0394
traincgb	0.4214	0.9263	18	0.5293
traincgf	0.5272	0.4695	17	0.5041
traincgp	0.1508	0.5901	4	0.5262
trainlm	**0.4706**	**0.2387**	**24**	**0.0174**
trainoss	0.2155	0.4998	9	0.5857
trainr	0.6236	0.7638	2	0.6274
trainrp	0.7356	0.6722	14	0.5351
trainscg	0.7724	0.1303	13	0.5661

4.4.1.4 Effect of Performing Dataset Categorization

In the previous investigation, all the training cases comprising of 11 types of faults are fed into the ANN to be trained together. However, further investigation is conducted to observe the effect of performing dataset categorization, where the training process is conducted separately for each category of fault types – BF, SLGF, LLGF and LLF types of fault. Here, the performance is evaluated based on both the average error and maximum error.

Table 4.19 shows the results and comparison when the dataset categorization is performed and each category of fault types is trained separately. As shown in the table, the obtained average error reduces significantly for SLGF and LLGF while the improvement is only marginal for BF and LLF if each type of faults is trained separately. Moreover, it is observed that the obtained maximum error decreases for all types of fault except for BF type of fault where it experiences a slight increase from 0.3539 to 0.3604.

Table 4.19: Results for separating different types of fault

Training	Fault type	Average error (km)	Maximum error (km)
Combined	BF	0.0623	0.3539
	SLGF	0.0278	0.2646
	LLGF	0.0341	0.1726
	LLF	0.0495	0.2151
Separate	BF	0.0592	0.3604
	SLGF	0.0089	0.0796
	LLGF	0.0130	0.1170
	LLF	0.0458	0.1924

4.4.1.5 Effect of Different Number and Combinations of Input Data

In this subsection, the effects of different number and combinations of input data being fed into the ANN are investigated. The comparison analysis is first conducted using 3 consistent input data in each level of MRA-DWT decompositions. Then, the comparative analysis is conducted for more input data comprising of consistent data from multiple

different combinations of MRA-DWT decompositions levels. Finally, the analysis for random selection of input data is also performed. A comparison of the results with and without the GWO technique in the above analysis is also conducted.

(a) ***Variation in the Number of Input Data***

In this investigation, the effects of a different number of input data to be fed into the ANN are observed. There are 5 scenarios wherein the number of input data is varied between 3, 6, 12, 18 and 24 input data. For each scenario, the best combination of input data is determined based on the average error. Then, this best combination of input data will be further trained with the application of GWO.

Table 4.20 shows the first scenario results when only 3 input data are fed into the ANN to estimate the fault distance. The input data can be either 3 phases of voltage or current energy contents from the same level of decomposition. This analysis is then repeated for every level of decomposition. The first column shows the level of decomposition, the second column represents the combination of input data and the third column shows the average error results. As shown in the table, the least value of the average error is 0.1818, which is obtained when the 1st level of 3 phases of voltage energy content is used.

Table 4.20: Average error results utilizing 3 input data

Level of decomposition	Input combination	Average error (km)
1st level	$sEV_a^1, sEV_b^1, sEV_c^1$	**0.1818**
	$sEI_a^1, sEI_b^1, sEI_c^1$	0.1840
2nd level	$sEV_a^2, sEV_b^2, sEV_c^2$	0.1821
	$sEI_a^2, sEI_b^2, sEI_c^2$	0.1834
3rd level	$sEV_a^3, sEV_b^3, sEV_c^3$	0.1825
	$sEI_a^3, sEI_b^3, sEI_c^3$	0.1839
4th level	$sEV_a^4, sEV_b^4, sEV_c^4$	0.1824
	$sEI_a^4, sEI_b^4, sEI_c^4$	0.1841

Whereas in Table 4.21, the average error results are shown when 6 input data consisting of 3 phases of voltage and current energy contents at the same level of decomposition are fed into the ANN. This analysis is then repeated for every level of decomposition. As depicted in the table, the least average error is obtained when the combination of 3 phases of voltage and current energy contents at the first level of decomposition is used. The obtained average error is 0.0976

Table 4.21: Average error results utilizing 6 input data

Level of decomposition	Input combination	Average error (km)
1st level	$sEV_a^1, sEV_b^1, sEV_c^1, sEI_a^1, sEI_b^1, sEI_c^1$	**0.0976**
2nd level	$sEV_a^2, sEV_b^2, sEV_c^2, sEI_a^2, sEI_b^2, sEI_c^2$	0.1465
3rd level	$sEV_a^3, sEV_b^3, sEV_c^3, sEI_a^3, sEI_b^3, sEI_c^3$	0.1400
4th level	$sEV_a^4, sEV_b^4, sEV_c^4, sEI_a^4, sEI_b^4, sEI_c^4$	0.1629

Table 4.22 shows the average error results when 12 input data are fed into the ANN. The input data consists of 3 phases of voltage and current energy contents from a combination of 2 decomposition levels as shown in the table. The least average error recorded is 0.0122, which is obtained when the 1st and 2nd levels of decomposition data are used.

Table 4.22: Average error results utilizing 12 input data

Level of decomposition	Input combination	Average error (km)
1st & 2nd level	$sEV_a^1, sEV_b^1, sEV_c^1, sEI_a^1, sEI_b^1, sEI_c^1$ $sEV_a^2, sEV_b^2, sEV_c^2, sEI_a^2, sEI_b^2, sEI_c^2$	**0.0122**
1st & 3rd level	$sEV_a^1, sEV_b^1, sEV_c^1, sEI_a^1, sEI_b^1, sEI_c^1$ $sEV_a^3, sEV_b^3, sEV_c^3, sEI_a^3, sEI_b^3, sEI_c^3$	0.0133
1st & 4th level	$sEV_a^1, sEV_b^1, sEV_c^1, sEI_a^1, sEI_b^1, sEI_c^1$ $sEV_a^4, sEV_b^4, sEV_c^4, sEI_a^4, sEI_b^4, sEI_c^4$	0.0143

2nd & 3rd level	$sEV_a^2, sEV_b^2, sEV_c^2, sEI_a^2, sEI_b^2, sEI_c^2$ $sEV_a^3, sEV_b^3, sEV_c^3, sEI_a^3, sEI_b^3, sEI_c^3$	0.0126
2nd & 4th level	$sEV_a^2, sEV_b^2, sEV_c^2, sEI_a^2, sEI_b^2, sEI_c^2$ $sEV_a^4, sEV_b^4, sEV_c^4, sEI_a^4, sEI_b^4, sEI_c^4$	0.0139
3rd & 4th level	$sEV_a^3, sEV_b^3, sEV_c^3, sEI_a^3, sEI_b^3, sEI_c^3$ $sEV_a^4, sEV_b^4, sEV_c^4, sEI_a^4, sEI_b^4, sEI_c^4$	0.0146

Table 4.23 and Table 4.24 show the average error results when the number of input data are increased to 18 and 24 respectively. As shown in Table 4.23, the least value of the average error is 0.0089, which is obtained when the combination of the 2nd, 3rd and 4th levels of decomposition is used. Whereas in Table 4.24, it shows that the obtained average error is 0.0084 when 24 input data are fed into the ANN altogether to estimate the fault distance.

Table 4.23: Average error results utilizing 18 input data

Level of decomposition	Input combination	Average error (km)
1st, 2nd & 3rd level	$sEV_a^1, sEV_b^1, sEV_c^1, sEI_a^1, sEI_b^1, sEI_c^1$ $sEV_a^2, sEV_b^2, sEV_c^2, sEI_a^2, sEI_b^2, sEI_c^2$ $sEV_a^3, sEV_b^3, sEV_c^3, sEI_a^3, sEI_b^3, sEI_c^3$	0.0098
1st, 2nd & 4th level	$sEV_a^1, sEV_b^1, sEV_c^1, sEI_a^1, sEI_b^1, sEI_c^1$ $sEV_a^2, sEV_b^2, sEV_c^2, sEI_a^2, sEI_b^2, sEI_c^2$ $sEV_a^4, sEV_b^4, sEV_c^4, sEI_a^4, sEI_b^4, sEI_c^4$	0.0096
1st, 3rd & 4th level	$sEV_a^1, sEV_b^1, sEV_c^1, sEI_a^1, sEI_b^1, sEI_c^1$ $sEV_a^3, sEV_b^3, sEV_c^3, sEI_a^3, sEI_b^3, sEI_c^3$ $sEV_a^4, sEV_b^4, sEV_c^4, sEI_a^4, sEI_b^4, sEI_c^4$	0.0097
2nd, 3rd & 4th level	$sEV_a^2, sEV_b^2, sEV_c^2, sEI_a^2, sEI_b^2, sEI_c^2$ $sEV_a^3, sEV_b^3, sEV_c^3, sEI_a^3, sEI_b^3, sEI_c^3$ $sEV_a^4, sEV_b^4, sEV_c^4, sEI_a^4, sEI_b^4, sEI_c^4$	**0.0089**

Table 4.24: Average error results utilizing 24 input data

Level of decomposition	Input combination	Average error (km)
1st, 2nd, 3rd & 4th level	$sEV_a^1, sEV_b^1, sEV_c^1, sEI_a^1, sEI_b^1, sEI_c^1$ $sEV_a^2, sEV_b^2, sEV_c^2, sEI_a^2, sEI_b^2, sEI_c^2$ $sEV_a^3, sEV_b^3, sEV_c^3, sEI_a^3, sEI_b^3, sEI_c^3$ $sEV_a^4, sEV_b^4, sEV_c^4, sEI_a^4, sEI_b^4, sEI_c^4$	**0.0084**

Based on the above observations, the best combination of input data with the least average error for each scenario is further investigated with the application of GWO technique. Table 4.25 shows the results for this investigation. The first column indicates the number of data being fed into the ANN. The second until fourth columns show the optimal values of ANN parameters given by GWO. Whereas, the fifth column shows the average error results. As shown in the table, it can be observed that the average error reduces as the number of input data increases. However, the obtained average errors from 12 to 24 input data do not show substantial improvement.

Table 4.25: Average error results with application of GWO

No. of data	*lr*	*mc*	*p*	Average error (km)
3	0.0754	0.0753	6	0.1640
6	0.4032	0.4091	11	0.0241
12	1.000	1.000	24	0.0077
18	0.3653	0.3653	35	0.0070
24	0.4900	0.4905	31	0.0069

A comparison in terms of average error between the stand-alone ANN with GWO-ANN for a different number of input data is shown in Table 4.26. As depicted in the table, the obtained average error is higher for the stand-alone ANN as compared to GWO-ANN for all different number of input data. The most promising result is obtained when GWO-

ANN with 12 input data delivered a lower average error than the stand-alone ANN with 24 input data.

Table 4.26: Comparison between stand-alone ANN with GWO-ANN

No. of input data	Average error (km)	
	Stand-alone ANN	GWO-ANN
3 inputs	0.1818	0.1640
6 inputs	0.0976	0.0241
12 inputs	0.0122	0.0077
18 inputs	0.0089	0.0070
24 inputs	0.0084	0.0069

Figure 4.12 illustrates the comparison between the stand-alone ANN with GWO-ANN for different numbers of input data. The average error for GWO-ANN is consistently lower than the stand-alone ANN, especially for 6 input data where the value of average error reduces significantly. Increasing the number of input data beyond 6 will only improve the accuracy slightly.

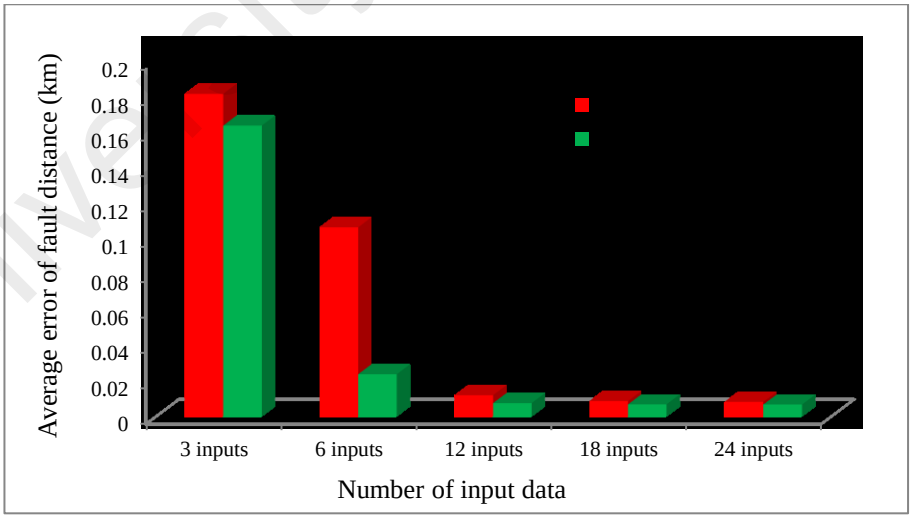

Figure 4.12: Average error results between stand-alone ANN with GWO-ANN

(b) ***Random Selection of Input Data (6 Input Data)***

In the previous investigation, it was observed that utilizing too many input data does not lead to corresponding linear improvement in the accuracy of ANN as the obtained average error for 12 input data and 24 input data represents a minimal improvement in accuracy. In this subsection, further investigation is conducted to select the minimum number of input data, which can still improve the ANN accuracy. For this purpose, 6 input data are considered because the difference of average error between 3 and 6 input data is quite big and the difference is only minimal for 6 and 12 input data as shown in Figure 4.12. To improve the ANN accuracy, the best random combination of 6 input data which are randomly selected from 24 available input data is determined. It is observed that in the previous investigation, the best combination of 6 input data is selected from the same level of decomposition. As such, the previous investigation had neglected the distinctive data from the other levels of decomposition. Therefore, in this investigation, it is to be expected that by evaluating the strength of each input data and its combinations might improve the ANN accuracy. For this purpose, an exhaustive technique is used to obtain the best random combination of 6 input data and there are a total of 134596 random combinations that can be obtained using this technique.

In this investigation, all 134596 random combinations are first evaluated using the stand-alone ANN and each random combinations is iterated for 50 times. Besides that, all the training cases are fed into the ANN altogether to be trained. The reason is to reduce the computational time. Table 4.27 shows the results for the 5 best random combinations with the least value of average error. As shown in the table, the least average error (0.0770) is obtained when the first level of phase-A and phase-B voltage decomposition, the second level of phase-C voltage and phase-B current together with the fourth level decomposition of phase-C voltage and current are selected.

Table 4.27: Average error for different random combinations of 6 input data

No.	Random combinations	Average error (km)
1	$V_a^1, V_b^1, V_c^2, I_b^2, V_c^4, I_c^4$	**0.0770**
2	$V_b^1, V_c^1, I_a^1, V_a^2, I_c^2, V_c^3$	0.0779
3	$V_a^1, V_c^1, I_c^1, V_b^3, I_b^3, V_b^4$	0.0786
4	$V_b^1, V_c^1, V_a^2, I_b^2, V_b^3, I_a^3$	0.0804
5	$V_c^1, I_a^1, V_a^2, V_b^2, I_c^3, V_a^4$	0.0819

Subsequently, the above analysis is repeated with the assistance of GWO-ANN. In this investigation, the best random combination of input data is first categorized into different types of fault, similar to the investigation conducted in Subsection 4.4.1.4, before the ANN can be trained with the application of GWO technique. Table 4.28 shows the comparison of average error results between the first level of decomposition input data and the best random combination of input data. It can be observed that the values of average error are reduced significantly for each category of fault types.

Table 4.28: Comparison of average error for different 6 input data using GWO

Type of fault	Average error (km)	
	Using 1st level of decomposition	Using the best random combination
BF	0.0592	0.0089
SLGF	0.0089	0.0014
LLGF	0.0130	0.0030
LLF	0.0458	0.0077

4.4.1.6 Effect of Different Objective Functions for GWO Technique

In this subsection, further investigation is conducted to evaluate the effect of different objective functions, *ObjFunc* for GWO technique. In the previous investigation, the *AverError* was assigned as the *ObjFunc*. However, in this subsection, the effects of different types of *ObjFunc* are evaluated and the best *ObjFunc* to be implemented in

GWO technique is selected. To evaluate the performance for each *ObjFunc*, the average error, maximum error and standard deviation of the estimated fault distance are evaluated. In this investigation, the best *ObjFunc* is the one that results in the least values of average error, maximum error and standard deviation altogether.

Table 4.29 shows the average error, maximum error and standard deviation results for different types of *ObjFunc* for the BF type of fault. The first column indicates the *ObjFunc* to be assigned in GWO. The second to the fourth columns represent the obtained average error, maximum error and standard deviation. As shown in the table, it can be observed that the least value of the average error is obtained when the *AverError* is used as the *ObjFunc*. Similar observations are noticed for the maximum error and standard deviation.

Table 4.29: The average error, maximum error and standard deviation for different *ObjFuncs* under BF

BF			
ObjFunc	Average error (km)	Maximum error (km)	Standard deviation (km)
AverError	**0.0592**	0.3604	0.0667
MaxError	0.0639	**0.3140**	0.0650
StD	0.0695	0.3551	**0.0621**

Table 4.30 shows the results for the SLGF. As shown in the table, it can be observed that the least value of the average error, maximum error and standard deviation altogether can be obtained if the *StD* is assigned as the *ObjFunc*.

Table 4.30: The average error, maximum error and standard deviation for different *ObjFuncs* under SLGF

SLGF			
ObjFunc	Average error (km)	Maximum error (km)	Standard deviation (km)
AverError	0.0089	0.0796	0.0080
MaxError	0.0102	0.0730	0.0097
StD	**0.0077**	**0.0343**	**0.0066**

Table 4.31 and Table 4.32 show the results for LLGF and LLF respectively. As shown in Table 4.31, the least values of average error and standard deviation are obtained when the *AverError* is assigned as the *ObjFunc*. Whereas the least value of the maximum error is obtained when *Std* is assigned. For the LLF shown in Table 4.32, similar observation as per the results for BF type of fault is obtained.

Table 4.31: The average error, maximum error and standard deviation for different *ObjFuncs* under LLGF

LLGF			
ObjFunc	Average error (km)	Maximum error (km)	Standard deviation (km)
AverError	**0.0130**	0.1170	**0.0132**
MaxError	0.0190	0.1170	0.0174
StD	0.0158	**0.1053**	0.0154

Table 4.32: The average error, maximum error and standard deviation for different *ObjFuncs* under LLF

LLF			
ObjFunc	Average error (km)	Maximum error (km)	Standard deviation (km)
AverError	**0.0458**	0.1924	0.0423
MaxError	0.0527	**0.1672**	0.0396
StD	0.0502	0.1736	**0.0386**

It is crucial to note that in this study, the GWO can only accept a single *ObjFunc*. Thus, based on the investigations above, *StD* is selected as a good candidate to represent the *ObjFunc*, where it delivered the highest number of best results.

4.4.1.7 Effect of Different Types of Optimization Techniques in Optimizing ANN Parameters

In this subsection, different types of optimization technique, which are the Particle Swarm Optimization (PSO) and Evolutionary Programming (EP) are implemented and compared against the GWO. The performance of these optimization techniques is compared in terms of accuracy and training time.

Table 4.33 to Table 4.36 show the average error results for all types of optimization technique for the BF, SLGF, LLGF and LLF types of fault respectively. The results for each type of fault show that the obtained average error was close to each other for all types of optimization techniques. It can be observed that for the BF and SLGF types of fault, the GWO technique delivered a slightly better performance as compared to the PSO and EP techniques. However, for the LLGF and LLF types of fault, EP and PSO techniques recorded the least value of average error respectively. In terms of the number of neurons utilized, it can be observed that the EP suggested the least number of neurons for the BF and LLF types of fault with 16 and 10 neurons respectively. Whereas for the SLGF and LLGF, the least number of neurons utilized are given by PSO and GWO with 14 and 27 neurons respectively.

Table 4.33: Different types of optimization techniques under BF

BF				
Optimization method	*lr*	*mc*	*p*	Average error (km)
GWO	**0.1991**	**0.2608**	**19**	**0.00858**
PSO	0.6713	0.6602	22	0.00862
EP	0.6449	0.1385	16	0.00862

Table 4.34: Different types of optimization techniques under SLGF

SLGF				
Optimization method	*lr*	*mc*	*p*	Average error (km)
GWO	**0.7276**	**0.1411**	**21**	**0.00136**
PSO	0.3965	0.6639	14	0.00194
EP	0.6704	0.9635	20	0.00163

Table 4.35: Different types of optimization techniques under LLGF

LLGF				
Optimization method	*lr*	*mc*	*p*	Average error (km)
GWO	0.2798	0.6545	27	0.00304
PSO	0.7264	0.5822	29	0.00287
EP	**0.4712**	**0.5858**	**52**	**0.00286**

Table 4.36: Different types of optimization techniques under LLF

LLF				
Optimization method	*lr*	*mc*	*p*	Average error (km)
GWO	0.3958	0.1943	60	0.00742
PSO	**0.1523**	**0.9579**	**40**	**0.00739**
EP	0.6423	0.3703	10	0.00745

It is important to note that all the optimization techniques delivered excellent results. It can be observed that GWO delivered a better performance in terms of accuracy as compared to the others, whereas EP delivered a good performance in terms of training time. However, GWO is selected to represent the best optimization technique because, in this analysis, the accuracy is more important than training time.

4.4.1.8 Summary for ANN Training in Fault Distance Estimation

The summary of the above investigations are as follows:

1) Different types of the mother wavelet: The Bior3.3 mother wavelet delivered better performance as compared to the Db4 and Sym8 mother wavelets.
2) Variations in ANN parameters: It was demonstrated that different values in ANN parameters influence the ANN accuracy. The implementation of GWO allows the optimal values for the ANN parameters to be identified and thus increasing the ANN accuracy.
3) Different types of ANN learning algorithm: *trainlm* delivered the best result as compared to the other learning algorithms.

4) Performing dataset categorization: The ANN accuracy improves significantly if each type of fault is trained separately in dedicated dataset category.
5) Different number and combinations of input data: Increasing the number of input data increases the accuracy. The best accuracy is obtained from a combination of 6 input data from different levels of MRA-DWT decomposition.
6) Different types of *ObjFunc:* The *StD* delivered better performance as compared to the *AverError* and *MaxError*.
7) Different types of optimization technique: GWO delivered better performance as compared to PSO and EP.

4.4.2 ANN Training for Fault Type Classification

In the previous section, thorough investigation for ANN training process to obtain the optimal ANN variables have been conducted to estimate the fault distance. As such, in this section, the previously obtained optimal ANN variables are utilized directly to classify the fault type. Here, the same process to estimate the fault distance is repeated to classify the fault types. As such, the best combination of 6 input data determined from Section 4.4.1.5 (b) is fed into the ANN and GWO technique with *Std* as the *ObjFunc* is used to provide the optimal values of ANN parameters. There are 11 types of fault to be classified namely AGF, BGF, CGF, ABGF, ACGF, BCGF, ABF, ACF, BCF, ABCGF and ABCF, with notations as shown in Table 4.37 .

Table 4.37: Fault types and its number notation

Types of fault	Number notation
AGF	1
BGF	2
CGF	3
ABGF	4
ACGF	5
BCGF	6
ABF	7
ACF	8
BCF	9
ABCGF	10
ABCF	11

Table 4.38 shows the results for the training of fault type classification. There are 363 ANN training cases consisting of 11 fault impedance values applied at 33 nodes for each type of fault. As shown in the table, it can be observed that the proposed method delivered high accuracies in which each type of fault can be classified accurately except for ABCGF and ABCF types of fault. A total of 21 and 12 ANN training cases that were misclassified by the proposed method for ABCGF and ABCF respectively. A thorough investigation found that the error is due to the similarity of the input data between the 50Ω ABCGF and 150Ω ABCF. For instance, the same data are obtained for the ABCGF type of fault that occurs at node 4 with 50Ω fault impedance and the ABCF type of fault that occurs at node 3 with 150Ω fault impedance as shown in Table 4.39. Therefore, the proposed method is facing difficulties to classify the fault type for this data, which can be either ABCGF or ABCF.

Table 4.38: Fault type identification

Type of fault	No. of ANN training cases	No. of ANN training cases that accurately identified by the proposed method
AGF	363	363
BGF	363	363
CGF	363	363
ABGF	363	363
ACGF	363	363
BCGF	363	363
ABF	363	363
ACF	363	363
BCF	363	363
ABCGF	363	342
ABCF	363	351

Table 4.39: Similarity data between two different scenarios

Node		1	2	3	4	5
50Ω (ABCGF)	1st data	-12.33	-12.38	-12.50	-12.50	-12.52
	2nd data	-12.05	-12.10	-12.22	-12.23	-12.25
	3rd data	-8.67	-8.72	-8.87	-8.88	-8.91
	4th data	3.97	3.96	3.93	3.92	3.91
	5th data	2.41	2.32	2.08	2.05	1.99
	6th data	4.71	4.70	4.66	4.66	4.64
150Ω (ABCF)	1st data	-12.38	-12.49	-12.50	-12.52	-12.54
	2nd data	-12.10	-12.22	-12.23	-12.25	-12.27
	3rd data	-8.72	-8.87	-8.88	-8.91	-8.93
	4th data	3.96	3.93	3.92	3.91	3.90
	5th data	2.32	2.08	2.05	1.99	1.93
	6th data	4.69	4.66	4.66	4.64	4.63

4.4.3 ANN Training for Fault Impedance Estimation

In this subsection, the fault impedance is estimated using the same method as in Subsection 4.4.2. The fault impedance value considered in this analysis ranges from 50Ω to 150Ω. Table 4.40 shows the training results for the estimation of fault impedance. The table only shows the maximum error of fault impedance estimation for each type of fault. It can be observed that all the fault impedances can be estimated accurately with the

maximum error of 0.24253Ω, 0.21269Ω, 0.22660Ω and 0.20346Ω for the SLGF, LLGF LLF and BF cases respectively.

Table 4.40: Maximum error of fault impedance estimation

Fault type	Maximum error of fault impedance estimation (Ω)
SLGF	0.24253
LLGF	0.21269
LLF	0.22660
BF	0.20346

4.4.4 ANN Testing for Fault Location Determination

As mentioned earlier, to evaluate the predictive capability of the saved network files, new testing data are generated in which the fault is applied in the middle of each line section with different fault types and fault impedances as shown in Table 4.41. The fault impedances are set systematically in increment by 10Ω for each type of fault in order to test the saved network file with all the possibilities of fault types and fault impedance values.

Table 4.41: Fault type and fault impedance for testing

Fault type		Fault impedance
SLGF	AGF	45Ω & 155Ω
	BGF	55Ω
	CGF	65Ω
LLGF	ABGF	75Ω
	ACGF	85Ω
	BCGF	95Ω
LLF	ABF	105Ω
	ACF	115Ω
	BCF	125Ω
BF	ABCGF	65Ω & 135Ω
	ABCF	95Ω & 145Ω

In this analysis, the fault distance is estimated by using the 3 best network files from a total of 50 network files obtained in Section 4.4.1.6. Subsequently, the average value of the estimated fault distances is calculated as shown in Table 4.42. The table shows an example when 45Ω of fault impedance with the AGF type of fault is applied in the middle of line Section 1. It can be observed that the first estimated fault distance is 0.1546km, which yields the absolute error of fault distance of 0.0954km. Whereas, the absolute error of 0.0899km and 0.1177km are obtained if only the second or the third network file is used respectively. However, if the average value is considered, then the final estimated fault distance will be 0.2874km. Thus, the absolute error is reduced considerably to the value of 0.0374km.

Table 4.42: AGF type of fault in the middle of line Section 1 with 45Ω of fault impedance

Section	Estimation of fault distance (km)				Actual fault distance (km)	Error fault distance (km)
	1st	2nd	3rd	Average		
1	0.1546	0.3399	0.3677	0.2874	0.2500	0.0374

4.4.4.1 Case Study – Single Line to Ground Fault (SLGF)

Figure 4.13 to Figure 4.16 show the results for the SLGF cases with fault impedances of 45Ω and 155Ω for AGF, 55Ω for BGF and 65Ω for CGF. As shown in the figures, the average estimated and actual fault distance values are shown by the bar chart whereas the line represents the absolute error of fault distance.

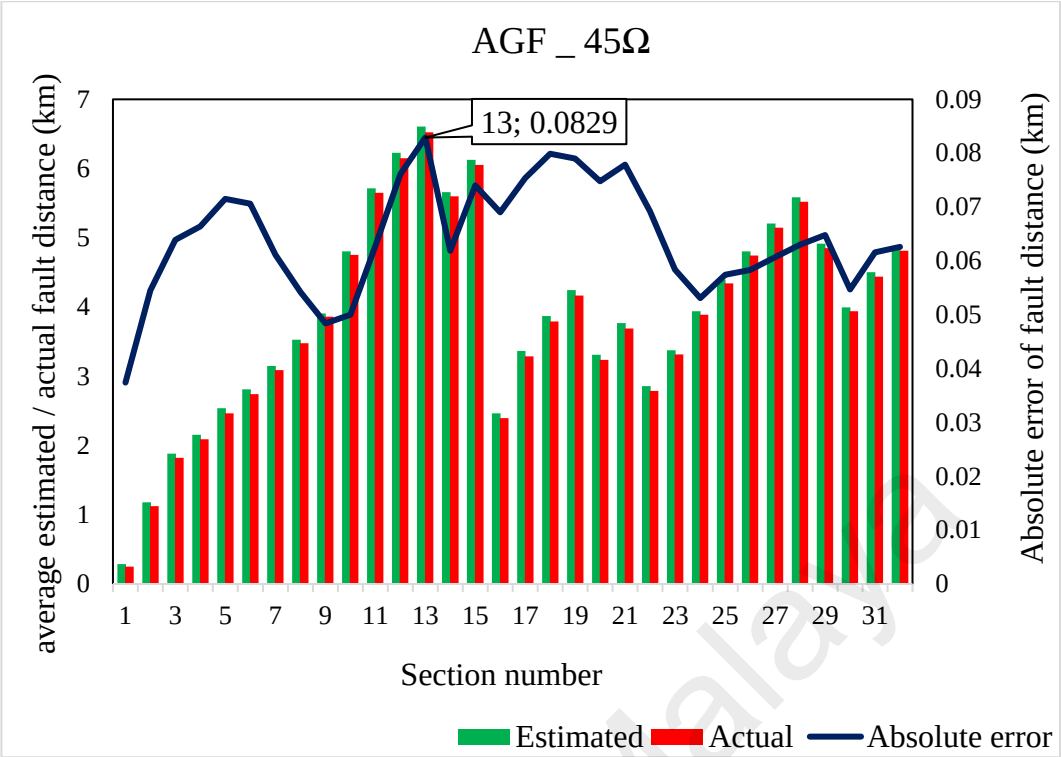

Figure 4.13: SLGF_AGF type of fault for 45Ω fault impedance

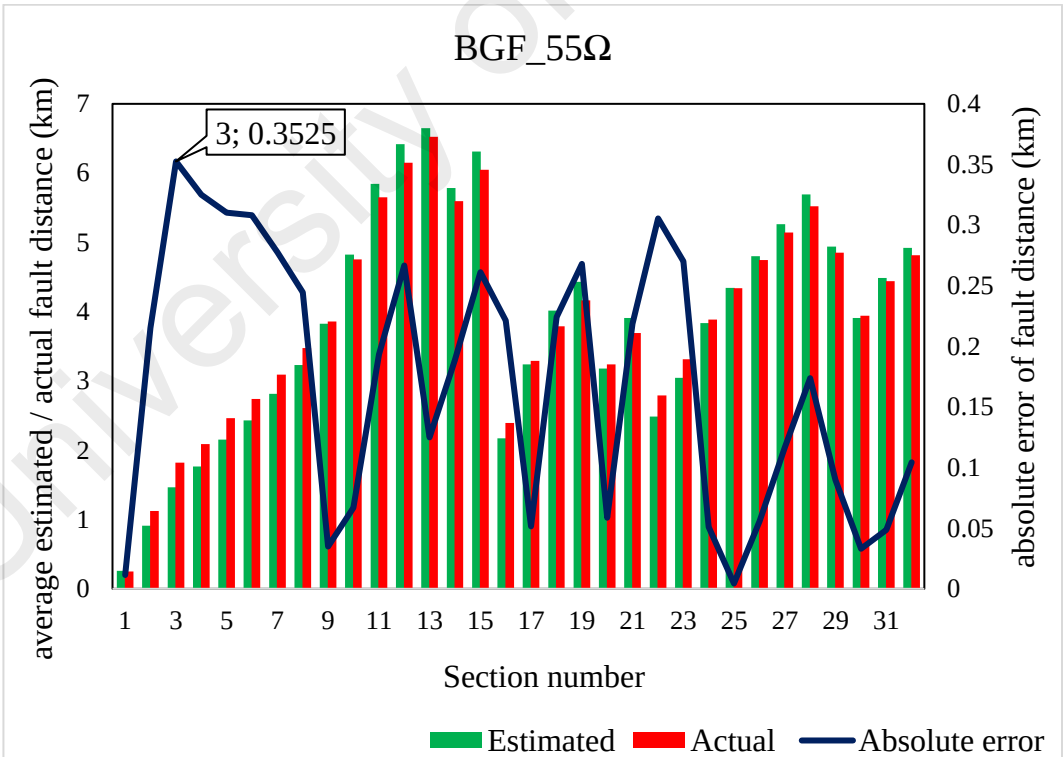

Figure 4.14: SLGF_BGF type of fault for 55Ω fault impedance

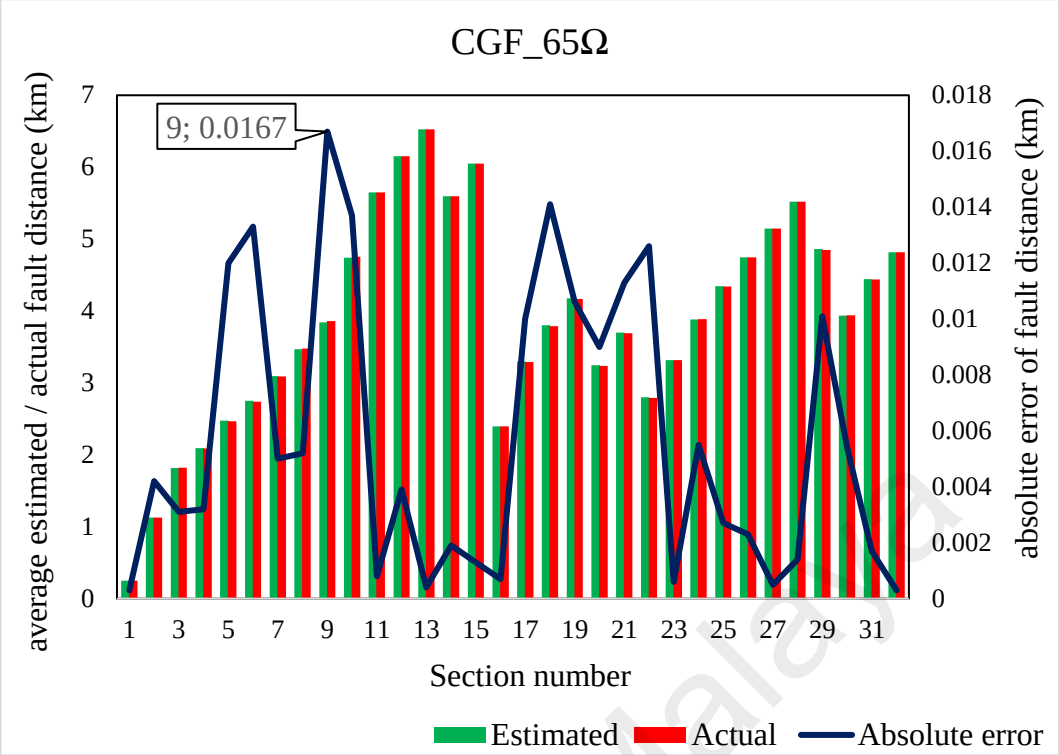

Figure 4.15: SLGF_CGF type of fault for 65Ω fault impedance

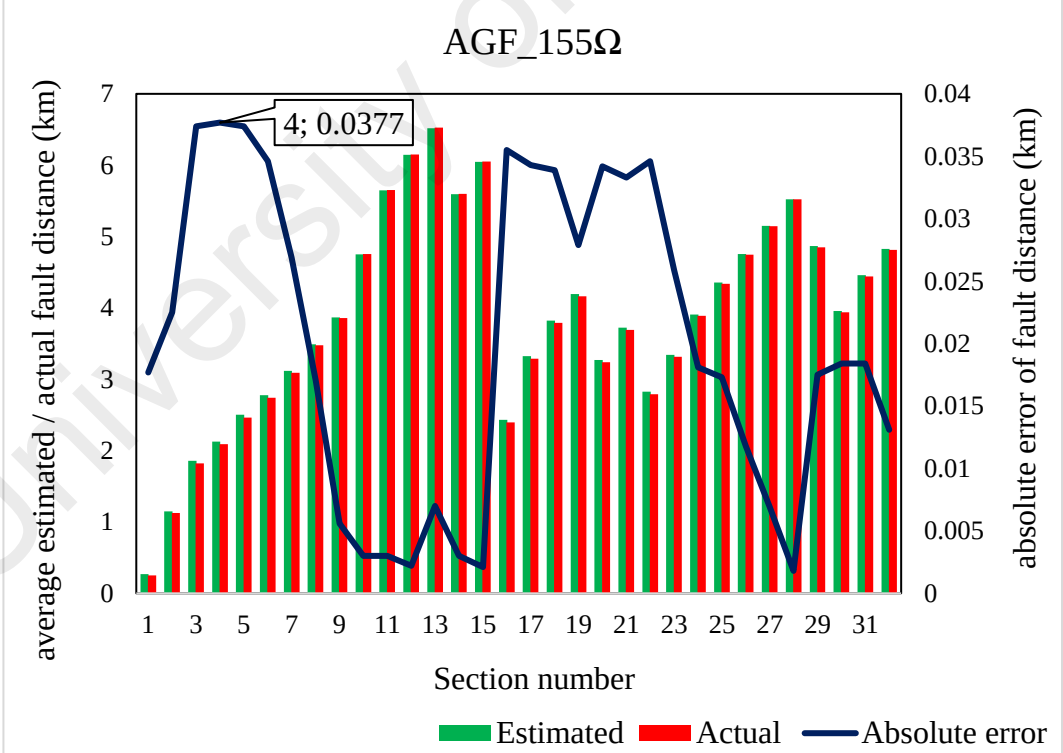

Figure 4.16: SLGF_AGF type of fault for 155Ω fault impedance

As shown in the above figures, the maximum value of the absolute error for the SLGF case is obtained when BGF type of fault with 55Ω of fault impedance value is applied in the middle of line section 3. The average estimated fault distance is 1.4675km while the actual fault distance is 1.82km. Therefore, the calculated absolute error is 0.3525km.

4.4.4.2 Case Study – Double Line to Ground Fault (LLGF)

Figure 4.17 to Figure 4.19 show the results for the LLGF cases with the applied fault impedance of 75Ω, 85Ω and 95Ω for ABGF, ACGF and BCGF types of fault respectively.

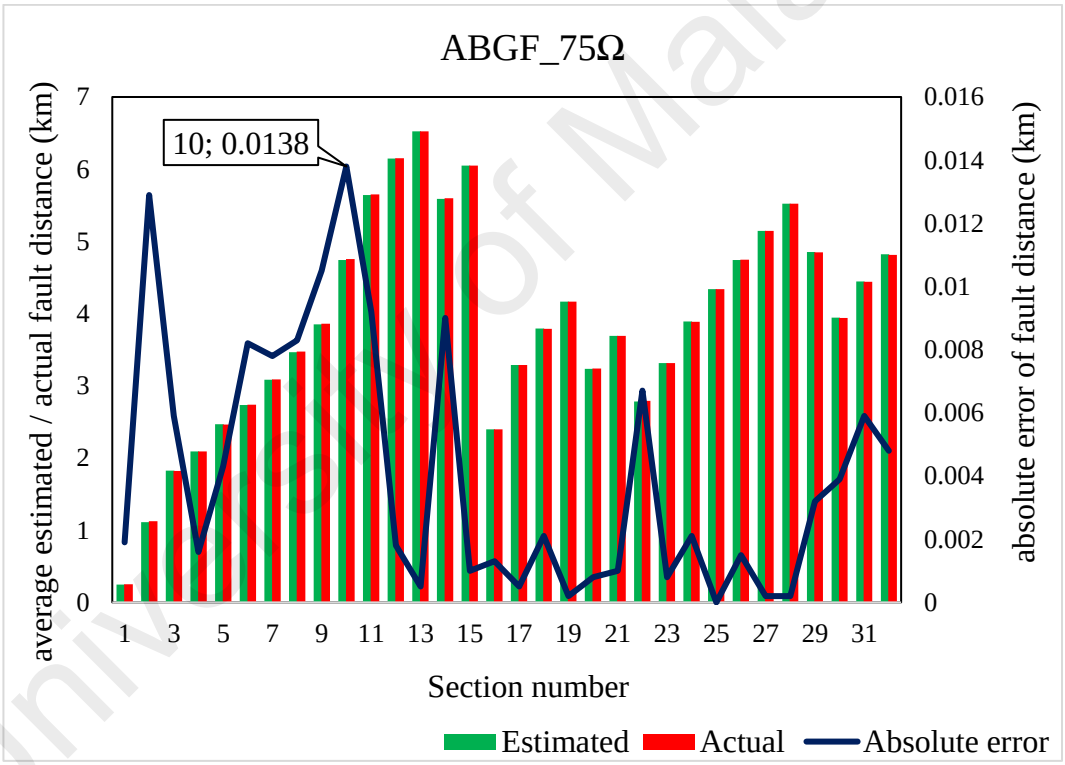

Figure 4.17: LLGF_ABGF type of fault for 75Ω fault impedance

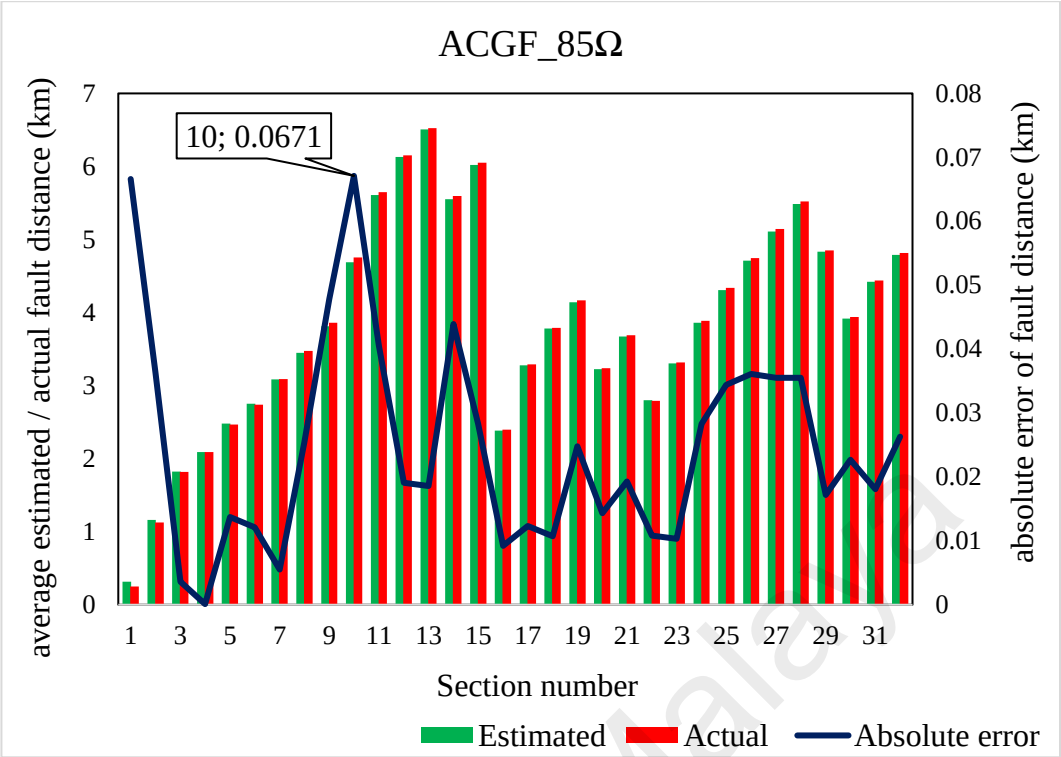

Figure 4.18: LLGF_ACGF type of fault for 85Ω fault impedance

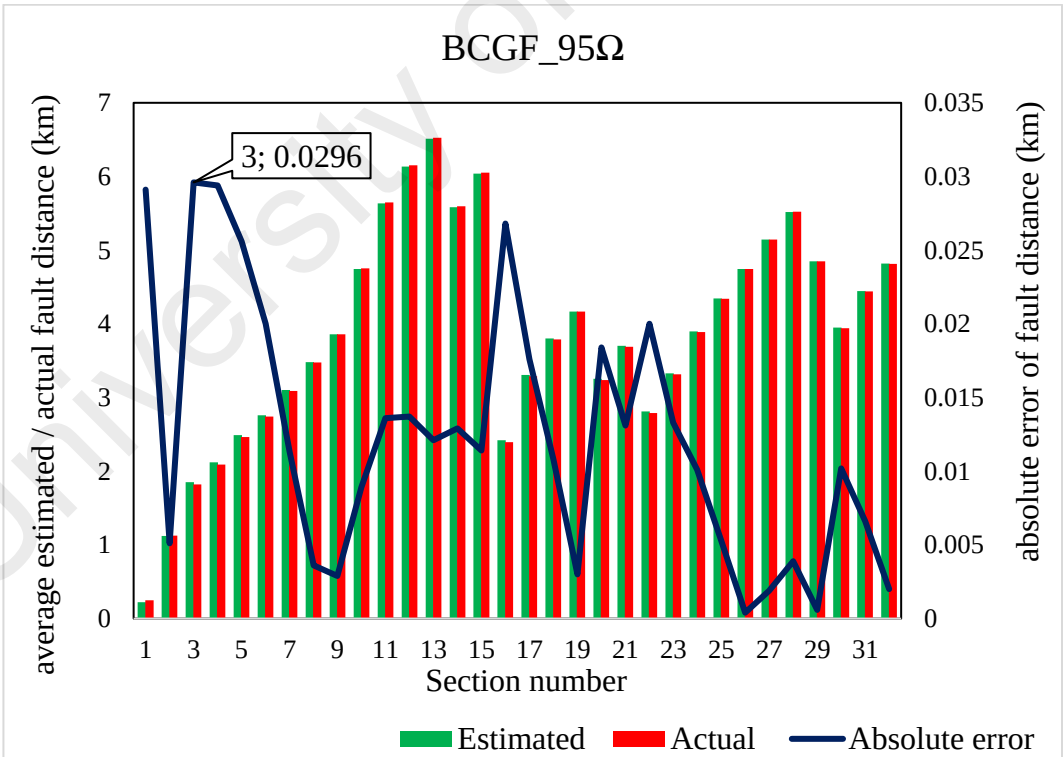

Figure 4.19: LLGF_BCGF type of fault for 95Ω fault impedance

As shown in the figures, the maximum absolute error for the LLGF case is obtained when the ACGF with 85Ω of fault impedance is applied in the middle of line section 10. The error recorded is 0.0671km when the average estimated and actual fault distance are 4.6879km and 4.755km respectively.

4.4.4.3 Case Study – Double Line Fault (LLF)

The results for LLF cases with 105Ω, 115Ω and 125Ω of fault impedances applied to ABF, ACF and BCF types of fault are shown in Figure 4.20 to Figure 4.22 respectively.

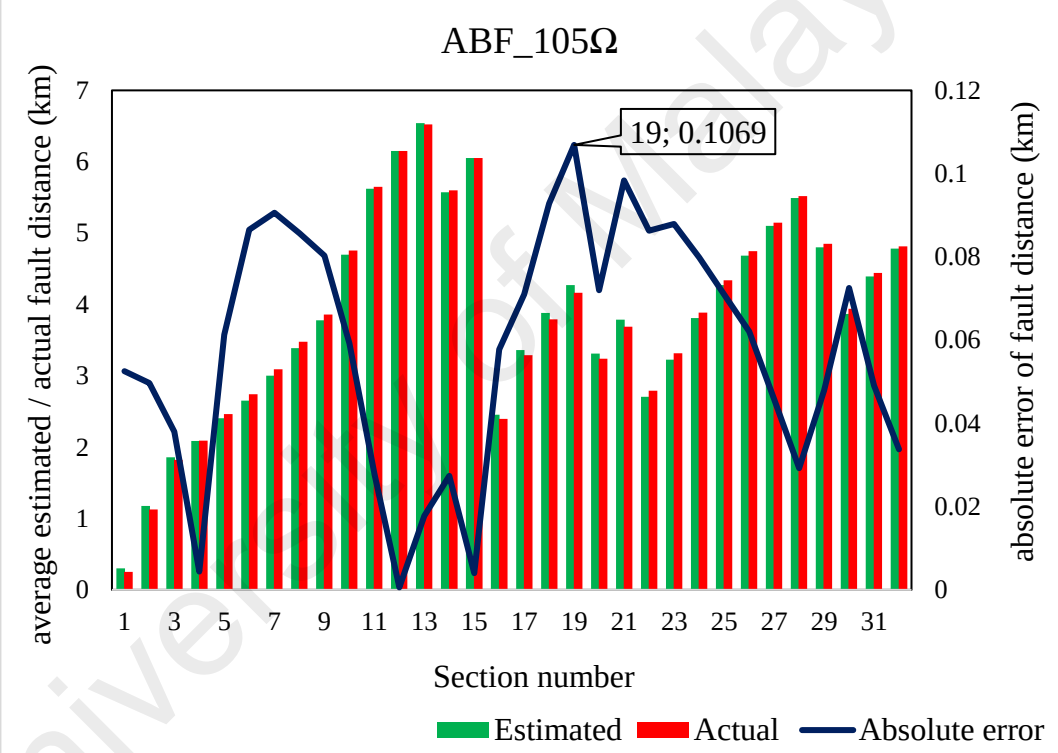

Figure 4.20: LLF_ABF type of fault for 105Ω fault impedance

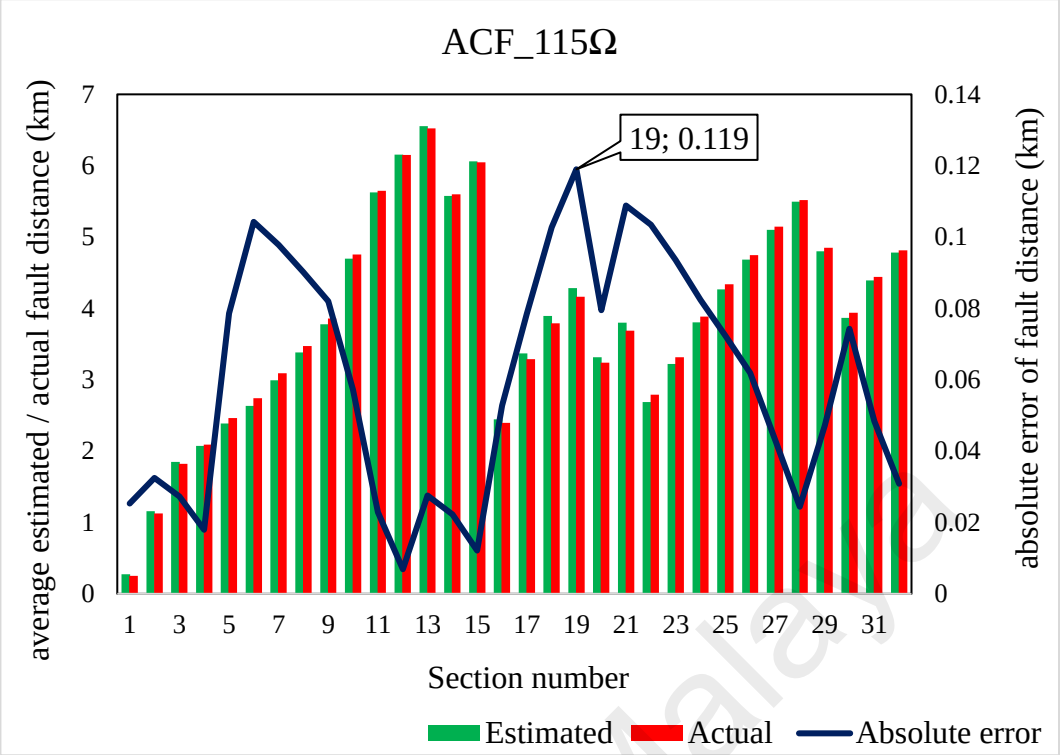

Figure 4.21: LLF_ACF type of fault for 115Ω fault impedance

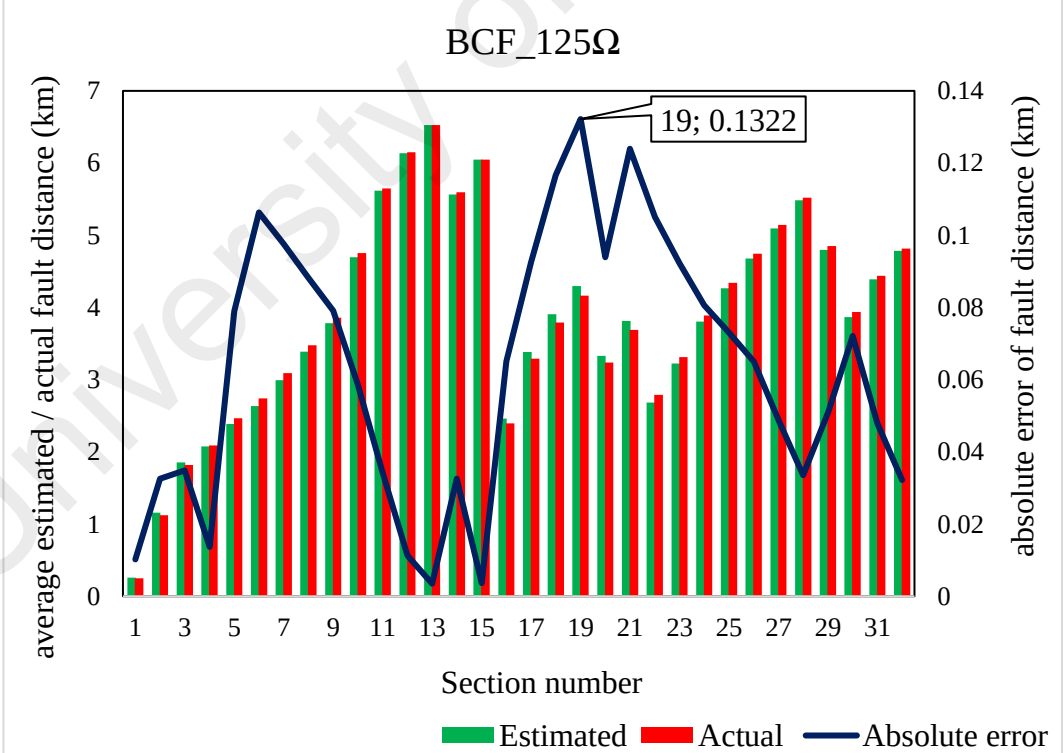

Figure 4.22: LLF_BCF type of fault for 125Ω fault impedance

Based on the results obtained in the figures above, it can be observed that the maximum absolute error for LLF case is obtained due to BCF type of fault with the fault impedance of 125Ω applied in the middle of line section 19. The obtained absolute error is 0.1322km.

4.4.4.4 Case Study – Balanced Fault (BF)

Lastly, Figure 4.23 to Figure 4.26 show the results for the BF cases consisting of ABCGF and ABCF types of fault with the fault impedances of 65Ω, 95Ω, 135Ω and 145Ω. Based on the results, it can be observed that the maximum absolute error (0.2430km) is obtained when the fault is applied in the middle of line section 19 with the fault impedance of 135Ω while the type of fault is ABCGF.

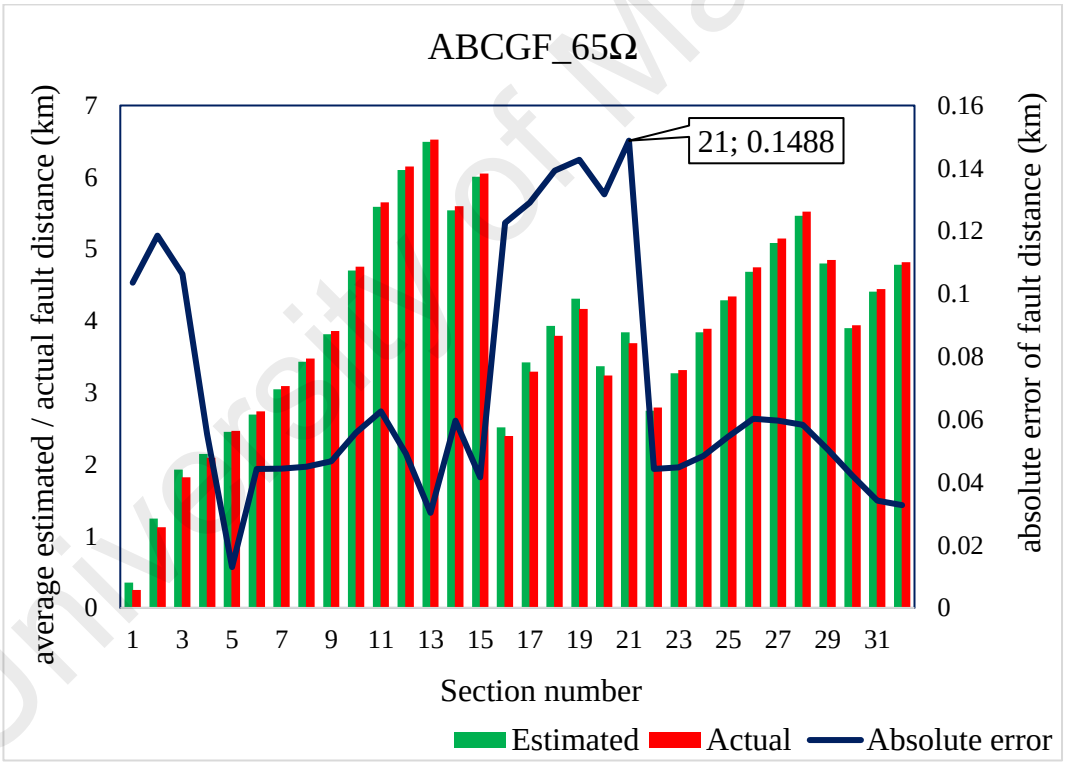

Figure 4.23: BF_ABCGF type of fault for 65Ω fault impedance

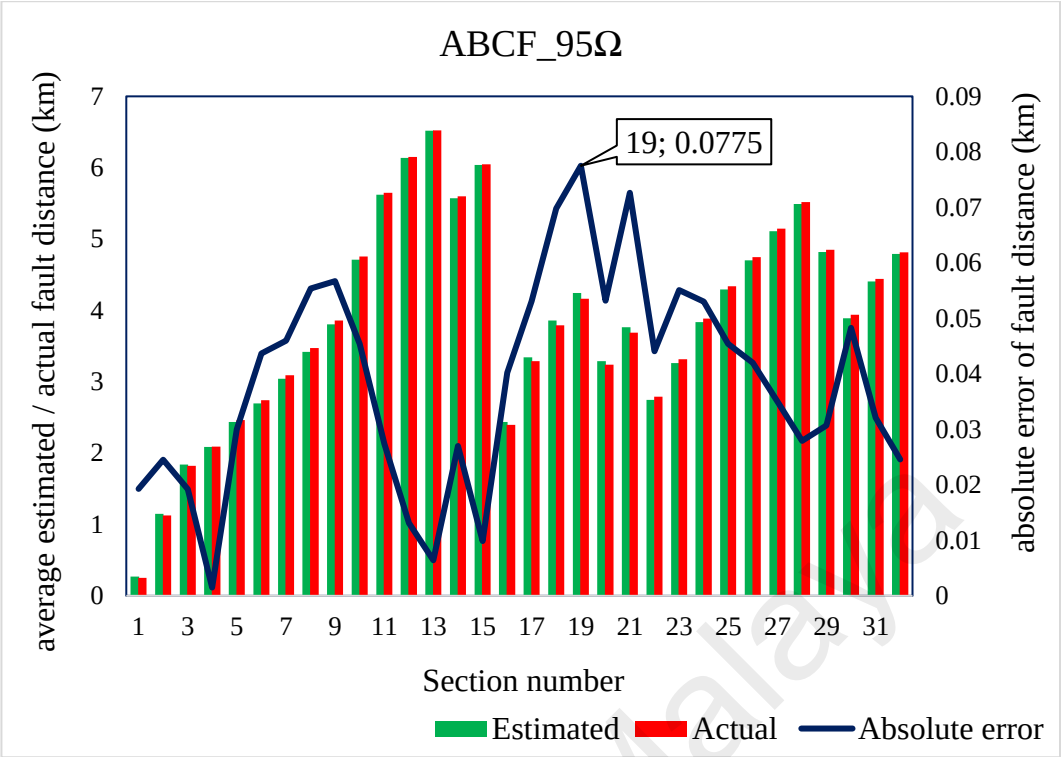

Figure 4.24: BF_ABCF type of fault for 95Ω fault impedance

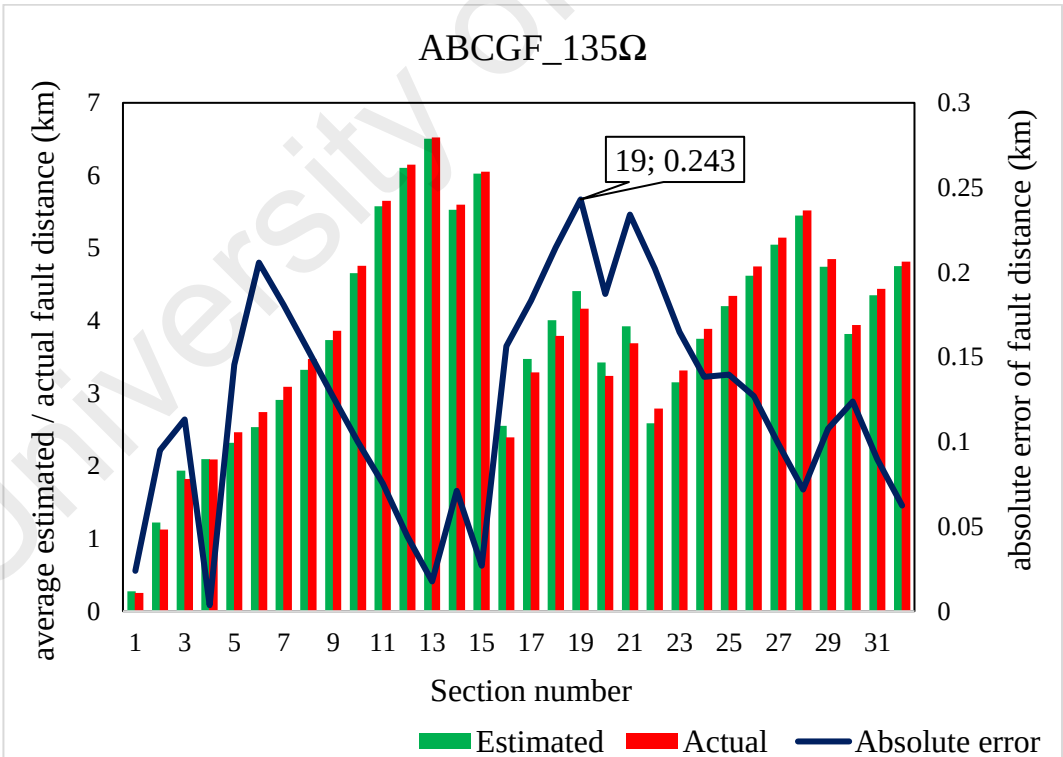

Figure 4.25: BF_ABCGF type of fault for 135Ω fault impedance

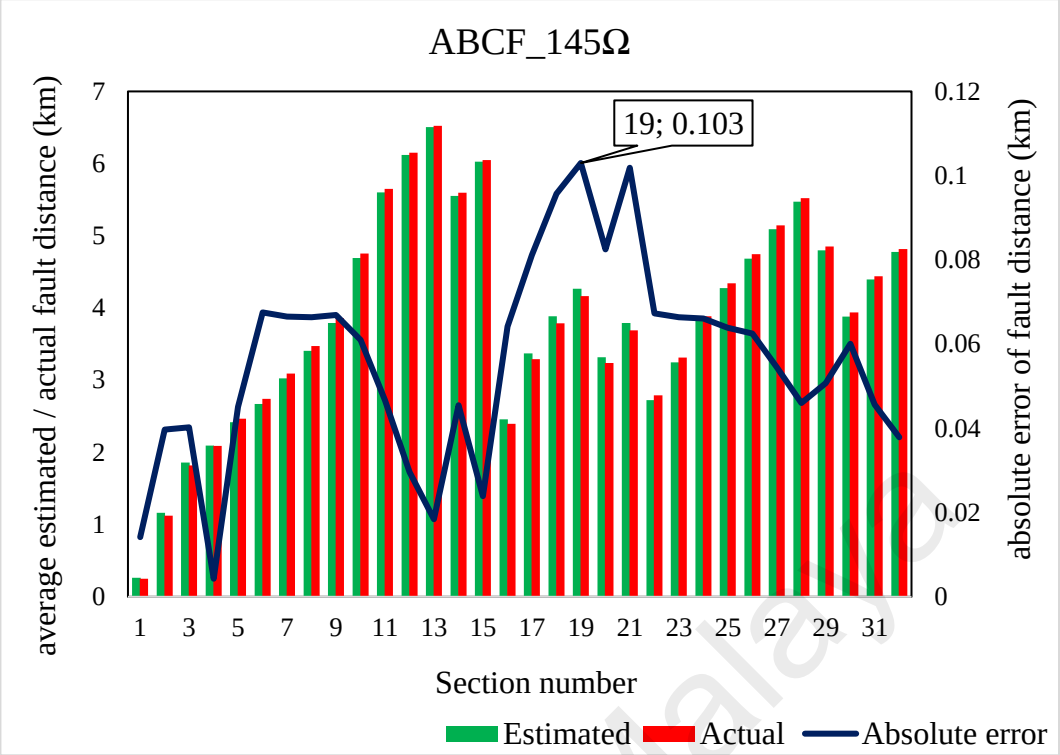

Figure 4.26: BF_ABCF type of fault for 145Ω fault impedance

4.4.4.5 Case Study - Random selection of testing data

Previously, testing analyses had been conducted with systematically varied fault impedances being applied in the middle of each line sections. However, in this subsection, the robustness of the proposed method is evaluated when fault impedances, fault points along the line section, fault types and faulty sections are randomly generated. In order to generate these random testing data, a random function is utilized. A total of 50 ANN testing cases are generated where, the randomized fault types and fault impedance values are shown in Figure 4.27, while Figure 4.28 shows the randomized line sections and the percentage of the line section length. The fault type notations in Figure 4.27 refers to the same notations as presented in Table 4.37.

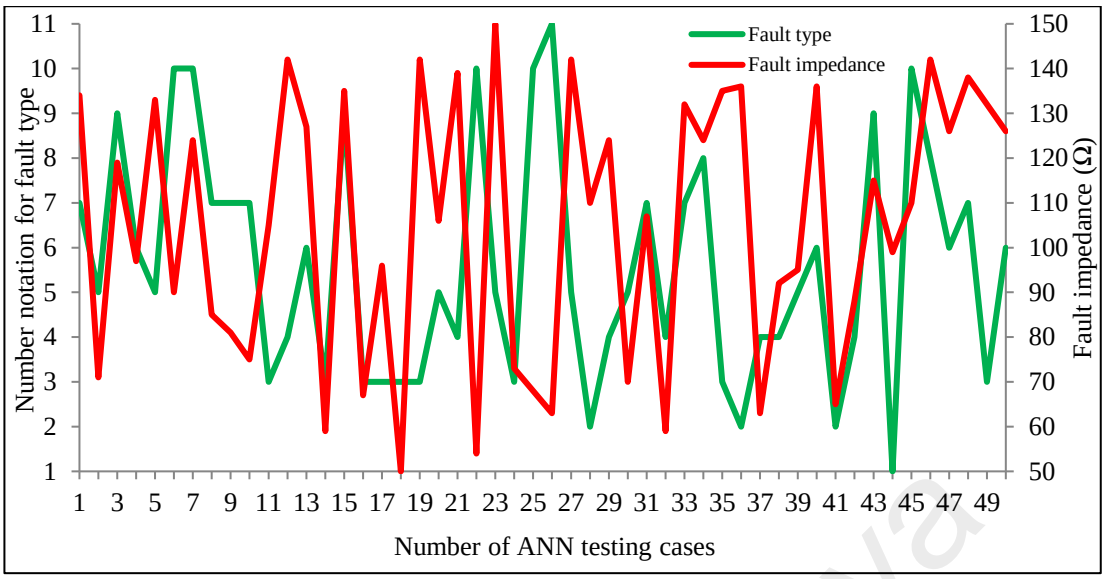

Figure 4.27: Random possible of fault type and fault impedance

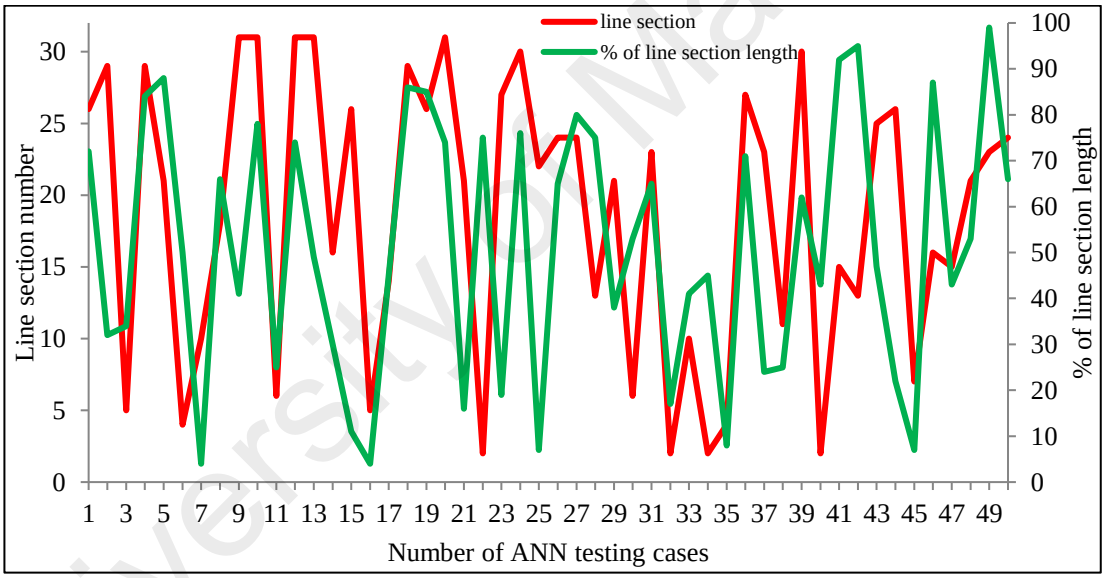

Figure 4.28: Random possible of line section and percentage of line section length

Table 4.43 shows the results for the fault distance estimation when random fault types, fault impedances, faulty sections and fault points are tested. The second, third, fourth and fifth columns represent the randomized fault types, fault impedances, line sections and percentage of line section length respectively. Whereas the sixth, seventh and eighth columns represent the estimated fault distance, actual fault distance and absolute error in fault distance estimation respectively. The estimated fault distance is the average value

obtained from three computed fault distances. As shown in the table, the fault distance can be estimated successfully with the maximum error in the distance of 0.2713km. This maximum error is recorded when the ACGF type of fault with 71Ω fault impedance is applied at 32% of the line section length of section 29.

Table 4.43: Results for random testing data

No.	Fault type	Fault impedance (Ω)	Line Section	Percentage of line section length (%)	Estimated fault distance (km)	Actual fault distance (km)	Absolute error in fault distance estimation (km)
1	ABF	134	26	72	4.7553	4.8110	0.0557
2	**ACGF**	**71**	**29**	**32**	**4.4869**	**4.7582**	**0.2713**
3	BCF	119	5	34	2.3505	2.4090	0.0585
4	BCGF	97	29	84	5.0158	5.0234	0.0076
5	ACGF	133	21	88	3.8941	3.8838	0.0103
6	ABCGF	90	4	50	2.0997	2.0900	0.0097
7	ABCGF	124	10	4	4.0652	4.1616	0.0964
8	ABF	85	18	66	3.9581	3.8700	0.0881
9	ABF	81	31	41	4.3650	4.3950	0.0300
10	ABF	75	31	78	4.5678	4.5800	0.0122
11	CGF	105	6	25	2.7049	2.6900	0.0149
12	ABGF	142	31	74	4.5724	4.5600	0.0124
13	BCGF	127	31	49	4.5448	4.4350	0.1098
14	CGF	59	16	30	2.1296	2.1370	0.0074
15	BCF	135	26	11	4.5654	4.6280	0.0626
16	CGF	67	5	4	2.3139	2.3040	0.0099
17	CGF	96	14	45	5.5693	5.5778	0.0085
18	CGF	50	29	86	5.0490	5.0336	0.0154
19	CGF	142	26	85	4.8478	4.8500	0.0022
20	ACGF	106	31	74	4.5720	4.5600	0.0120
21	ABGF	139	21	16	3.5186	3.5356	0.0170
22	ABCGF	54	2	75	1.4326	1.4375	0.0049
23	ACGF	150	27	19	4.9767	4.9900	0.0133
24	CGF	73	30	76	4.0633	4.0700	0.0067
25	ABCGF	68	22	7	2.6085	2.6610	0.0525
26	ABCF	63	24	65	3.9371	3.9468	0.0096
27	ACGF	142	24	80	3.9978	4.0060	0.0082
28	BGF	110	13	75	6.5875	6.5875	0.0000
29	ABGF	124	21	38	3.6317	3.6478	0.0161
30	ACGF	70	6	53	2.7678	2.7460	0.0218
31	ABF	107	23	65	3.3410	3.4275	0.0865
32	ABGF	59	2	17	0.6979	0.7125	0.0146
33	ABF	132	10	41	4.5881	4.6389	0.0508
34	ACF	124	2	45	1.0925	1.0625	0.0300
35	CGF	135	4	8	1.9195	1.9220	0.0025
36	BGF	136	27	71	5.2547	5.2500	0.0047

37	ABGF	63	23	24	3.1232	3.1200	0.0032
38	ABGF	92	11	25	5.5106	5.5250	0.0144
39	ACGF	95	30	62	3.9965	4.0000	0.0035
40	BCGF	136	2	43	1.2171	1.0375	0.1796
41	BGF	65	15	92	6.4355	6.2642	0.1713
42	ABGF	88	13	95	6.6328	6.6375	0.0047
43	BCF	115	25	47	4.2678	4.3247	0.0569
44	AGF	99	26	22	4.7074	4.6610	0.0464
45	ABCGF	110	7	7	2.6911	2.8750	0.1839
46	ACF	142	16	87	2.9611	2.8723	0.0888
47	BCGF	126	15	43	6.1390	6.0143	0.1247
48	ABF	138	21	53	3.8508	3.7243	0.1265
49	CGF	132	23	99	3.6770	3.6825	0.0055
50	BCGF	126	24	66	4.0382	3.9507	0.0875

4.5 Validation of Proposed Enhanced Fault Location Method

As shown in the previous subsection, the proposed fault location method generated good results. However, the estimated fault distance may lead to multiple possible points of fault location due to the existence of lateral branches of equal distances from the measurement point. As such, in the proposed enhanced fault location method, the faulty section identification method is used to determine the most likely faulty section. Then, each of the previously estimated fault distance will be re-evaluated with respect to the identified faulty section to improve the fault location results.

4.5.1 Faulty Section Identification Process

Table 4.44 shows an example of BGF type of fault occurring in the middle of line section 6 with 55Ω of fault impedance. At first, the average estimated fault distance is calculated. Then, the multiple possible faulty sections are identified based on the average estimated fault distance if the average estimated fault distance falls in between the length of any line section. Subsequently, all the possible faulty sections are ranked from the most likely to the least likely faulty section. To rank all the possible faulty sections, the measured data are first compared against the stored data for each of the identified faulty sections. Based on the example in Table 4.44, there are 5 possible faulty sections are

identified comprising of Section 4, Section 5, Section 6, Section 16, and Section 22. If the measured data fall in between the minimum and maximum values of the stored data, then it will be counted as '√', otherwise, it will be counted as '×'. Then, the total number of '√' for each identified faulty section is calculated and ranked according to the highest number of '√'.

Table 4.44: Comparing measured data with stored data (BGF - 55Ω - Section 6)

Measured data	381.32	-686.68	375.53	2.92	456.33	-0.0042
Stored data (Section 4)	352.61 424.29	-755.94 -640.21	346.92 397.98	2.61 3.39	416.73 424.53	-0.0043 -0.0035
	√	√	√	√	×	√
Stored data (Section 5)	350.82 421.37	-750.87 -637.00	344.76 394.49	2.59 3.36	413.80 419.92	-0.0045 -0.0037
	√	√	√	√	×	√
Stored data (Section 6)	350.14 418.84	-746.50 -635.73	343.85 411.97	2.59 3.33	412.58 506.81	-0.0045 -0.0038
	√	√	√	√	√	√
Stored data (Section 16)	349.21 425.33	-757.73 -633.92	342.53 410.08	2.58 3.41	410.81 504.26	-0.0041 -0.0034
	√	√	√	√	√	×
Stored data (Section 22)	349.80 418.84	-746.50 -635.08	343.40 411.33	2.58 3.33	411.97 505.95	-0.0046 -0.0038
	√	√	√	√	√	√

Table 4.45 summarizes the obtained results from Table 4.44. It shows that only Section 6 and 22 have the highest number of 6 '√'. Since both sections have the same total number of '√', thus, these sections will be sorted in incremental order. As such, Section 6 is ranked as first and followed by Section 22. As the actual fault occurs in the middle of line section 6, therefore, the proposed method has successfully identified the faulty section accurately in the first rank.

Table 4.45: List of possible faulty sections (BGF - 55Ω - Section 6)

Possible faulty section	Total number of measured data that falls in between the stored data
4	5
5	5
6	**6**
16	5
22	**6**
Sorted possible faulty section	Rank
6	**1**
22	2
4	3
5	4
16	5

4.5.2 Implementation of the Proposed Enhanced Fault Location Method

In the previous subsections, the fault distance has been estimated and multiple possible faulty sections have been identified and ranked. However, the fault location accuracy can be further improved by an enhanced fault distance algorithm. In this proposed enhanced method, the previously estimated fault distance will be re-evaluated with respect to the identified faulty section. Here, the average value of fault distance will only consider the estimated fault distances that fall in between the length of the identified faulty section.

Table 4.46 shows the comparison of fault distance estimation calculation between the previously proposed fault location and newly proposed enhanced fault location methods when the ABCGF type of fault occurs in the middle of line section 5 with 135Ω of fault impedance. In the proposed fault location method in Section 4.4.4, the estimation of fault distance is obtained from the average value of 3 estimated fault distances. As such, the estimated fault distance is 2.3195km and the calculated fault distance error is 0.1455km. Whereas, in the newly proposed enhanced fault location method, the calculation of

average value for the enhanced fault distance only consider the first and third estimations of fault distance. The second fault distance estimation is not considered in the calculation because the estimated fault distance (2.2642km) is not in between the length of line section 5 (2.2900 – 2.6400km). As such, the enhanced fault distance recorded 2.3472km and the calculated fault distance error is 0.1178km, which is less than the previously proposed method with an error of 0.1455km.

Table 4.46: Comparison between the previously and newly proposed enhanced method for Section 5 (2.2900 – 2.6400km)

Previously proposed method					
1st estimated fault distance (km)	2nd estimated fault distance (km)	3rd estimated fault distance (km)	Average value of estimated fault distance (km)	Actual fault distance (km)	Error of fault distance (km)
2.3832	2.2642	2.3112	2.3195	2.4650	0.1455
Newly proposed enhanced method					
1st estimated fault distance (km)	2nd estimated fault distance (km)	3rd estimated fault distance (km)	Average value of estimated fault distance (km)	Actual fault distance (km)	Error of fault distance (km)
2.3832	**2.2642**	2.3112	2.3472	2.4650	0.1178

4.5.2.1 Performance of the Proposed Enhanced Fault Location Method under Random Selection of Testing Data

Table 4.47 shows the results for the random fault analysis, using the same ANN test cases as in Subsection 4.4.4.5. The 1st to 4th columns indicate the actual fault types, fault distances, fault impedances and faulty sections respectively. The 5th to 8th columns show the estimated fault types, fault distances, fault impedances and faulty sections respectively. The 9th column indicates the fault type classification results. The 10th and 11th columns show the absolute error between the actual and estimated values for both fault distance and fault impedance respectively. The 12th column indicates the ranking for the correctly identified faulty section.

As shown in the table, all types of fault are correctly classified by the proposed method. For the faulty section identification, the worst result is obtained when the fault occurs at line section 23 where it can only be correctly identified at the 8th rank. Nevertheless, the fault distance can be estimated accurately with the absolute error of 86.5m. The maximum error for the fault impedance estimation is 1.37Ω when the ABCGF type of fault occurs at line section 2 with the actual and estimated fault impedances of 54Ω and 55.37Ω respectively. Whereas, the maximum error for fault distance estimation is 179.6m when the BCGF type of fault occurs at line section 2 with the actual and estimated fault distance of 1.0375km and 1.2171km respectively.

Table 4.47: Random Fault Analysis

Actual				Estimated				Absolute error / Results			
Fault Type	Fault Distance (km)	Fault Impedance (Ω)	Faulty Section	Fault Type	Fault Distance (km)	Fault Impedance (Ω)	Faulty Section	Classification	Fault Distance (km)	Fault Impedance (Ω)	Ranking
7	4.811	134	26	7	4.7553	134.04	26	classified	0.0557	0.04	1
5	4.7582	71	29	5	4.7261	71.04	29	classified	0.0321	0.04	4
9	2.409	119	5	9	2.3505	119.09	5	classified	0.0585	0.09	2
6	5.0234	97	29	6	5.0158	97.05	29	classified	0.0076	0.05	7
5	3.8838	133	21	5	3.8941	133.01	21	classified	0.0103	0.01	3
10	2.09	90	4	10	2.0997	90.01	4	classified	0.0097	0.01	1
10	4.1616	124	10	10	4.1100	124.34	10	classified	0.0516	0.34	2
7	3.87	85	18	7	3.9581	84.96	18	classified	0.0881	0.04	5
7	4.395	81	31	7	4.3650	81.00	31	classified	0.0300	0.00	5
7	4.58	75	31	7	4.5678	75.04	31	classified	0.0122	0.04	6
3	2.69	105	6	3	2.7049	105.17	6	classified	0.0149	0.17	2
4	4.56	142	31	4	4.5724	142.04	31	classified	0.0124	0.04	6
6	4.435	127	31	6	4.5448	127.03	31	classified	0.1098	0.03	6
3	2.137	59	16	3	2.1296	58.91	16	classified	0.0074	0.09	3
9	4.628	135	26	9	4.5950	135.08	26	classified	0.0330	0.08	4
3	2.304	67	5	3	2.3139	67.04	5	classified	0.0099	0.04	2
3	5.57775	96	14	3	5.5693	96.06	14	classified	0.0085	0.06	3
3	5.0336	50	29	3	5.0490	50.04	29	classified	0.0154	0.04	4
3	4.85	142	26	3	4.8478	142.05	26	classified	0.0022	0.05	2
5	4.56	106	31	5	4.5720	106.00	31	classified	0.0120	0.00	5
4	3.5356	139	21	4	3.5186	138.95	21	classified	0.0170	0.05	3
10	1.4375	54	2	10	1.4326	55.37	2	classified	0.0049	1.37	1
5	4.99	150	27	5	4.9767	150.03	27	classified	0.0133	0.03	4
3	4.07	73	30	3	4.0633	72.97	30	classified	0.0067	0.03	6

10	2.661	68	22	10	2.6469	69.20	22	classified	0.0141	1.20	5
11	3.94675	63	24	11	3.9371	62.96	24	classified	0.0096	0.04	6
5	4.006	142	24	5	3.9978	142.04	24	classified	0.0082	0.04	2
2	6.5875	110	13	2	6.5875	110.04	13	classified	0.0000	0.04	1
4	3.6478	124	21	4	3.6317	123.95	21	classified	0.0161	0.05	2
5	2.746	70	6	5	2.7678	70.07	6	classified	0.0218	0.07	1
7	3.4275	107	23	7	3.3410	107.04	23	classified	0.0865	0.04	8
4	0.7125	59	2	4	0.6979	59.04	2	classified	0.0146	0.04	1
7	4.6389	132	10	7	4.5881	131.97	10	classified	0.0508	0.03	2
8	1.0625	124	2	8	1.0925	123.89	2	classified	0.0300	0.11	1
3	1.922	135	4	3	1.9195	134.91	4	classified	0.0025	0.09	2
2	5.25	136	27	2	5.2547	136.02	27	classified	0.0047	0.02	4
4	3.12	63	23	4	3.1232	63.01	23	classified	0.0032	0.01	5
4	5.525	92	11	4	5.5106	91.98	11	classified	0.0144	0.02	1
5	4	95	30	5	3.9965	94.97	30	classified	0.0035	0.03	5
6	1.0375	136	2	6	1.2171	135.93	2	classified	0.1796	0.07	1
2	6.2642	65	15	2	6.2920	65.02	15	classified	0.0278	0.02	3
4	6.6375	88	13	4	6.6328	87.98	13	classified	0.0047	0.02	1
9	4.3247	115	25	9	4.2678	115.05	25	classified	0.0569	0.05	5
1	4.661	99	26	1	4.7074	99.01	26	classified	0.0464	0.01	2
10	2.875	110	7	10	2.8400	110.00	7	classified	0.0350	0.00	1
8	2.8723	142	16	8	2.9611	141.96	16	classified	0.0888	0.04	3
6	6.0143	126	15	6	6.1390	126.00	15	classified	0.1247	0.00	3
7	3.7243	138	21	7	3.8508	137.90	21	classified	0.1265	0.10	1
3	3.6825	132	23	3	3.6770	132.02	23	classified	0.0055	0.02	6
6	3.9507	126	24	6	3.9936	126.04	24	classified	0.0429	0.04	5

In order to justify the effectiveness of the proposed method, different methods used in other literature were compared as shown in Table 4.48. The comparison is based on the maximum error of fault distance in a kilometer. As shown in the table, it can be observed that the proposed method delivered results with higher accuracies where the maximum error is 0.180km.

Table 4.48: Comparison with the previous methods

Technique proposed in other presented paper	Maximum error of fault distance (in km)
Wavelet, SVR (Borghetti, Bosetti et al. 2008)	0.214
Wavelet, ANN, FLS (Pourahmadi-Nakhli and Safavi 2011)	0.248
EMD, CVR (Liang, Fu et al. 2015)	0.393
Unsynchronized phasor (Xiu and Liao 2014)	0.557
Proposed method	0.180

4.6 Conclusion

In this chapter, the validation of the proposed techniques for HIF detection and localization has been performed. At first, the occurrence of HIF event was detected and identified. Once the occurrence of HIF event was identified, the location of the event can be estimated.

In the proposed technique for HIF detection and identification, the occurrence of HIF event was differentiated from non-HIF events based on the smoothed PDC pattern. The HIF event was detected based on the smoothed PDC pattern that rises until it reaches a plateau without subsequent dip. To simplify the HIF detection and identification process, an automatic HIF classification algorithm was proposed. The event was considered to occur in the system if the value of *D-index* is lower than -200. Subsequently, the event was identified as HIF event if the value of *Id-index* is lower than 0.01. Based on the

obtained results, it was observed that the proposed algorithm successfully detected and identified the HIF from non-HIF events.

Subsequently, a thorough investigation has been conducted to determine the fault location during the occurrence of HIF event. Hybrid technique comprising of Multi-Resolution Analysis-Discrete Wavelet Transform (MRA-DWT), Artificial Neural Network (ANN) and Grey Wolf Optimization (GWO) technique have successfully classified the fault type and estimated the fault impedance and distance values.

It was observed that the estimated fault distance had led to multiple possibilities of faulty sections. In this proposed enhanced fault location method, the multiple possibilities of faulty sections were successfully identified and ranked. Besides that, the estimated fault distance was enhanced with respect to the identified faulty section.

CHAPTER 5: CONCLUSION AND FUTURE WORK

5.1 Conclusion

The work reported in this thesis can be divided into three parts. In the first part, a new algorithm for HIF detection and classification called the Phase Displacement Computation (PDC) was proposed. It utilized three-phase voltage waveforms to detect HIF and other disturbances that occurred in a distribution system and subsequently identified the events as HIF or non-HIF. In the algorithm, the data were calculated between the measured and reference three-phase voltage waveforms. The reference waveforms were the clean ones without any anomaly, while the measured waveforms were the ones that contain distortions caused by the event that occurred in the system. The event was classified based on the pattern of smoothed PDC. The HIF event was detected if the smoothed PDC pattern rises until it reaches a plateau without subsequent dip. Otherwise, it was regarded as a non-HIF event such as capacitor switching, motor starting and load switching. However, it was difficult to discriminate the event based on the pattern alone. Thus, an automatic HIF classification algorithm based on pre-defined indices was proposed. Two indices introduced for this purpose were detection index (*D-index*) and identification index (*Id-index*). First, the *D-index* was used to detect any extraordinary event that occurred in the system. If an event was found to occur in the system, the *Id-index* was checked to classify it into HIF or non-HIF. An event was considered as a HIF if it has an *Id-index* value that was lower than 0.01. Otherwise, the event was classified as a non-HIF. As such, the first objective to detect and identify the occurrence of HIF event had been accomplished.

In the second part of the work, if the detected event was considered as a HIF, the fault distance needs to be estimated using the three-phase voltage and current waveforms. Firstly, important features were extracted from the measured waveforms using the MRA-

DWT with Bior3.3 mother wavelet. Only the best 6 out of 24 features were selected from the 4 decomposition levels of the three-phase voltage and current waveforms. Then, the selected features were fed into the ANN to estimate the fault distance. To improve the accuracy of the proposed ANN in estimating the fault distance, an optimization method was adopted. For this purpose, the GWO method was implemented to provide the optimal values of the ANN parameters. Besides estimating the fault distance, the proposed method also identified the fault type and its impedance value using the same input data. As such, the second objective to classify the fault type, estimate the fault distance and impedance values had been achieved.

To improve the accuracy of the estimated fault distance, an enhanced fault location method was proposed in the third part of the work. In the proposed enhanced fault location method, a number of possible faulty sections were determined using the average value of fault distance estimation. The average value was calculated from 3 estimated fault distance using 3 different network files. Then, the multiple possibilities of faulty sections were ranked from the most likely to the least likely using a database and matching approach. The database to be used was chosen using the estimated fault impedance value. Subsequently, the input features were compared against the stored data in the database. The faulty section with the highest number of matching data will be ranked as the first. If more than one possible faulty sections have the same number of matching data, then they will be sorted in increment order based on the line section number. Subsequently, the estimated fault distance was re-evaluated with respect to the identified faulty section. For this purpose, the average value will only considers the estimated fault distance that falls within the range of the line section length of the faulty section. As such, the fault distance estimation had been enhanced and thus the third objective had been fulfilled.

The proposed methods for HIF detection and localization had also been compared with the previous methods. The comparisons show that the proposed methods delivered accurate results as compared to the previous techniques. Besides that, the proposed methods comprise of simple algorithm that can detect, classify and locate HIF in a distribution network accurately with less computational time. The methods were inexpensive and practical since it required only voltage and current waveforms from a single measurement unit. Therefore, the fourth objective of the research had been met.

5.2 Future Work

The following suggestions are made to improve the proposed HIF detection, classification and localization technique. They are as follows:

1) HIF detection and classification technique
   - In the proposed method, only the three-phase voltage waveforms are used to detect and classify the HIF from non-HIF events. In order to increase the accuracy and reliability of the method, the measured three-phase current waveforms can be considered as well to provide a double verification of the occurrence of a HIF event.
   - Different types of non-HIF events such as harmonic event, noise and others can be included to show the robustness of the proposed method.
2) HIF localization technique
   - In the proposed technique, the GWO technique is utilized to provide the optimal value of the ANN parameters. In the future, a more advanced and new optimization technique can be adopted.
   - Instead of ANN, another AI classifier such as Support Vector Machine (SVM) can be utilized to estimate the fault distance.
   - Different types of digital signal processing techniques such as an Empirical Mode Decomposition (EMD) and Short Time Fourier Transform (STFT) can be tested to extract features from the three-phase voltage and current waveforms.

REFERENCES

IEEE Guide for Determining Fault Location on AC Transmission and Distribution Lines. (2005). IEEE Std C37.114-2004: 0_1-36.

Abraham, S., Dhaliwal, H., et al. (2004). Final Report on the August 14, 2003 Blackout in the United States and Canada: Causes and Recommendations, U.S.-Canada Power System Outage Task Force.

Adamiak, M., Wester, C., et al. High Impedance Fault Detection On Distribution Feeders.

Aggarwal, R. K., Aslan, Y., et al. (1997). New concept in fault location for overhead distribution systems using superimposed components. *IEEE Proceedings on Generation, Transmission and Distribution, 144*(3), 309-316.

Akorede, M. F. and Katende, J. (2010). Wavelet Transform Based Algorithm for High-Impedance Faults Detection in Distribution Feeders. *European Journal of Scientific Research, 41*(2), 238-248.

Aslan, Y. and Yağan, Y. E. (2016). Artificial neural-network-based fault location for power distribution lines using the frequency spectra of fault data. *Electrical Engineering*, 1-11.

Avdakovic, S., Nuhanovic, A., et al. (2012). Wavelet transform applications in power system dynamics. *Electric Power Systems Research, 83*(1), 237-245.

Aziz, M. S. A., Hassan, M. A. M., et al. (2012). An Artificial Intelligence Based Approach for High Impedance Faults Analysis in Distribution Networks. *International Journal of System Dynamics Aplications, 1*(2), 44-59.

Bansal, A. and Pillai, G. N. (2007). High impedance fault detection using LVQ neural networks. *International Journal of Computer Systems Science and Engineering, 1*(3), 148–152.

Baqui, I., Zamora, I., et al. (2011). High impedance fault detection methodology using wavelet transform and artificial neural networks. *Electric Power Systems Research, 81*(7), 1325-1333.

Barakat, S., Eteiba, M. B., et al. (2014). Fault location in underground cables using ANFIS nets and discrete wavelet transform. *Journal of Electrical Systems and Information Technology, 1*(3), 198-211.

Bernadić, A. and Leonowicz, Z. (2012). Fault location in power networks with mixed feeders using the complex space-phasor and Hilbert–Huang transform. *International Journal of Electrical Power and Energy Systems, 42*(1), 208-219.

Bhalja, B. and Maheshwari, R. P. (2008). Wavelet-based Fault Classification Scheme for a Transmission Line Using a Support Vector Machine. *Electric Power Components and Systems, 36*(10), 1017-1030.

Borghetti, A., Bosetti, M., et al. (2008). Continuous-Wavelet Transform for Fault Location in Distribution Power Networks: Definition of Mother Wavelets Inferred From Fault Originated Transients. *IEEE Transactions on Power Systems, 23*(2), 380-388.

Borghetti, A., Corsi, S., et al. (2006). On the use of continuous-wavelet transform for fault location in distribution power systems. *International Journal of Electrical Power and Energy Systems, 28*(9), 608-617.

Bretas, A. S., Moreto, M., et al. (2006). A Novel High Impedance Fault Location for Distribution Systems Considering Distributed Generation. *Transmission and Distribution Conference and Exposition, Latin America, TDC '06. IEEE/PES*.

Briassouli, A., Matsiki, D., et al. (2010). Continuous wavelet transform for time-varying motion extraction. *IET Image Processing, 4*(4), 271-282.

Cardoso, G., Rolim Jr, J. G., et al. (2004). Application of neural-network modules to electric power system fault section estimation. *IEEE Transactions on Power Delivery, 19*(3), 1034-1041.

Chanda, D., Kishore, N. K., et al. (2003). A wavelet multiresolution analysis for location of faults on transmission lines. *International Journal of Electrical Power and Energy Systems, 25*(1), 59-69.

Chunju, F., Li, K. K., et al. (2007). Application of wavelet fuzzy neural network in locating single line to ground fault (SLG) in distribution lines. *International Journal of Electrical Power and Energy Systems, 29*(6), 497-503.

Cnockaert, L., Migeotte, P. F., et al. (2008). A Method for the Analysis of Respiratory Sinus Arrhythmia Using Continuous Wavelet Transforms. *IEEE Transactions on Biomedical Engineering, 55*(5), 1640-1642.

Costa, F. B., Souza, B. A., et al. (2015). Real-Time Detection of Transients Induced by High-Impedance Faults Based on the Boundary Wavelet Transform. *IEEE Transactions on Industry Applications, 51*(6), 5312-5323.

David, C. T. W., Xia, Y. (1998). A novel technique for high impedance fault identification. *IEEE Transactions on Power Delivery, 13*(3), 738-744.

Dilokratanatrakool, C., Na Ayudhya, P. N., et al. (2003). Automatic detection-localization of fault point on waveform and classification of power quality disturbance waveshape fault using wavelet and neural network. *IEEE International Conference on Robotics, Intelligent Systems and Signal Processing.*

Elhaffar, A. M. (2008). Power Transmission Line Fault Location Based on Current Traveling Waves. Faculty of Electronics, Communications and Automation, Helsinki University of Technology. *Degree of Doctor of Science in Technology*.

Elkalashy, N. I., Lehtonen, M., et al. (2007). DWT-based extraction of residual currents throughout unearthed MV networks for detecting high-impedance faults due to leaning trees. *European Transactions on Electrical Power, 17*(6), 597-614.

Elkalashy, N. I., Lehtonen, M., et al. (2008). DWT-Based Detection and Transient Power Direction-Based Location of High-Impedance Faults Due to Leaning Trees in Unearthed MV Networks. *IEEE Transactions on Power Delivery, 23*(1), 94-101.

Elkalashy, N. I., Lehtonen, M., et al. (2008). A novel selectivity technique for high impedance arcing fault detection in compensated MV networks. *European Transactions on Electrical Power, 18*(4), 344-363.

Elkalashy, N. I., Lehtonen, M., et al. (2008). Verification of DWT-Based Detection of High Impedance Faults in MV Networks. *IET 9th International Conference on Developments in Power System Protection, DPSP 2008*.

Etemadi, A. H. and Sanaye-Pasand, M. (2008). High-impedance fault detection using multi-resolution signal decomposition and adaptive neural fuzzy inference system. *IET Generation, Transmission and Distribution, 2*(1), 110-118.

Ferraz, R. G., Iurinic, L. U., et al. (2014). High impedance fault location formulation: A least square estimator based approach. *12th IET International Conference on Developments in Power System Protection, DPSP 2014*.

Filomena, A. D., Resener, M., et al. (2009). Fault location for underground distribution feeders: An extended impedance-based formulation with capacitive current compensation. *International Journal of Electrical Power and Energy Systems, 31*(9), 489-496.

Gaouda, A. M., Salama, M. M. A., et al. (1999). Power quality detection and classification using wavelet-multiresolution signal decomposition. *IEEE Transactions on Power Delivery, 14*(4), 1469-1476.

Garcia-Santander, L., Bastard, P., et al. (2005). Down-conductor fault detection and location via a voltage based method for radial distribution networks. *IEE Proceedings-Generation, Transmission and Distribution, 152*(2), 180-184.

Gazzana, D. S., Ferreira, G. D., et al. (2014). An integrated technique for fault location and section identification in distribution systems. *Electric Power Systems Research, 115*, 65-73.

Ghaderi, A., Ginn, H. L., et al. (2017). A review: High impedance fault detection. *Electric Power Systems Research, 143*, 376-388.

Ghaderi, A., Mohammadpour, H. A., et al. (2015). High-Impedance Fault Detection in the Distribution Network Using the Time-Frequency-Based Algorithm. *IEEE Transactions on Power Delivery, 30*(3), 1260-1268.

Ghaffarzadeh, N. and Vahidi, B. (2010). A New Protection Scheme for High Impedance Fault Detection using Wavelet Packet Transform. *Advances in Electrical and Computer Engineering, 10*(3), 17-20.

Girgis, A. A., Fallon, C. M., et al. (1993). A fault location technique for rural distribution feeders. *IEEE Transactions on Industry Applications, 29*(6), 1170-1175.

Girgis, A. A., Hart, D. G., et al. (1992). A new fault location technique for two- and three-terminal lines. *IEEE Transactions on Power Delivery, 7*(1), 98-107.

Glik, K. and Rasolomampionona, D. D. (2013). Travelling wave fault location algorithm in HV lines -Simulation test results for arc and high impedance faults. *Eurocon 2013*.

Glinkowski, M. T. and Wang, N. C. (1995). ANNs pinpoint underground distribution faults. *IEEE Computer Applications in Power, 8*(4), 31-34.

Gohokar, V. N. and Khedkar, M. K. (2005). Faults locations in automated distribution system. *Electric Power Systems Research, 75*(1), 51-55.

Goudarzi, M., Vahidi, B., et al. (2015). Improved fault location algorithm for radial distribution systems with discrete and continuous wavelet analysis. *International Journal of Electrical Power and Energy Systems, 67*, 423-430.

Guler, S. I. and Menendez, M. (2014). Part B: Methodological on Analytical formulation and empirical evaluation of pre-signals for bus priority. *Transportation Research, 64*, 41-53.

Haghifam, M., Sedighi, A. R., et al. (2006). Development of a fuzzy inference system based on genetic algorithm for high-impedance fault detection. *IEE Proceedings-Generation, Transmission and Distribution, 153*(3), 359-367.

Hong, Y. Y. and Huang, W. S. (2015). Locating High-Impedance Fault Section in Electric Power Systems Using Wavelet Transform, Means, Genetic Algorithms, and Support Vector Machine. *Mathematical Problems in Engineering, 9*.

Hulzink, J., Konijnenburg, M., et al. (2011). An Ultra Low Energy Biomedical Signal Processing System Operating at Near-Threshold. *IEEE Transactions on Biomedical Circuits and Systems, 5*(6), 546-554.

Iurinic, L., Orozco, A. H., et al. (2015). Distribution Systems High Impedance Fault Location: a Parameter Estimation Approach. *IEEE Transactions on Power Delivery, 99*, 1-1.

Jarventausta, P., Verho, P., et al. (1994). Using fuzzy sets to model the uncertainty in the fault location process of distribution networks. *IEEE Transactions on Power Delivery, 9*(2), 954-960.

Jensen, K. J., Munk, S. M., et al. (1998). Feature extraction method for high impedance ground fault localization in radial power distribution networks. *IEEE International Conference on Acoustics, Speech and Signal Processing*.

John Tengdin, C., Ron Westfall, V. C., et al. (1996). High Impedance Fault Detection Technology. Report of PSRC Working Group D15.

Jung, C. K., Kim, K. H., et al. (2007). Wavelet and neuro-fuzzy based fault location for combined transmission systems. *International Journal of Electrical Power and Energy Systems, 29*(6), 445-454.

Khorramdel, B., Marzooghi, H., et al. (2014). Fault locating in large distribution systems by empirical mode decomposition and core vector regression. *International Journal of Electrical Power and Energy Systems, 58*, 215-225.

Krajnak, D. J. (2000). Faulted circuit indicators and system reliability. *Rural Electric Power Conference.*

Kumano, S., Ito, N., et al. (1993). Development of expert system for operation at substation. *IEEE Transactions on Power Delivery, 8*(1), 56-65.

Lai, T. M., Snider, L. A., et al. (2005). High-impedance fault detection using discrete wavelet transform and frequency range and RMS conversion. *IEEE Transactions on Power Delivery, 20*(1), 397-407.

Lee, H. and Mousa, A. M. (1996). GPS travelling wave fault locator systems: investigation into the anomalous measurements related to lightning strikes. *IEEE Transactions on Power Delivery, 11*(3), 1214-1223.

Liang, R., Fu, G., et al. (2015). Fault location based on single terminal travelling wave analysis in radial distribution network. *International Journal of Electrical Power and Energy Systems, 66*, 160-165.

Macedo, J. R., Resende, J. W., et al. (2015). Proposition of an interharmonic-based methodology for high-impedance fault detection in distribution systems. *IET Generation, Transmission & Distribution, 9*(16), 2593-2601.

Martin, F. and Aguado, J. A. (2003). Wavelet-based ANN approach for transmission line protection. *IEEE Transactions on Power Delivery, 18*(4), 1572-1574.

Martinez, E. M. and Richards, E. F. (1991). An expert system to assist distribution dispatchers in the location of system outages. *Rural Electric Power Conference*. Papers Presented at the 35th Annual Conference.

Mathworks (2016). Neural Network Toolbox. Training Functions, Mathwork, Inc.

Melhorn, C. J., Davis, T. D., et al. (1998). Voltage sags: their impact on the utility and industrial customers. *IEEE Transactions on Industry Applications, 34*(3), 549-558.

Michalik, M., Lukowicz, M., et al. (2007). Verification of the Wavelet-Based HIF Detecting Algorithm Performance in Solidly Grounded MV Networks. *IEEE Transactions on Power Delivery, 22*(4), 2057-2064.

Michalik, M., Rebizant, W., et al. (2006). High-impedance fault detection in distribution networks with use of wavelet-based algorithm. *IEEE Transactions on Power Delivery, 21*(4), 1793-1802.

Mirjalili, S., Mirjalili S. M., et al. (2014). Grey Wolf Optimizer. *Advances in Engineering Software, 69*, 46-61.

Mohamed, S. S., El-Saadany, E. F., et al. (2003). ANN-based technique for fault location estimation using TLS-ESPRIT. *IEEE 46th Midwest Symposium on Circuits and Systems*.

Mora-Flòrez, J., Meléndez, J., et al. (2008). Comparison of impedance based fault location methods for power distribution systems. *Electric Power Systems Research, 78*(4), 657-666.

Moravej, Z., Mortazavi, S. H., et al. (2015). DT-CWT based event feature extraction for high impedance faults detection in distribution system. *International Transactions on Electrical Energy Systems 25*(12), 3288-3303.

Moshtagh, J. and Aggarwal, R. K. (2006). A New Approach to Ungrounded Fault Location in a Three-Phase Underground Distribution System using Combined Neural Networks and Wavelet Analysis. *Canadian Conference on Electrical and Computer Engineering, CCECE '06*.

Muro, C., Escobedo, R., et al. (2011). Wolf-pack (Canis lupus) hunting strategies emerge from simple rules in computational simulations. *Behavioural Processes, 88*(3), 192-197.

Nam, S. R., Kang, S. H., et al. (2012). Single line-to-ground fault location based on unsynchronized phasors in automated ungrounded distribution systems. *Electric Power Systems Research, 86*, 151-157.

Nath, S., Sinha, P., et al. (2012). A wavelet based novel method for the detection of harmonic sources in power systems. *International Journal of Electrical Power and Energy Systems, 40*(1), 54-61.

Novosel, D., Hart, D. G., et al. (1998). System for locating faults and estimating fault resistance in distribution networks with tapped loads. *Google Patents.*

Novosel, D., Hart, D. G., et al. (1996). Unsynchronized two-terminal fault location estimation. *IEEE Transactions on Power Delivery, 11*(1), 130-138.

Pinnegar, C. R. and Mansinha, L. (2003). A method of time–time analysis: The TT-transform. *Digital Signal Processing, 13*(4), 588-603.

Poisson, O., Rioual, P., et al. (2000). Detection and measurement of power quality disturbances using wavelet transform. *IEEE Transactions on Power Delivery, 15*(3), 1039-1044.

Pourahmadi-Nakhli, M. and Safavi, A. A. (2011). Path Characteristic Frequency-Based Fault Locating in Radial Distribution Systems Using Wavelets and Neural Networks. *IEEE Transactions on Power Delivery, 26*(2), 772-781.

Prabhavathi, D., Surya Kalavathi, M., et al. (2016). Detection and Location of Faults in Three-Phase 11 kV Underground Power Cables by Discrete Wavelet Transform. *Proceeding of International Conference on Intelligent Communication, Control and Devices, ICICCD 2016.*

Rafinia, A. and Moshtagh, J. (2014). A new approach to fault location in three-phase underground distribution system using combination of wavelet analysis with ANN and FLS. *International Journal of Electrical Power and Energy Systems, 55*, 261-274.

Ranjan, R. K., Pai, M. A., et al. (1993). Analytical formulation of small signal stability analysis of power systems with nonlinear load models. *Sadhana, 18*(5), 869-889.

Raza, S., Mokhlis, H., et al. (2016). Minimum-features-based ANN-PSO approach for islanding detection in distribution system. *IET Renewable Power Generation.*

S. Nath, A. D. and Chakrabarti, A. (2009). Detection of power quality disturbances using wavelet transform. *World Academy of Science Engineering and Technology, 49*, 869-873.

Samantaray, S. R., Panigrahi, B. K., et al. (2008). High impedance fault detection in power distribution networks using time-frequency transform and probabilistic neural network. *IET Generation, Transmission and Distribution, 2*(2), 261-270.

Santoso, S., Dugan, R. C., et al. (2000). Distance estimation technique for single line-to-ground faults in a radial distribution system. *IEEE Power Engineering Society Winter Meeting.*

Sarlak, M. and Shahrtash, S. M. (2011). High impedance fault detection using combination of multi-layer perceptron neural networks based on multi-resolution morphological gradient features of current waveform. *IET Generation, Transmission and Distribution, 5*(5), 588-595.

Sedighi, A. R., Haghifam, M., et al. (2005). High impedance fault detection based on wavelet transform and statistical pattern recognition. *IEEE Transactions on Power Delivery, 20*(4), 2414-2421.

Sekar, K., Mohanty, N. K., et al. (2018). High impedance fault detection using wavelet transform. *2018 Technologies for Smart-City Energy Security and Power (ICSESP).*

Sharaf, A. M. and Abu-Azab, S. I. (2000). A smart relaying scheme for high impedance faults in distribution and utilization networks. *Canadian Conference on Electrical and Computer Engineering.*

Shinde, V. B. and Hase, S. G. (2012). Identification of L-G Fault Transients & Capacitors Switching Transients by Using Wavelet. *International Journal of Advancement in Electronics and Computer Engineering, 1*(2), 69-76.

Shyh-Jier, H. and Cheng-Tao, H. (1999). High-impedance fault detection utilizing a Morlet wavelet transform approach. *IEEE Transactions on Power Delivery, 14*(4), 1401-1410.

Siddiqui, M. R., AlOthman, Z. A., et al. (2017). Analytical techniques in pharmaceutical analysis: A review. *Arabian Journal of Chemistry, 10,* Supplement 1, 1409-1421.

Sidhu, T. S. and Zhihan, X. (2010). Detection of Incipient Faults in Distribution Underground Cables. *IEEE Transactions on Power Delivery, 25*(3), 1363-1371.

Stockwell, R. G., Mansinha, L., et al. (1996). Localization of the complex spectrum: the S-transform. *IEEE Transactions on Signal Processing, 44*(4), 998-1001.

Takagi, T., Yamakoshi, Y., et al. (1982). Development of a New Type Fault Locator Using the One-Terminal Voltage and Current Data. *IEEE Transactions on Power Apparatus and Systems, 101*(8), 2892-2898.

Thomas, M. S., Bhaskar, N., et al. (2016). Voltage Based Detection Method for High Impedance Fault in a Distribution System. *Series B: Journal of The Institution of Engineers (India), 97*(3), 413-423.

Thukaram, D., Khincha, H. P., et al. (2005). Artificial neural network and support vector Machine approach for locating faults in radial distribution systems. *IEEE Transactions on Power Delivery, 20*(2), 710-721.

Torres, V., Guardado, J. L., et al. (2014). Modeling and detection of high impedance faults. *International Journal of Electrical Power & Energy Systems, 61*, 163-172.

Tria, M., Ovarlez, J. P., et al. (2007). Discriminating real objects in radar imaging by exploiting the squared modulus of the continuous wavelet transform. *IET Radar, Sonar and Navigation, 1*(1), 27-37.

Uriarte, F. M. and Centeno, V. (2005). High-impedance fault detection and localization in distribution feeders with microprocessor based devices. *Proceedings of the 37th Annual North American, Power Symposium.*

Vahidi, B., Ghaffarzadeh, N., et al. (2010). An Approach to Detection of High Impedance Fault Using Discrete Wavelet Transform and Artificial Neural Networks. *Simulation, 86*(4), 203-215.

Wavelet Transform. MATLAB Toolbox.

Wen-Hui, C., Chih-Wen, L., et al. (2000). On-line fault diagnosis of distribution substations using hybrid cause-effect network and fuzzy rule-based method. *IEEE Transactions on Power Delivery, 15*(2), 710-717.

Wen, F. and Han, Z. (1995). Fault section estimation in power systems using a genetic algorithm. *Electric Power Systems Research, 34*(3), 165-172.

Wenzhong, G. and Jiaxin, N. (2011). Wavelet-Based Disturbance Analysis for Power System Wide-Area Monitoring. *IEEE Transactions on Smart Grid, 2*(1), 121-130.

Xiu, W. and Liao, Y. (2014). Novel fault location methods for ungrounded radial distribution systems using measurements at substation. *Electric Power Systems Research, 106*, 95-100.

Ye, L., You, D., et al. (2014). An improved fault-location method for distribution system using wavelets and support vector regression. *International Journal of Electrical Power and Energy Systems, 55*, 467-472.

Ying-Hong, L., Chih-Wen, L., et al. (2002). A new fault locator for three-terminal transmission lines using two-terminal synchronized voltage and current phasors. *IEEE Transactions on Power Delivery, 17*(2), 452-459.

Yuan-Yih, H., Lu, F. C., et al. (1991). An expert system for locating distribution system faults. *IEEE Transactions on Power Delivery, 6*(1), 366-372.

Zadeh, H. K. (2005). An ANN-Based High Impedance Fault Detection Scheme: Design and Implementation. *International Journal of Emerging Electric Power Systems, 4*(2).

Zanjani, M. G. M. and Kargar, H. K. (2012). High impedance fault detection of distribution network by phasor measurement units. *Proceedings of 17th Conference on Electrical Power Distribution Networks.*

Zayandehroodi, H., Mohamed, A., et al. (2013). An optimal radial basis function neural network for fault location in a distribution network with high penetration of DG units. *Measurement, 46*(9), 3319-3327.

Zayandehroodi, H., Mohamed, A., et al. (2012). A novel neural network and backtracking based protection coordination scheme for distribution system with distributed generation. *International Journal of Electrical Power and Energy Systems, 43*(1), 868-879.

Zimath, S. L., Dutra, C. A., et al. (2014). Traveling wave fault location applied to high impedance events. 12th IET International Conference on Developments in Power System Protection (DPSP 2014).

LIST OF PUBLICATIONS AND PAPERS PRESENTED

Mohd Syukri Ali, Ab Halim Abu Bakar, ChiaKwang Tan, Hamzah Arof, Hazlie Mokhlis. "Studies on the Application of Wavelet Families for HIF Location Algorithm in Distribution Network" Turkish Journal of Electrical Engineering & Computer Sciences (2016), Volume 24, Issue 6, Pages 5043-5054. https://doi:10.3906/elk-1412-148

Mohd Syukri Ali, Ab Halim Abu Bakar, ChiaKwang Tan, Hamzah Arof, Hazlie Mokhlis, Mohamad Sofian Abu Talip. "High Impedance Fault Localization Using Discrete Wavelet Transform for Single Line to Ground Fault" Arabian Journal for Science and Engineering (2017), Volume 42, Issue 12, Pages 5031–5044. https://doi.org/10.1007/s13369-017-2545-8

Mohd Syukri Ali, Ab Halim Abu Bakar, ChiaKwang Tan, Hamzah Arof, Hazlie Mokhlis, "High Impedance Fault Detection and Identification based on Pattern Recognition of Phase Displacement Computation" IEEJ Transactions on Electrical and Electronic Engineering (2018). http://doi.org/10.1002/tee.22600